FRACTURE MECHANICS AND CONTACT PROBLEMS IN MATERIALS INVOLVING GRADED COATINGS AND INTERFACIAL ZONES

Final Technical Report

Fazil Erdogan

Lehigh University
Bethlehem, PA 18105

April 2001

Prepared for

US Air Force Office of Scientific Research
Grant No. F49620-98-1-0028

FRACTURE MECHANICS AND CONTACT PROBLEMS IN MATERIALS INVOLVING GRADED COATINGS AND INTERFACIAL ZONES

Final Technical Report

Fazil Erdogan

Lehigh University
Bethlehem, PA 18105

April 2001

Prepared for

US Air Force Office of Scientific Research
Grant No. F49620-98-1-0028

SF 298 MASTER COPY KEEP THIS COPY FOR REPRODUCTION PURPOSES

REPORT DOCUMENTATION PAGE

Form Approved
OMB NO. 0704-0188

1. AGENCY USE ONLY *(Leave blank)*	2. REPORT DATE	3. REPORT TYPE AND DATES COVERED
	April 2001	Final 10/15/97 - 4/15/01

4. TITLE AND SUBTITLE

Fracture Mechanics and Contact Problems in Materials Involving Graded Coatings and Interfacial Zones

5. FUNDING NUMBERS

AFOSR - Grant

F49620-98-1-0028

6. AUTHOR(S)

Fazil Erdogan

7. PERFORMING ORGANIZATION NAMES(S) AND ADDRESS(ES)

Lehigh University, ME - MECH Department
19 Memorial Drive West,
Bethlehem, PA 18015

8. PERFORMING ORGANIZATION REPORT NUMBER

533 046

9. SPONSORING / MONITORING AGENCY NAME(S) AND ADDRESS(ES)

Dr. H. Thomas Hahn, IPA Program Manager
AFOSR/NA
801 N. Randolph St. Room 947
Arlington, VA 22203

10. SPONSORING / MONITORING AGENCY REPORT NUMBER

11. SUPPLEMENTARY NOTES

The results obtained during the course of this program have been submitted in the form of AFOSR Technical Project Reports. The views and findings contained in these reports are those of author and should not be construed as official AFOSR position. The technical monitors for this project were Dr. Ozden O. Ochoa and Dr. H. Thomas Hahn.

12a. DISTRIBUTION / AVAILABILITY STATEMENT

Approved for public release; distribution unlimited

12 b. DISTRIBUTION CODE

13. ABSTRACT *(Maximum 200 words)*

Continuously grading the thermomechanical properties of materials is becoming a powerful tool in designing new materials for specific applications. Even though the potential application of the concept is very nearly unlimited, in the near future most likely fields of application of graded materials appear to be high-temperature components, load transfer components, components with high impact resistance and improved bonding strength, and thermoelectric cells. Thus, the primary objectives of this research program have been to identify specific fracture and contact problems the solutions of which are needed in the relevant failure analysis, to develop the necessary analytical and numerical methods for solving these problems, and to provide meaningful benchmark solutions in each area identified for investigation. Particular emphasis in the program has been on the investigation of failure-oriented problems. Considering the present and future applications, the main research efforts are therefore, concentrated on fracture mechanics, contact mechanics and elastodynamics of graded materials. In this report after presenting the necessary review and background information on the application of graded materials, the objectives of the research program and the summary of a series of benchmark solutions in the fields of fracture and contact mechanics involving graded coatings and interfaces are described.

14. SUBJECT TERMS

Funtionally graded materials, fracture mechanics, contact mechanics, surface cracking, graded coatings, sliding contact, graded interfacial zones.

15. NUMBER IF PAGES

16. PRICE CODE

17. SECURITY CLASSIFICATION OR REPORT	18. SECURITY CLASSIFICATION OF THIS PAGE	19. SECURITY CLASSIFICATION OF ABSTRACT	20. LIMITATION OF ABSTRACT
UNCLASSIFIED	UNCLASSIFIED	UNCLASSIFIED	UL

TABLE OF CONTENTS

Report Documentation Page i

Cover Page ii

Table of Contents iii

Abstract 1

1. Functionally Graded Materials - A Brief Introduction and Potential Applications 2

1.1 High Temperature Applications 3

1.2 Tribology - Contact Mechanics 5

1.3 Cracking Due to Sliding Contact 6

1.4 Impact Resistance - Wave Propagation in Graded Materials 6

1.5 Thermoelectric Cells 7

2. Objectives of the Research Program 8

3. Fracture and Contact Mechanics: Basic Concepts 9

3.1 Fracture Mechanics of Graded Materials: Basic Concepts 9

3.2 Debonding Problems in Graded Materials 12

3.3 Cracking Perpendicular to Interfaces and Surfaces 13

3.4 End Effects 15

3.5 Contact Mechanics of Graded Materials: Basic Concepts 15

4. Fracture Mechanics of Graded Materials / Benchmark Solutions 17

4.1 The Effect of Material Orthotropy in Graded Materials 18

4.2 Spallation of Graded Materials: A Penny Shaped Crack 20

4.3 Interface Cracking of Graded Coatings 20

4.4 Buckling of Graded Coatings - A Continuum Model 21

4.5 Surface Cracking in a Graded Medium under General Loading Conditions 21

4.6 Cracking of a Graded Layer Bonded to a Homogeneous Substrate 22

5. Contact Mechanics of Graded Materials / Benchmark Solutions 23

5.1 Basic Contact Mechanics Problems in FGM Coatings 23

5.2 Surface Cracking of Homogeneous Materials Due to Sliding Contact 24

5.3 Surface Cracking of Graded Materials Due to Sliding Contact 24

6. Elastodynamics of Graded Materials 25

7. Some Concluding Remarks 26

8. References 27

9. Personnel 30

10. List of AFOSR Technical Project Reports and Articles 30

10.1 Technical Reports 30

10.2 Journal Articles 30

10.3 Proceedings Articles 31

Appendix A A1

Appendix B B1

Appendix C C1

FRACTURE MECHANICS AND CONTACT PROBLEMS IN MATERIALS INVOLVING GRADED COATINGS AND INTERFACIAL ZONES

ABSTRACT

Continuously grading the thermomechanical properties of materials is becoming a powerful tool in designing new materials for specific applications. Even though the potential application of the concept is very nearly unlimited, in the near future most likely fields of application of graded materials appear to be high-temperature components, load transfer components, components with high impact resistance and improved bonding strength, and thermoelectric cells. Thus, the primary objectives of this research program have been to identify specific fracture and contact problems the solutions of which are needed in the relevant failure analysis, to develop the necessary analytical and numerical methods for solving these problems, and to provide meaningful benchmark solutions in each area identified for investigation. Particular emphasis in the program has been on the investigation of failure-oriented problems. Considering the present and future applications, the main research efforts are therefore, concentrated on fracture mechanics, contact mechanics and elastodynamics of graded materials. In this report after presenting the necessary review and background information on the application of graded materials, the objectives of the research program and the summary of a series of benchmark solutions in the fields of fracture and contact mechanics involving graded coatings and interfaces are described.

1. Functionally Graded Materials - A Brief Introduction and Potential Applications

To meet the highly stringent demands of future technologies in power generation, transportation, aerospace and microelectronics, in current research a greater emphasis will have to be placed on material design, more specifically, on developing new materials or material systems tailored for specific applications. Generally such materials tend to be composites and intermetallics with homogeneous bulk properties. The composites may be fiber or filament-reinforced, particulate or layered in structure. Many of the laminated materials, thin films and coatings also fall into this category. A common feature of composites is that they consist of bonded dissimilar homogeneous materials. Consequently, in studying the mechanics, particularly the failure mechanics of such materials, the structure of interfaces or interfacial regions would play an extremely important role. From a mechanics stand point material property discontinuities across the interfaces have generally two undesirable features, namely higher stress concentration and weaker bonding strength. To circumvent these difficulties, the interfacial regions are modified by introducing a third medium along the interface in the form of an interlayer, by mechanically roughening the contacting surfaces or by using chemical coupling agents.

A relatively new alternative concept which may be used to overcome some of the shortcomings of bonded dissimilar homogeneous materials, particularly that of the layered materials would be the introduction of interfacial regions or coatings with graded thermomechanical properties [1-7]. Thus, by varying the volume fractions of the constituents in the coating or the interface from zero to one hundred percent, and thereby obtaining a continuous through thickness thermomechanical property variation, it is possible to obtain not only smoother stress distributions and lower stress concentrations [8], but also higher bonding strength [9]. For example, in [8] it was shown that the points of intersection of free surfaces and interfaces between dissimilar materials are points of stress singularity and, consequently, potential locations of debonding fracture initiation. On the other hand, if the sharp interface is eliminated by introducing a graded layer, the singularity disappears and the stress distribution becomes considerably smoother [8,10].

In many deposition and bonding processes used in ceramic coatings it is difficult to obtain the desired strength for the interfacial zones. This is due largely to poor adhesion and partly to high stress concentrations. The adverse influence of both of these factors can be reduced significantly by introducing a graded interfacial zone between the two materials. The technique can be particularly useful for material pairs in which bonding is inherently difficult. For example, in [9] it was shown that a diamond film deposited over a

50/50 W/Mo alloy by using a DC plasma jet, the bonding strength obtained was less than 10 kg/cm^2. On the other hand if a graded interfacial zone is introduced by first plasma spraying the substrate with tungsten carbide and then gradually adding increasing amounts of methane and hydrogen before growing the diamond film, the adhesive strength was measured to be over 150 kg/cm^2.

These mostly particulate composites with continuously varying volume fractions are called *functionally graded materials* (FGMs). By controlling not only the composition profile but also the microstructure, the concept of FGMs could provide a great deal of flexibility in material design. As the processing techniques improve, the potential for special applications of FGMs appear to be nearly unlimited. However, in the immediate future the primary application of these materials will most likely be limited to thermal barrier coatings, tribology (with wear and corrosion-resistant coatings), abradable seals, impact-resistant structures, and thermoelectric cells. In the remainder of this section these potential applications of FGMs will be briefly described. The primary objectives of the research program will be outlined in Section 2.

1.1 High Temperature Applications

Within the past decade considerable progress has been made in using ceramic coatings to protect metallic components from high temperatures. These *thermal barrier coatings* (TBCs) are currently being used in conjunction with air cooling to prolong the life of hot section turbine components in aircraft engines. The application of ceramic TBCs also offers the possibility of increasing the thermodynamic efficiency of landbased turbines by increasing the inlet temperature of gases. TBC technology is thus considered to be a viable means for developing more efficient aircraft engines and stationary gas turbines. There are, however, several major technical issues involving the next generation of TBCs that need to be addressed: (a) improvement in processing techniques from both economic and performance standpoints, (b) understanding the failure mechanisms of TBCs in simulated and actual turbine environments and developing the appropriate techniques for their modeling and analysis, and (c) developing thermomechanical material characterization and test methodologies to measure the material properties necessary for the application of life prediction models.

The current approach for accommodating the material property mismatch between the ceramic coating and the metallic substrate is to make the ceramic layer to be more compliant or strain-tolerant by introducing a segmented columnar structure (or in some

cases pores or microcracks). The difficulty with this solution is that the particular microstructural features that provide compliant coatings also provide rapid diffusion paths for oxygen. The experience seems to indicate that by far the most critical factor limiting the performance of the state-of-the-art TBCs is the spallation of ceramic layers which take place either along a plane parallel to the ceramic/oxide layer interface (as in plasma spray coatings) or bond coat/oxide interface (as in coatings processed by using electron beam physical vapor deposition). Usually a micron-thick oxide layer (generally Al_2O_3) forms between the bond coat and the top coat during processing. It then gradually grows during operation as the system is subjected to sustained high temperature until most of the aluminum in the bond coat is depleted. Thus, the life of TBCs seems to be controlled by the number and exposure time of thermal cycles and the process of local initiation, growth and coalescence of micro cracks.

The main desirable characteristics of an ideal TBC appear to be low conductivity for thermal insulation, high coefficient of thermal expansion to match that of the metallic substrate, and high resistance to oxygen diffusion. It is highly unlikely to find all these favorable properties in a single material. Many of the well-known ceramics have either high conductivity and low oxygen diffusivity or low conductivity and high oxygen diffusivity. To prevent oxygen diffusion at some point a layer of Al_2O_3 or mullite (Al_2O_3 $2SiO_2$) may be needed. However, these materials have considerably higher thermal conductivity than that of, for example, YSZ (ytria-stabilized zirconia). Thus, the problem appears to be an optimal design of a multi-layered structure, including graded interfacial zones and coatings.

Typically, the current design of TBCs consists of a partially stabilized zirconia coating deposited on an intermediate metallic bond coat (e.g., NiCrAlY) which is plasma sprayed on the (superalloy) substrate [7]. The main function of the bond coat is to protect the substrate against oxidation. It also helps to reduce thermal expansion mismatch between the ceramic coating and the metallic substrate, and provides the surface texture needed to improve bonding. At high temperatures an oxide (Al_2O_3) scale is formed along the PSZ-bond coat interface. Even though this Al_2O_3 layer forms an oxygen diffusion barrier, it also introduces a weak cleavage plane which, under thermal cycling may lead to spallation. This difficulty may be overcome by introducing a graded ($NiCrAl_2Y$-PSZ) layer between the bond coat and the ceramic layer [7].

The basic premise behind using the FGM concept is that by replacing sharp interfaces with graded interfacial zones or by replacing homogeneous ceramics layers with graded

metal/ceramic composites, it is possible to improve the resistance of the coating to spallation as a result of reduced stress levels and improved bonding strength.

A broad outline of the benchmark problems studied in this area is presented in Section 4. The details of these studies are described in Appendices A, B and C and in the Technical Project Reports [10], [11], [12] and the Article [13].

1.2 Tribology - Contact Mechanics

An obvious application of ceramic coatings seems to be to provide the necessary hardness or wear resistance to the surfaces of structural components transmitting forces through contact such as gears, bearings, cams and machine tools. Intuitively, it is clear that the fatigue life of these components may be improved quite considerably by using graded rather than homogeneous ceramic coatings on the main load-bearing metallic substrate. In these load-transfer components FGM coatings would provide the necessary surface hardness without sacrificing toughness.

A wear related application of FGM coatings or interfacial zones may be found in abradable seals used in some stationary gas turbines to help minimize the gas leakage through the gap between the tips of the rotating blades and turbine shroud. Here the main components in the shroud are the metallic structure or the substrate, the bond coat, a layer of high density ceramic and a layer of very low density ceramic with a graded zone replacing every sharp interface [14]. The underlying mechanics problem is again a contact problem and the primary desirable material property requirements are toughness and abradability.

In the past wear and corrosion resistant coatings have been used quite extensively in industrial machinery. Coating materials have been metals such as stainless steels, Mo based alloys and WC-Co as well as ceramics such as Al_2O_3/NiCr have been extensively used in aircraft industry to coat various turbine/compressor components and mid-span stiffeners for improved wear resistance. Other applications of wear-resistant coatings have been in printing rolls, steel mills, petrochemical industry and transportation industry. Most of these coatings have been deposited by using a thermal spray technique. Since thermal spray processes are readily suitable for composition grading, service life improvement can be obtained in all applications of wear and corrosion-resistant coatings by using the FGM concept.

The basic mechanics of crack and contact problems associated with the failure of wear and corrosion-resistant coatings and abradable seals is described in Section 3 of this

report. The analytical details and extensive results for the contact problems in FGM coatings are presented in the Technical Report [15].

1.3 Cracking Due to Sliding Contact

Many of the present and potential applications of FGMs involve contact problems. These are mostly the load transfer problems in deformable solids, generally in the presence of friction. From the standpoint of failure mechanics an important aspect of contact problems is the surface cracking which is caused by friction forces and which invariably leads to fretting fatigue. In most applications material property grading near the surface is used as a substitute for homogeneous ceramic coatings. In both cases, that is in both homogeneous and graded coatings the surface of the medium consists of 100% ceramic which is generally a brittle solid. Hence, the "maximum tensile stress" criterion may be used for crack initiation on the surface. Once the crack is initiated, its subcritical growth under repeated loading by a sliding stamp is controlled by stress intensity factors at the crack tip. The main objective of this study is, therefore, the evaluation of peak tensile stresses on the surface for the purpose of studying crack initiation and the stress intensity factors for modeling subcritical crack growth. Specifically, the objective is the examination of the influence of friction coefficient and material nonhomogeneity parameters on the peak surface stresses and stress intensity factors. The problem is considered under the assumption of plane strain, Coulomb friction and linear nonhomogeneous elasticity.

The details of the analysis and very extensive results for the coupled crack/contact problems involving homogeneous and graded materials are presented in the Technical Project Reports [16] and [17], respectively. A brief introduction of the problem and some results may also be found in Appendix C. In all these studies the emphasis has been on examining the influence of the material nonhomogeneity constants and the friction coefficient on the surface crack initiation stress and crack tip stress intensity factors.

1.4 Impact Resistance - Wave Propagation in Graded Materials

A first step in studying the failure mechanics of structural components usually is a detailed stress analysis for identifying the likely sites of failure initiation and for determining the peak values of stresses. In some cases the loading of these nonhomogeneous components may be dynamic in nature. Thus, an important area of

interest in considering the applications of graded materials would be to study the dynamic response of the component to, for example, impact or blast loading. In elastodynamics of materials with continuously varying properties, usually the pulse shape is distorted in time, the wave propagation speed is not constant, and there are no sharp interfaces that would cause wave reflections. Consequently, even in the simple case of one-dimensional wave propagation the locations and magnitudes of peak stresses can not be determined by inspection.

Because of its relevance in geophysics and soil mechanics, in the past there has been quite considerable interest in elastodynamics of nonhomogeneous media. In 1946 Friedlander [18] proposed a solution that consists of a series of terms the first of which describes the wave motion predicted by geometrical optics and the subsequent terms account for certain types of diffraction effects. Karal and Keller [19] extended this method to treat general wave propagation problems in nonhomogeneous elastic media by formulating the problem in terms of displacements and displacement potentials. Pekeris [20] used an asymptotic method to solve the problem for a half-space with a variable speed of sound and reduced the solution to Fourier-Bessel series. Since then geophysics-oriented contributions to the field have been quite voluminous.

Among many others, there are two important reasons for studying the problem of wave propagation and impact in FGMs. The first is the interpretation and analysis of possible nondestructive testing and evaluation results. The second is related to service life and reliability of FGM components, specifically, to the evaluation of peak stresses for the purpose of spallation studies. A one-dimensional benchmark problem was considered in [21]

1.5 Thermoelectric Cells

In many conductors generally the electrical current and the thermal flux are coupled. This coupling can be used, in principle, to construct refrigerators or electric power generators. A temperature difference ΔT across any conductor would generate a voltage ΔV. Generally $S = \Delta V/\Delta T$ is a measure of the efficiency of the device where S is the Seebeck coefficient. A commonly known such device is the thermocouple. The efficiency of the device is also dependent on thermal conductivity k and electrical resistivity ρ. Thus, it has been shown that the dimensionless constant defined by $Z = TS^2/k\rho$ is the measure of device efficiency at temperature $T(K)$, where Z is known as the figure of merit. Most metallic materials have very small values of Z and, consequently, are not suitable for

thermoelectric cell applications. The group of materials most suitable for refrigeration as well as power generation appears to be certain doped semiconductors [22], [23]. Some of the typical applications for thermoelectric devices are power for deep space probes, remote weather stations, and underwater and remote navigational systems in power generation area and spot cooling of electronic devices, infrared and X-ray detectors, fiber optic laser packages, and computer central processing units in refrigeration area.

In semiconductors suitable for thermoelectric cell application, the figure of merit is highly temperature dependent. In a typical temperature range such as 300 - 1000 (K) the use of a single material would be very inefficient. Thus, to optimize the power efficiency a layered material is necessary. This result of increasing overall device efficiency can be best accomplished by using bonded dissimilar materials containing many layers each operating near its optimum temperature. To a lesser extent, it can also be accomplished by using a single semi-conductor with graded dopant concentration. In either case, the underlying mechanics is one of bonded dissimilar materials with stress-free surfaces subjected to steep temperature gradients. Here, because of stress singularities, debonding is a common mode of failure. It is, therefore, clear that, from the viewpoint of failure mechanics as well as device efficiency, the FGM concept is very highly suitable for application to thermoelectric cells.

2. Objectives of the Research Program

The primary objectives of this research program on the fracture and contact mechanics in graded materials have been

- To identify specific crack and contact problems the solutions of which are needed in the relevant failure analysis
- To develop the necessary analytical and numerical methods for solving these crack and contact problems
- To examine the singular behavior of crack, contact and coupled crack/contact problems in FGMs and compare them with the corresponding results in homogeneous and piecewise homogenous materials
- To provide meaningful analytical benchmark solutions in each area identified for the investigation

A particular emphasis in the research program has been on the investigation of failure-oriented problems. Thus, considering the present and potential applications of the graded materials, the main efforts were concentrated in the following three specific areas:

- Fracture mechanics of graded materials
- Contact mechanics of graded materials
- Elastodynamics of graded materials

In general *the results of the research program are intended to provide technical support for material scientists and engineers who are trying to develop techniques for processing new graded materials with certain desirable properties and for design engineers who are interested in their applications. Also, the analytically obtained singularities and benchmark solutions are intended to help the development and testing of new finite element models for solving more complex problems involving fracture and contact mechanics of graded materials.*

3. Fracture and Contact Mechanics: Basic Concepts

In this section the basic concepts of fracture and contact mechanics in graded elastic solids are very briefly described.

3.1 Fracture Mechanics of Graded Materials: Basic Concepts

In a broad sense "fracture" is the creation of new surfaces in solids. The fundamental criterion of fracture initiation and propagation is based on the energy balance concept. Let the solid contain a dominant flaw which is usually considered to be a planar crack of surface area A. Under given external loads if the crack grows by an amount dA in time dt, the thermodynamic equilibrium of the solid requires that

$$\frac{dU}{dt} = \frac{dV}{dt} + \frac{dT}{dt} + \frac{dD}{dt}, \tag{1}$$

where U, V, T and D respectively are the work of the external loads, the recoverable internal energy, the kinetic energy, and the sum of all dissipated energies such as surface tension, plastic work, viscous dissipation, etc. If the energy dissipation takes place only

around the advancing periphery of the crack, in a quasi-static case T is negligible and defining $dD/dA = G_c$ (1) may be expressed as

$$\frac{d}{dA}(U - V) = G_c. \tag{2}$$

In the fracture criterion given by (2) the left hand side is the energy available and G_c is the energy required to create a unit area of new fracture surface. They are also known as the *crack driving force* and the *fracture toughness*, respectively. By using the concept of crack closure it can then be shown that the increment $d(U - V)$ of the energy available for fracture may be evaluated from the asymptotic stresses and the crack opening displacements near the crack tip which, in homogeneous solids, may be obtained from the three dimensional elasticity solution as follows:

$$\sigma_{ij}(r,\theta) \cong \frac{k_1}{\sqrt{2r}} f_{1ij}(\theta) + \frac{k_2}{\sqrt{2r}} f_{2ij}(\theta), \qquad (i,j = x,y), \tag{3}$$

$$\sigma_{iz}(r,\theta) \cong \frac{k_3}{\sqrt{2r}} f_{3i}(\theta), \quad (i = x,y), \tag{4}$$

$$v^+ - v^- \cong \frac{2(1-\nu^2)}{E} k_1 \sqrt{2r}, \qquad u^+ - u^- \cong \frac{2(1-\nu^2)}{E} k_2 \sqrt{2r}, \tag{5}$$

$$w^+ - w^- \cong \frac{k_3}{\mu} \sqrt{2r}, \tag{6}$$

where k_1, k_2 and k_3 are the modes I, II and III stress intensity factors, f_{1ij}, f_{2ij} and f_{3i} are known functions and E, ν and μ are the elastic constants, $E = 2\mu(1+\nu)$. From the crack closure energy it may then be shown that

$$G_1 = \frac{\pi(1-\nu^2)}{E} k_1^2, \qquad G_2 = \frac{\pi(1-\nu^2)}{E} k_2^2, \qquad G_3 = \frac{\pi}{2\mu} k_3^2, \tag{7}$$

$$G = \frac{d}{dA}(U - V) = G_1 + G_2 + G_3, \tag{8}$$

where G is total energy available for fracture.

Equation (7) indicates that one may also use k_i in place of G_i as the measure of the crack driving force. For mode I loading conditions, for example defining

$$K_I = k_1 \sqrt{\pi}, \qquad G_{1c} = G_{IC}, \qquad K_{IC} = \sqrt{G_{IC} E (1-\nu^2)}, \tag{9}$$

the fracture criterion (2) may be expressed as

$$K_I \leq K_{IC}. \tag{10}$$

Equation (10) has proved to be very useful in considering the fracture stability. However, perhaps the most useful application of the stress intensity factors may be found in analyzing the subcritical crack growth processes.

In studying the fracture mechanics of graded materials one may have to deal with a number of distinct singularity problems. The first is the investigation of the nature of stress singularities near the tip of a crack embedded in a nonhomogeneous medium. The second is the general problem of debonding and the effect of a possible "kink" in material property distributions on stress singularities. And the third is the basic surface cracking problems and the nature of the stress singularities for cracks intersecting the interfaces.

To examine the influence of the material nonhomogeneity on the asymptotic stress state near the crack tips, we first consider the plane elasticity problem for an infinite medium containing a line crack. For simplicity we will assume that the Poisson's ratio ν of the medium is constant and the shear modulus is approximated by

$$\mu(x,y) = \mu_0 \exp(\beta x + \gamma y), \tag{11}$$

where μ_0, β and γ are known constants. This problem was solved for a crack along $y = 0, \ -a < x < a,$ under arbitrary loading conditions [24]. It was shown that near the crack tip $x = a$ the stresses have the following asymptotic behavior:

$$\sigma_{ij}(x,y) = \exp(r(\beta\cos(\theta) + \gamma\sin(\theta)))\left[\frac{k_1}{\sqrt{2r}} f_{1ij}(\theta) + \frac{k_2}{\sqrt{2r}} f_{2ij}(\theta)\right], \ (i,j = x,y), \tag{12}$$

where the stress intensity factors k_1 and k_2 are defined by

$$k_1(a) = \lim_{x \to a} \sqrt{2(x-a)}\sigma_{yy}(x,0), \qquad k_2(a) = \lim_{x \to a} \sqrt{2(x-a)}\sigma_{xy}(x,0), \tag{13}$$

and the functions f_{1ij} and f_{2ij} are identical to those found for the homogeneous materials given in (3). Note that the asymptotic stress states for homogeneous materials (3) and FGMs (12) are identical only at $r = 0$. However, since the crack opening displacement is also influenced in a way similar to stresses, the crack driving force (or, for "fixed grip" conditions, the strain energy release rate) was found to be identical to that calculated for the homogeneous materials, namely

$$G = \frac{\pi(1+\kappa)}{8\mu(a,0)}(k_1^2 + k_2^2), \tag{14}$$

where $\kappa = 3 - 4\nu$ for plane strain and $\kappa = (3-\nu)/(1+\nu)$ for plane stress conditions.

For results regarding the stress intensity factors in FGMs see [12], [13] and [24], [30].

3.2 Debonding Problems in Graded Materials

Consider the crack problems shown in Figs. 1a and 1b. Figure 1a describes the debonding problem in piecewise homogeneous materials, whereas Fig. 1b refers to an FGM bonded to a homogeneous substrate. In both cases $h = 0$ refers to an "interface crack". In terms of the unknown functions

$$f_1(x) = \frac{\partial}{\partial x}(v^+ - v^-), \qquad f_2(x) = \frac{\partial}{\partial x}(u^+ - u^-), \tag{15}$$

in each case the formulation of the problem may be reduced to a system of integral equations of the form

$$\frac{1}{\pi}\int_{-a}^{a}\sum_{1}^{2}\left[\frac{\delta_{ij}}{t-x} + k_{ij}^s(x,t) + k_{ij}^f(x,t)\right] f_j(t)dt = \frac{1+\kappa}{2\mu_1(0)}p_i(x), \ (i=1,2),$$
$$-a < x < a, \tag{16}$$

where the kernels k_{ij} are known functions which depend on h and material parameters, k_{ij}^s is associated with the infinite medium, k_{ij}^f represents the geometry of the medium, and

$$p_1(x) = \sigma_{yy}(x,0), \qquad p_2(x) = \sigma_{xy}(x,0), \tag{17}$$

are the crack surface tractions which may be expressed in terms of the external load. The kernels k_{ij}^f are bounded for all values of h. For $h > 0$ the functions k_{ij}^s are also bounded. Thus, for $h > 0$ the crack is an embedded crack and (16) would lead to the asymptotic stresses given by (3) and (12) for problems described by Figs. 1a and 1b respectively. On the other hand, for $h = 0$ in problem 1a the kernels k_{11}^s and k_{22}^s would become a Cauchy kernel $(t-x)^{-1}$ and k_{12}^s and k_{21}^s would degenerate to a delta function $\delta(t-x)$ [31,32]. Consequently, in this interface crack problem the integral equations become one of the second kind leading to the well known anomalous stress oscillation behavior very near the crack tips.

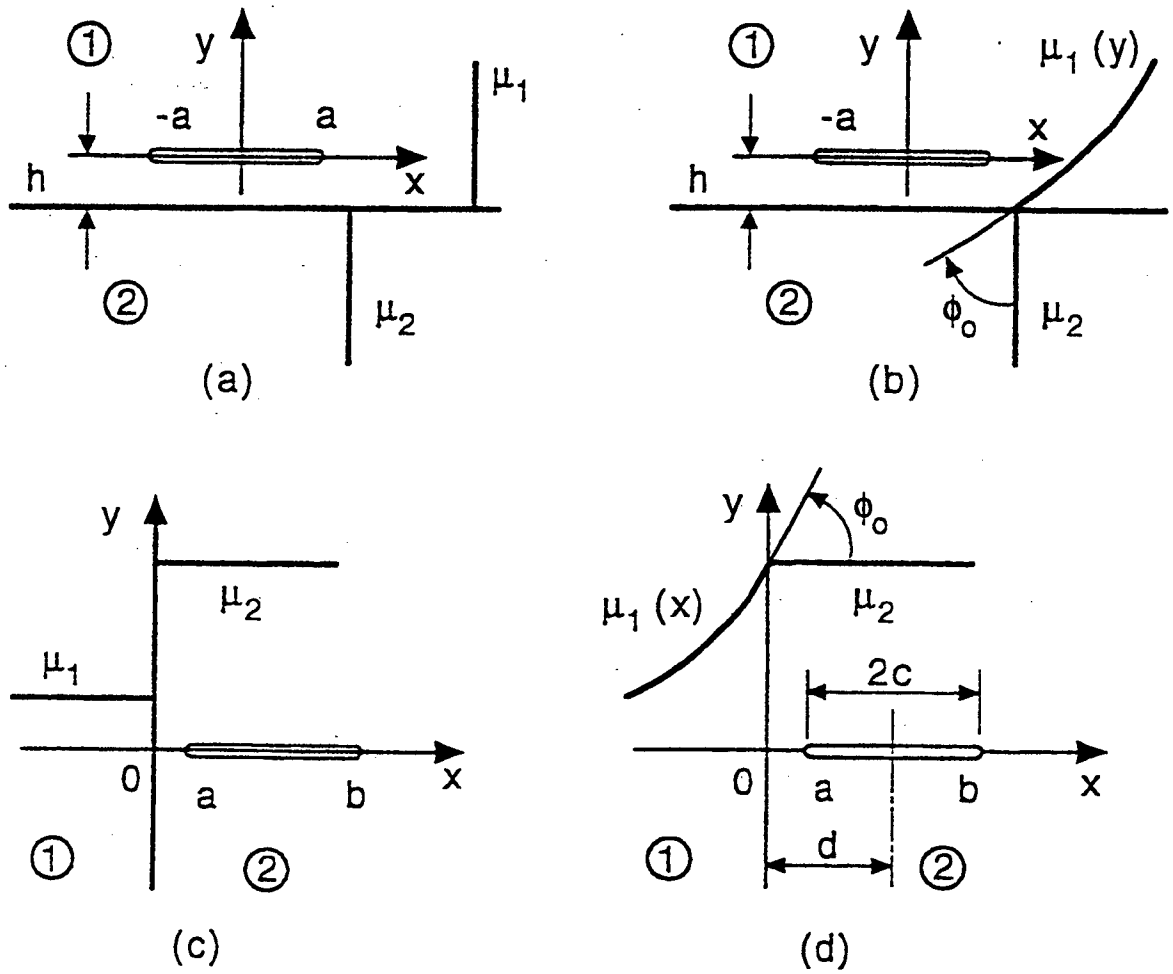

Figure 1: Geometry and notation for a plane crack in bonded homogeneous and nonhomogeneous media.

For $h = 0$ in problem 1b, however, the leading terms of the kernels k_{ij}^s become

$$k_{11}^s = k_{22}^s = -\frac{\pi\gamma|t-x|}{8(t-x)},$$

$$k_{12}^s = -k_{21}^s = \frac{\gamma}{4}\log|t-x|, \qquad \gamma = \tan(\phi_0), \tag{18}$$

which would indicate that (16) would remain to be an ordinary system of singular integral equations, of the first kind and would have the asymptotic solution given by (12). It is, therefore, seen that the anomalous behavior of the crack tip stress oscillations may be eliminated by "smoothing" the material property distribution (or by removing the property discontinuity). A qualitative description of the interface crack geometries and the singular kernels k_{ij}^s may be seen in Fig. 2.

3.3 Cracking Perpendicular to Interfaces and Surfaces

In ceramic and ceramic/metal FGM components generally a common mode of failure is surface cracking which could penetrate to the interface and cause debonding. The main problem here is assessing the influence of material nonhomogeneity on the fracture mechanics parameters (such as G and k_1) for surface cracks and cracks terminating at an interface. Figures 1c and 1d show the crack geometry for the latter problem in piecewise homogeneous and in nonhomogeneous materials. Because of symmetry, generally these are all mode I problems. Thus, if we define the unknown function and crack surface traction by

$$g(x) = \frac{\partial}{\partial x}(v(x,+0) - v(x,-0)), \qquad p(x) = \sigma_{yy}(x,0), \qquad a < x < b, \tag{19}$$

the integral equation for the general problem may be expressed as

$$\frac{1}{\pi}\int_a^b \left[\frac{1}{t-x} + k_s(x,t) + k_f(x,t)\right] g(t)dt = \frac{1+\kappa_2}{2\mu_2}p(x), \qquad a < x < b, \tag{20}$$

where, again k_s is associated with two bonded semi-infinite media and k_f represents the geometry of the composite medium and is always bounded. For an embedded crack, $a > 0$ and k_s is also bounded. However, for $a = 0$, k_s could be singular. In fact, for $a = 0$ in piecewise homogenous materials (Fig. 1c) it is known that

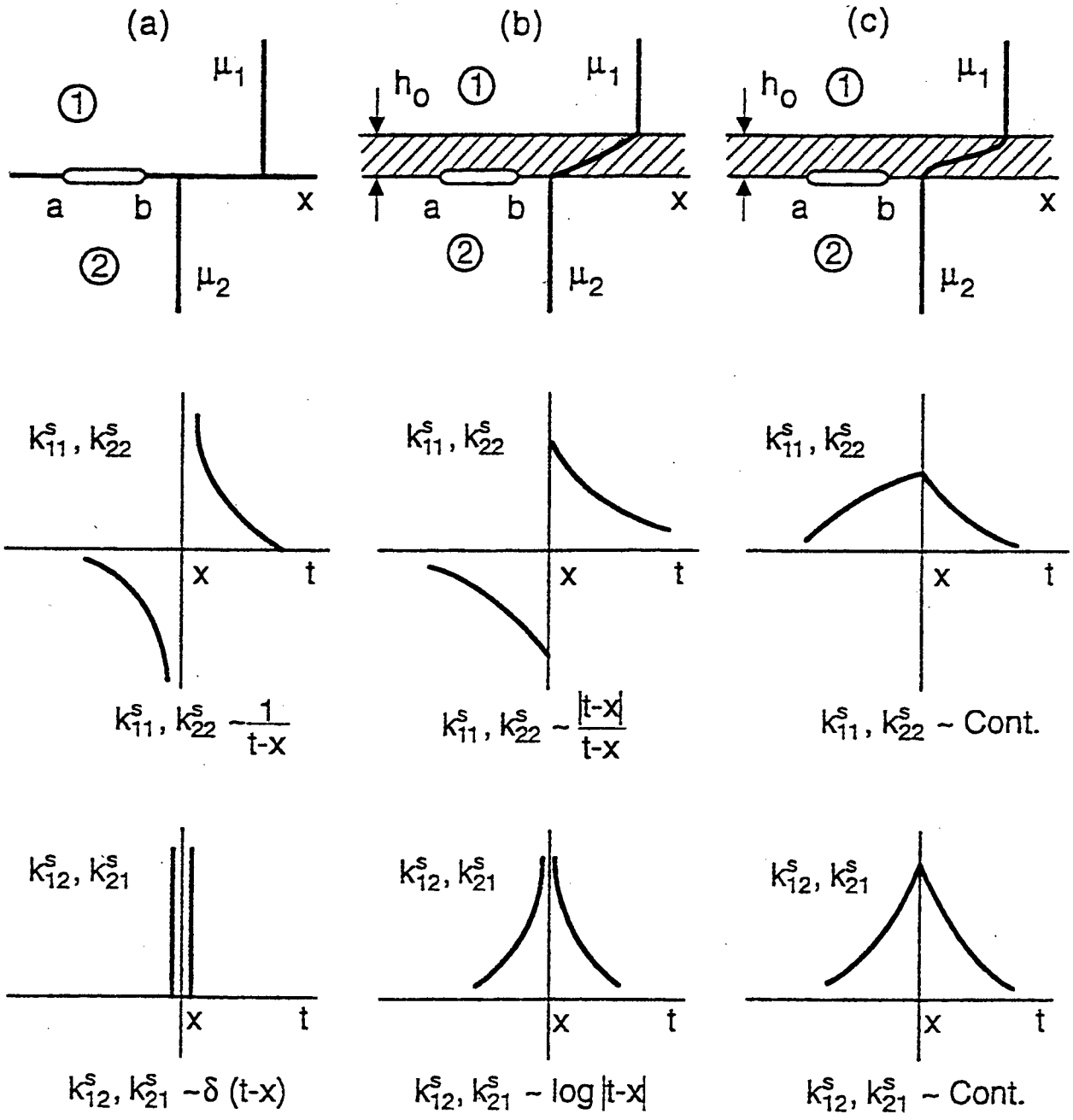

Figure 2: Singular behavior of the irregular kernels for an interface crack in bonded dissimilar materials.

$$k_s(x,t) = \frac{c_1}{t+x} + \frac{c_2 x}{(t+x)^2} + \frac{c_3 x^2}{(t+x)^3}, \qquad 0 < (t,x) < b, \tag{21}$$

where c_1, c_2 and c_3 are bimaterial constants [33]. Note that as t and x approach the end point $x = 0$, k_s tends to infinity and, hence, would contribute to the singular behavior of the solution giving

$$\sigma_{ij}(r,\theta) = \frac{k_1}{r^\alpha} g_{ij}(\theta), \qquad 0 < \theta < \pi, \ (i,j = x,y), \qquad 0 < \alpha < 1, \tag{22}$$

where g_{ij} are known functions, k_1 is a "stress intensity factor" and the power of stress singularity $\alpha > 1/2$ for $\mu_2 > \mu_1$ and $\alpha < 1/2$ for $\mu_2 < \mu_1$, $\alpha = 1/2$ being the value for $\mu_2 = \mu_1$. From the viewpoint of fracture mechanics, the consequence of having $\alpha \neq 1/2$ is that as the crack intersects the interface, the stress and deformation states would not remain self-similar and, hence, it would not be possible to use the fracture theories based on the energy balance concept to calculate a strain energy release rate or to use the stress intensity factors as the crack driving force. This, then, is the second anomalous behavior regarding the stress state near the crack tip in bonded dissimilar homogeneous materials.

If we now "smooth" the material property distribution and assume that medium 1 is a graded material (Fig. 1d), it can be shown that for $a = 0$ the leading terms of k_s become [34]

$$k_s(x,t) \cong \frac{d_1 t}{t+x} + \frac{d_2 x}{t+x} + \frac{d_3 t x}{(t+x)^2} + d_4 \log(t+x), \tag{23}$$

where, $d_1, \ldots, d_4$ are bimaterial constants. Note that the kernel given by (23) is square integrable and, therefore, would have no contribution to the stress singularity at $x = 0$. Consequently, the stresses would have the standard square-root singularity and, by smoothing the material property distribution through the introduction of material property grading, the anomalous behavior of the stress state would again be eliminated.

Figure 3 shows the mode I stress intensity factor for $a = 0$ and $p(x) = -\sigma_0$ in Fig. 1d. The normalized stress intensity factors shown in the figure are defined by

$$k(a) = k_1(0)/\sigma_0\sqrt{b/2}, \qquad k(b) = k_1(b)/\sigma_0\sqrt{b/2}, \tag{24}$$

$$k_1(0) = \lim_{x\to 0}\sqrt{-2x}\sigma_{1yy}(x,0), \qquad k_1(b) = \lim_{x\to b}\sqrt{2(x-b)}\sigma_{2yy}(x,0). \tag{25}$$

The shear modulus of FGM in Fig. 1d is assumed to be

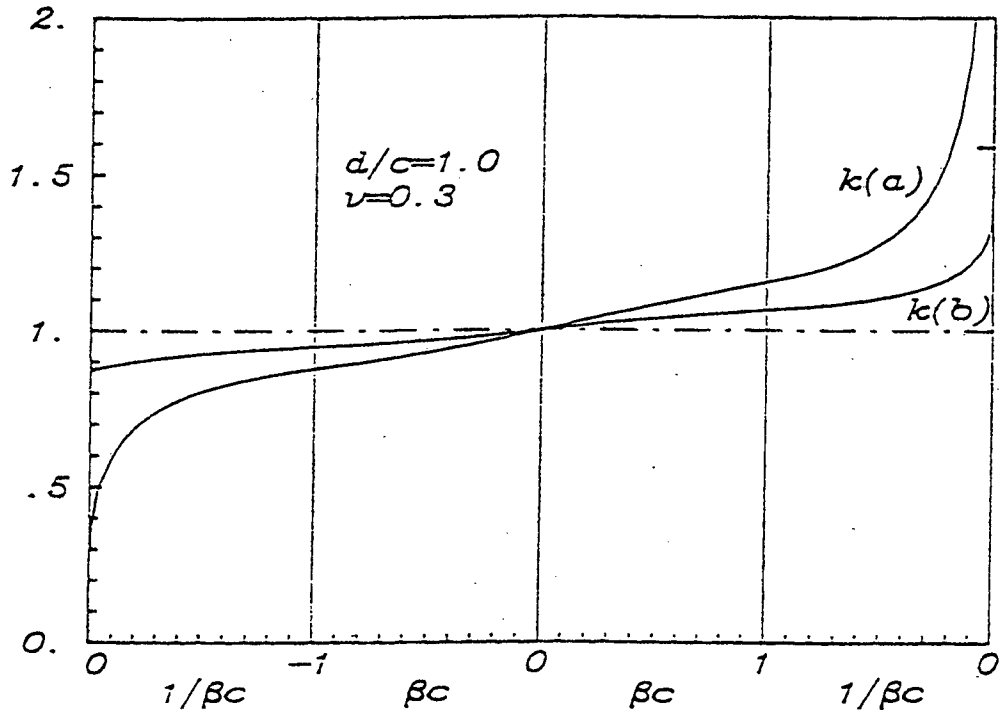

Figure 3: Normalized stress intensity factors for a plane crack terminating at the interface between a homogeneous medium and an FGM half-space.

$$\mu_1(x) = \mu_2 \exp(\beta x), \tag{26}$$

where μ_2 is constant. It is thus seen that for $\beta \to \infty$, $\mu_1 \to 0$ and the problem becomes an ordinary edge crack problem in a homogeneous half space for which

$$k_1(0) \to \infty, \quad k_1(b) \to 1.5861\sigma_0\sqrt{b/2}. \tag{27}$$

For $\beta = 0$ the medium is homogeneous and

$$k_1(0) = k_1(b) = \sigma_0\sqrt{b/2}. \tag{28}$$

In the other limiting case of $\beta = -\infty$, μ_1 becomes infinite and for the resulting problem of a crack terminating at the interface we have

$$k_1(0) \to 0, \quad k_1(b) \to 0.8710\sigma_0\sqrt{b/2}. \tag{29}$$

The analytical details and further results for this problem may be found in [33].

3.4 End Effects

Generally the stress-free ends in bonded materials are locations of high stress concentrations and potential debonding fracture. In bonded dissimilar homogeneous materials the point at which the interface intersects the free boundary (or the apex of two 90-degree bonded wedges) is, in fact, a point of singularity near which the stress state is given by [35]

$$\sigma_{ij}(r,\theta) = \frac{K}{r^\beta} F_{ij}(\theta), \qquad (i,j = x,y), \quad 0 < \beta < 1/2, \tag{30}$$

when (r,θ) are the polar coordinates, β and F_{ij} depend on the bimaterial constants and K is a measure of the load amplitude or stress intensity. For β to be positive the material properties need to be discontinuous across the interface. In FGM coatings, since the material properties are made continuous through composition grading, it can be shown that the singularity β becomes zero and consequently, the stresses become finite.

3.5 Contact Mechanics of Graded Materials: Basic Concepts

The contact mechanics for a graded elastic medium acted upon by a rigid stamp of arbitrary profile is described in the Technical Project Report [15]. In the most general case

of two elastic nonhomogeneous solids in contact in the presence of friction, the integral equation of the problem may be expressed as follows:

$$Ap(x)+\frac{B}{\pi}\int_{-a}^{b}\frac{p(t)}{t-x}dt+\int_{-a}^{b}k(x,t)p(t)dt=f(x),\qquad a<x<b, \tag{31}$$

$$\int_{-a}^{b}p(t)dt=P, \tag{32}$$

$$A=\eta\left(\frac{\kappa^{+}(0)-1}{4\mu^{+}(0)}-\frac{\kappa^{-}(0)-1}{4\mu^{-}(0)}\right),\qquad B=\frac{\kappa^{+}(0)+1}{4\mu^{+}(0)}+\frac{\kappa^{-}(0)+1}{4\mu^{-}(0)}, \tag{33}$$

where P is the resultant compressive force, $p(x)=-\sigma_{yy}(x,0)$, and $q(x)=\eta p(x)=-\sigma_{xy}(x,0)$ are the contact stresses, η is the coefficient of friction, $\mu^{+}(y)$, $\kappa^{+}(y)$, $\mu^{-}(y)$, $\kappa^{-}(y)$ are elastic parameters of the contacting solids and $-a<x<b$, $y=0$ is the contact area, Fig. 4. It is assumed that the curvatures of the contacting solids near the contact zone are smooth $a+b=l<<R_i$ where R_1 and R_2 are the radii of curvature, and both curvatures may be positive or one may be negative. Defining, now the sectionally holomorphic function

$$F(z)=\frac{1}{\pi}\int_{-a}^{b}\frac{p(t)}{t-z}dt, \tag{34}$$

and by using the Plemelj formulas

$$F^{+}(x)-F^{-}(x)=\begin{cases}2ip(x), & -a<x<b\\ 0, & -\infty<x<-a,\ b<x<\infty\end{cases} \tag{35}$$

$$F^{+}(x)-F^{-}(x)=\begin{cases}\dfrac{2}{\pi}\displaystyle\int_{-a}^{b}\frac{p(t)}{t-x}dt, & -a<x<b\\ 4iF(x), & -\infty<x<-a,\ b<x<\infty\end{cases} \tag{36}$$

the fundamental solution and the fundamental function of (31) may be obtained as follows

$$X(z)=(z-b)^{\alpha}(z+a)^{\beta}, \tag{37}$$

$$w(x)=(b-x)^{\alpha}(x+a)^{\beta}, \tag{38}$$

$$\alpha=\frac{1}{2\pi i}\log\left(\frac{A-iB}{A+iB}\right)+N,\qquad -1<\Re(\alpha)<1, \tag{39}$$

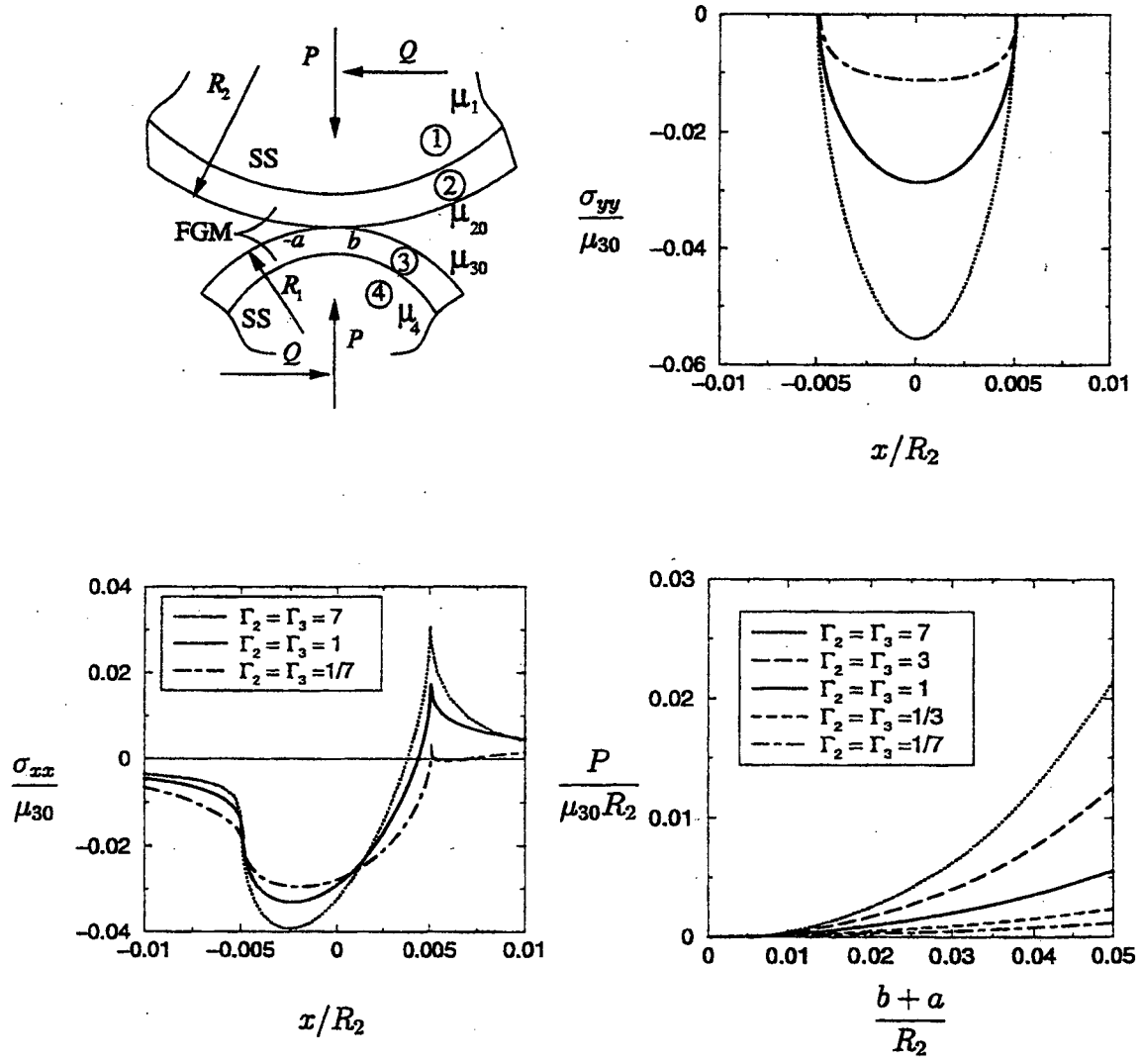

Figure 4: Stress distribution on the surface of an FGM coating for various values of the stiffness ratio $\Gamma_2 = \mu_1/\mu_{20} = , \Gamma_3 = \mu_4/\mu_{30}$, $\mu_{30}/\mu_{20} = 0.5$, $R_2/R_1 = 5.0$, $(b + a)/R_2 = 0.01$, $R_2/h_3 = 100$, $h_2/h_3 = 1$, $\eta = 0.3$.

$$\beta = -\frac{1}{2\pi i}\log\left(\frac{A-iB}{A+iB}\right) + M, \qquad -1 < \Re(\beta) < 1, \tag{40}$$

In (39) and (40) N and M are arbitrary positive and negative integers or zero. The index of the problem is defined by

$$\kappa_0 = -(\alpha+\beta) = -(N+M). \tag{41}$$

In the problem under consideration the index is $+1$, 0 or -1 and is determined from physical considerations. From (39) and (40) it may be seen that

$$\alpha = -\frac{\theta}{\pi} + N, \quad \beta = \frac{\theta}{\pi} + M, \qquad \theta = \arctan(B/A). \tag{42}$$

After determining the fundamental function $w(x)$, the solution (36) may be expressed as

$$p(x) = g(x)w(x), \qquad -a < x < b, \tag{43}$$

where $g(x)$ is an unknown bounded function and is dependent on the geometry and material properties of the contacting media. The arbitrary constants N and M are determined in such a way that, for example, at the end point $x = b$, $\Re(\alpha) > 0$ if the contact is smooth and $\Re(\alpha) < 0$ of one of the contacting solids has a sharp corner (implying stress singularity).

It is important to observe that in contact problems involving graded materials the fundamental function w or singularities α and β are independent of the material nonhomogeneity parameter and are dependent on the coefficient of friction η and the surface values of the elastic constants μ^+, κ^+, μ^- and κ^- of the contacting surfaces.

Figure 4 shows an example for the surface stress distributions and the resultant force P vs the contact length in two contacting elastic cylinders coated by graded layers. In this example $\eta = 0.3$ and σ_{yy} and σ_{xx} are stresses on the surface $y = 0$ of the cylinder 1. The stiffness distributions are exponential, namely $\mu_2(y) = \mu_{20}\exp(\gamma_2 y)$, $\mu_3(y) = \mu_{30}\exp(\gamma_3 y)$, $\mu_1 = \mu_2(h_2)$, $\mu_4 = \mu_3(-h_3)$.

4. Fracture Mechanics of Graded Materials / Benchmark Solutions

In this section a summary of benchmark problems relating to the fracture mechanics of graded materials studied under the current research grant is presented. Nearly all results

are obtained analytically. The only exception is the investigation of various crack geometries in a thermal barrier coating system that consists a homogeneous substrate, a homogenous bond coat, a thermally grown oxide and a graded (metal/ceramic) top coat. (see Section 4.3 for a brief discussion and the Technical Project Report [36] for details). Similarly, nearly all results obtained in this project are described in detail in Appendices A, B, C, articles [13] and [21] and Technical Project Reports [10], [11], [12], [15], [16], [17] and [36]. Again, the exception is the analytical investigation of the homogeneous substrate, homogeneous bond coat and FGM top coat TBC system containing an interface crack and subjected to arbitrary symmetric loading. This study is currently in progress [37].

4.1 The Effect of Material Orthotropy in Graded Materials

Generally, in FGM coatings the subcritical crack propagation and spallation related failures involve two types of cracks, namely a surface crack growing perpendicular to the boundary and a debond crack parallel to the interface. This is partly due to the fact that, because of the techniques used in processing, the graded medium is seldom isotropic and the crack planes mentioned usually correspond to the principal planes of material orthotropy and, consequently, to relatively weak fracture planes. For example, the materials processed by using plasma spray technique have generally a lamellar structure. Flattened splats and relatively weak splat boundaries provide an oriented material that has a higher stiffness and weaker cleavage planes parallel to the surface. On the other hand, graded materials processed by using an electron beam vapor deposition technique would invariably have a columnar structure, resulting in a higher stiffness in thickness direction and weaker fracture planes perpendicular to the boundary. Clearly, in studying the fracture mechanics of these materials assuming the medium to be isotropic would be rather unrealistic. A closer approximation would be to assume that the nonhomogeneous medium is orthotropic with the principal directions parallel and perpendicular to the boundary.

In FGM coatings since the material property grading is usually in the thickness direction and dominant components of the residual and thermal stresses are generally parallel to the boundary, in the first crack problem of interest, namely in the surface crack problem the plane of the crack is a plane of symmetry in material properties as well as in loading. Consequently, the resulting problem is a mode I crack problem for an orthotropic nonhomogeneous medium. Such a problem is considered in [28] which is solved for fixed

grip loading away from the crack region and for polynomial crack surface tractions in order to accommodate more general loading conditions. It is assumed that x_1 and x_2 are the principal axes of orthotropy, the crack is located along $x_2 = 0$, $|x_1| < a$ and material properties vary in x_1 direction only. In the crack problems for orthotropic nonhomogeneous materials analytically the problem is intractable if all material parameters are assumed to be variable. However, by replacing the four engineering parameters E_{11}, E_{22}, G_{12} and ν_{12} by a stiffness parameter $E = \sqrt{E_{11}E_{22}}$, a stiffness ratio $\delta = (E_{11}/E_{22})^{1/4}$, a Poisson's ratio $\nu = \sqrt{\nu_{12}\nu_{21}}$ and a shear parameter $\kappa_0 = (E/2G_{12}) - \nu$, assuming that ν is constant and the moduli E_{11}, E_{22}, G_{12} vary proportionately, and by using δ as a scaling constant for the coordinates, stresses and displacements, it is shown that the problem becomes tractable and one can study the influence of the material orthotropy on the stress intensity factors and the crack opening displacement. The solution of mode I problem is given in [28]. Some of the main conclusions drawn from this study is that the results depend on the nonhomogeneity parameter α and the elastic constants ν and κ_0 but not on E_0 and δ, where $E(x_1) = E_0\exp(\alpha x_1)$, and the stress component $\sigma_{22}(x_1, 0)$ and the mode I stress intensity factors at the crack tips $x = \mp a$ are invariant with respect to a 90^0 material rotation (see [28] for details). It is further shown that the results are relatively insensitive to the change in ν.

The mixed mode crack problem that provides a benchmark for debonding problems is considered in [13]. In this problem again the crack is located along $x_2 = 0$, $|x_1| < a$ and the same assumptions as in the mode I crack problem are made with regard to the material parameters and scaling. However, here it is assumed that the material properties vary in a direction perpendicular to the plane of the crack. Hence, the plane of the crack is no longer a plane of symmetry and consequently, the problem is one of mixed mode. The solution is obtained for polynomial crack surface tractions $\sigma_{22}(x_1, 0) = \sigma_0(x_1)$ and $\sigma_{12}(x_1, 0) = \tau_0(x_1)$, $|x| < a$. The main calculated results are the modes I and II stress intensity factors, the strain energy release rate and the crack opening displacement. Other than the load amplitude, the primary variables are the material nonhomogeneity parameter α, the shear parameter κ_0 and the stiffness ratio δ. Again, the results are shown to be relatively insensitive to the variation in Poisson's ratio ν. It is found that generally the stress intensity factors increase with increasing α and κ_0 and with decreasing δ. The main results are described in [13]. The general formulation and extensive results for the problem of collinear cracks in a graded medium are given in the Technical Report [12].

4.2 Spallation of Graded Materials: A Penny-Shaped Crack

The basic benchmark problem considered in Appendix A consists of a penny-shaped crack parallel to the surface of a semi-infinite graded medium. The problem is an axisymmetric mixed mode problem in which crack surfaces may be subjected to shear as well as normal tractions. The main objective of the study is to determine the influence of material nonhomogeneity constants and the dimensionless length parameter h/a on the stress intensity factors, where h is the distance of the crack from the surface and a is the radius of the crack. The problem is solved analytically by reducing it to a system of singular integral equations. The results are obtained for polynomial normal and shear tractions acting on the crack surfaces. As expected, generally the stress intensity factors increase with decreasing h/a and increasing material nonhomogeneity. In addition to results regarding the stress intensity factors, Appendix A also includes the corresponding crack opening displacements (for extensive details see [38]).

4.3 Interface Cracking of Graded Coatings

Various fracture problems in a basic TBC system that consists of a homogeneous substrate (SS), a homogeneous bond coat (BC), a thermally grown oxide (TGO) and a homogeneous or graded top coat (TC) are considered in [36]. Assuming that heating and cooling take place sufficiently slowly so that the time-dependent transient effects may be neglected and there are no mechanical loads, the problem is solved under a uniform temperature change (ΔT of the order 1000 ^{0}C). The basic crack geometries considered are axisymmetric and plane strain edge cracks at various locations parallel to the interfaces, plane strain surface crack propagating in and terminating at or crossing the interfaces between various layers, *T*-shaped crack branching from a surface crack and growing parallel to the interfaces at various critical locations and periodic cracks at the peaks of interface asperities between TGO and BC. Due to complexity of the problem, a finite element technique is used in its solution. An enriched crack tip element is used to simulate the asymptotic behavior of the stress and displacement fields at and near the crack tips and to evaluate the stress intensity factors. The detailed results may be found in the Technical Report [36].

An analytical benchmark solution for the interface crack problem is also being developed, in part, to verify the purely numerical results [37]. Here the TGO is neglected and it is assumed that the composite medium consisting of a substrate, a bond coat and a

graded top coat is under plane strain conditions, contains an interface crack between the TC and BC, and is subjected to arbitrary general loading conditions. The main results of this study will be the stress intensity factors, strain energy release rate and crack opening displacements.

4.4 Buckling of Graded Coatings - A Continuum Model

In structural components such as thermal barrier and other protective coatings spallation is a serious mode of failure. At high temperatures the medium is generally stress-free. Upon cooling, because of the mismatch in thermal expansion coefficients, the coating would be subjected to severe compressive stresses. In the final stages of the failure process, a highly weakened or fully cracked interface could then pose a buckling instability problem. Considered as a problem in linear elasticity, it is shown that for flat components the result would be trivial and in the presence curvature (as in, for example, turbine blades) highly misleading. The objective of this part of the project is to study the influence of geometric nonlinearity and curvature on the crack opening δ and the strain energy release rate G. The example considered is shown in Fig. 5a where (simulating a turbine blade at various locations) it is assumed that a ceramic-rich FGM coating of thickness $h_c = 130\,\mu$m is bonded to a 3 mm thick superalloy substrate and the interface contains a 5.2 mm long crack. The loading is the temperature drop ΔT. Figs. 5b and 5c show, respectively, the crack opening δ at the midpoint $x = 0$ and the strain energy release rate G at the crack tips $x = \pm a$ for various values of radius of curvature R. Note that for flat specimen ($R = \infty$) the linear theory gives $\delta = 0$, $G = 0$ and the nonlinear model predicts a distinct instability load ($\Delta T_{cr} \cong 450\,^0$C). Also note that as R decreases the difference between the linear and nonlinear results becomes insignificant. The details of the analysis and extensive results are given in AFOSR Technical Project Report [11].

4.5 Surface Cracking in a Graded Medium under General Loading Conditions

In this part of the project the problem of a plane strain surface crack in an elastic graded medium under general loading conditions is considered. It is assumed that first by solving the original thermomechanical problem for the graded material in the absence of a crack, it is reduced to a local perturbation problem with arbitrary self-equilibrating crack surface tractions. It is further assumed that the length of the surface crack is relatively small in comparison with the in-plane dimensions of the medium and, consequently, the

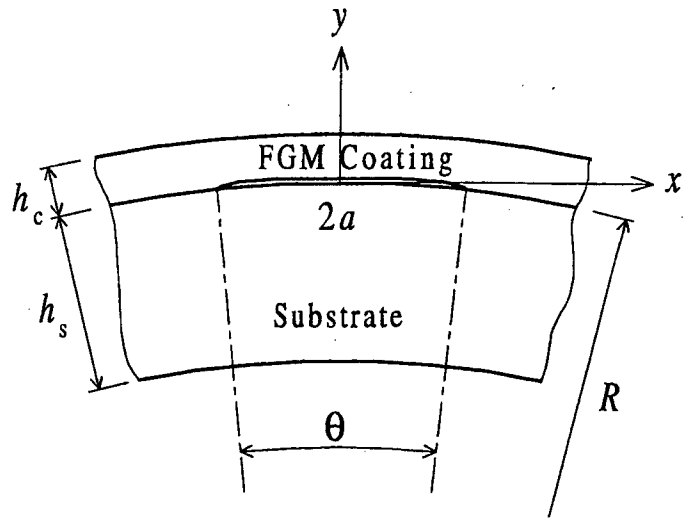

(a)

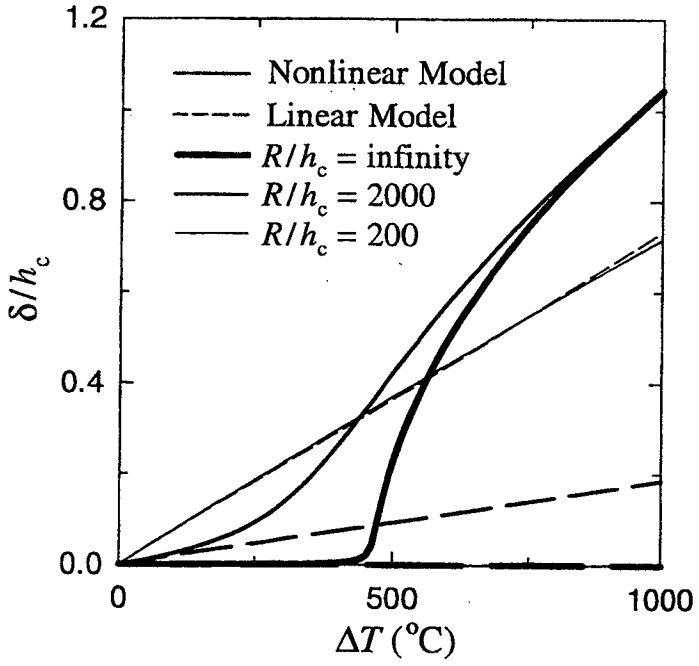

(b)

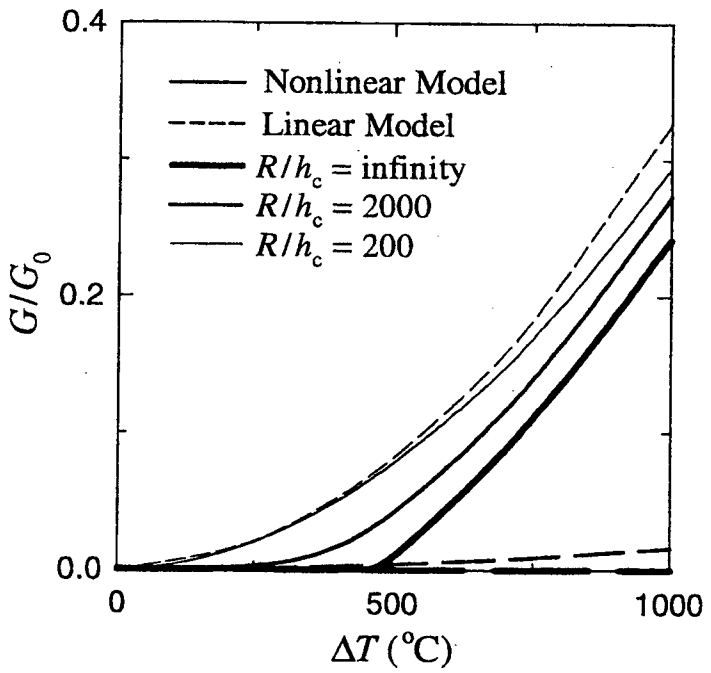

(c)

Figure 5: The effect of geometric nonlinearity and curvature on the spallation behavior of *functionally graded* (FGM) *coatings*. ΔT (°C): the temperature drop, δ: the crack opening, G: strain energy release rate, substrate: superalloy, coating: ceramic rich zirconia/superalloy FGM.

local problem may be approximated by that of a surface crack in a semi-infinite graded medium under known crack surface tractions. The local problem is then solved by approximating the known normal and shear tractions on the crack surfaces by polynomials. The main calculated results of the study are the modes I and II stress intensity factors and the crack opening displacements. As an application the results for a graded medium loaded by a sliding circular stamp with constant coefficient of friction is presented. The complete solution of the problem and extensive results are given in Appendix B.

4.6 Cracking of a Graded Layer Bonded to a Homogeneous Substrate

This is the basic FGM coating problem in which various collinear internal and surface cracks in a homogeneous elastic substrate coated by a graded layer under arbitrary mechanical and thermal loadings are investigated. The thermo-mechanical properties of the FGM coating are assumed to vary exponentially with the thickness coordinate. The equilibrium equations are solved using integral transforms. The resulting singular integral equations are solved using numerical integration. The results of interest for this mode I formulation are the stress intensity factors and the crack opening displacements. The effects of the nonhomogeneity parameter and various dimensionless length parameters are studied.

One of the most important outcomes of this study is the theoretical proof that a "kink" in material property at the interface does not introduce any singularity. In the numerical results it is observed that generally the stress intensity factors tend to increase with material nonhomogeneity. Also, it is observed that the substrate thickness tends to suppress cracking in the coating. In pure thermal loading, the surface cracks may either be arrested or there might be crack closure. The stress intensity factors from different loadings can be added up to obtain the resultant stress intensity factor for multiple loading.

Some interesting and important results are obtained from thermal loading of the surface crack problem in which near and at the free surface crack closure may occur and the problem becomes nonlinear. In the examples considered a simple iteration scheme is used to solve the problem.

Results in this study have wide-ranging applications. They can be applied to thermal barrier coatings on turbine components, combustion chambers, parts of the airframe for the "Space Plane", soil mechanics, bone fractures and many more applications where the

material is macroscopically nonhomogeneous. Thus this study solves a basic problem common to a variety of applications in diverse fields.

The analytical details, numerous examples and extensive results are given in AFOSR Technical Project Report [10].

5. Contact Mechanics of Graded Materials / Benchmark Solutions

5.1 Basic Contact Mechanics Problems in FGM Coatings

One of the potentially important applications of graded materials involves protective coatings against mechanically applied loads. In these load transfer applications, because of the possibility of fretting fatigue, the friction plays a particularly important role. Grading the surface coating adds another dimension to the design of load transfer components in order to optimize their performance. Keeping in mind the likely applications of FGM coatings in load transfer components in the immediate future, the related problems in contact mechanics may be studied under two broad categories: (a) a rigid stamp with an arbitrary profile acting on a homogeneous elastic substrate with FGM coating and (b) two FGM-coated elastic media with arbitrary but smooth profiles that are in contact. As a practical example for the first group of contact problems one may mention the abradable seal design in stationary gas turbines. In this case the shroud is coated by a low density metal/ceramic FGM and in order to prevent gas leakage (and consequently to increase the efficiency) the blades are allowed to touch the coating. The repeated loading may directly result in fretting fatigue. Cylinder linings and brake disks may be mentioned as other applications of the concept. A typical example for that group of problems is shown in Fig. 6 where the distribution of contact pressure $\sigma_{yy}(x,0)$ and the in-plane component of the surface stress $\sigma_{xx}(x,0)$, and the dependence of the resultant force P on the contact area are given for various values of the stiffness ratio $\Gamma_3 = \mu_4/\mu_{30}$, μ_4 and μ_{30} being the shear moduli of the substrate and coating on the surface respectively.

The main practical applications of the second group of contact problems are gears, bearings, cams and possibly large earth moving and other construction equipment. In this case specially designed FGM coatings may be used to reduce wear and to increase the fatigue life. The general contact problem is formulated and extensive results are obtained for various geometries and material nonhomogeneity parameters of the contacting solids. In order to address a possible microcrack inititation on the surfaces of the contacting FGM coatings, the stress state σ_{xx} on the surfaces within and outside the contact regions

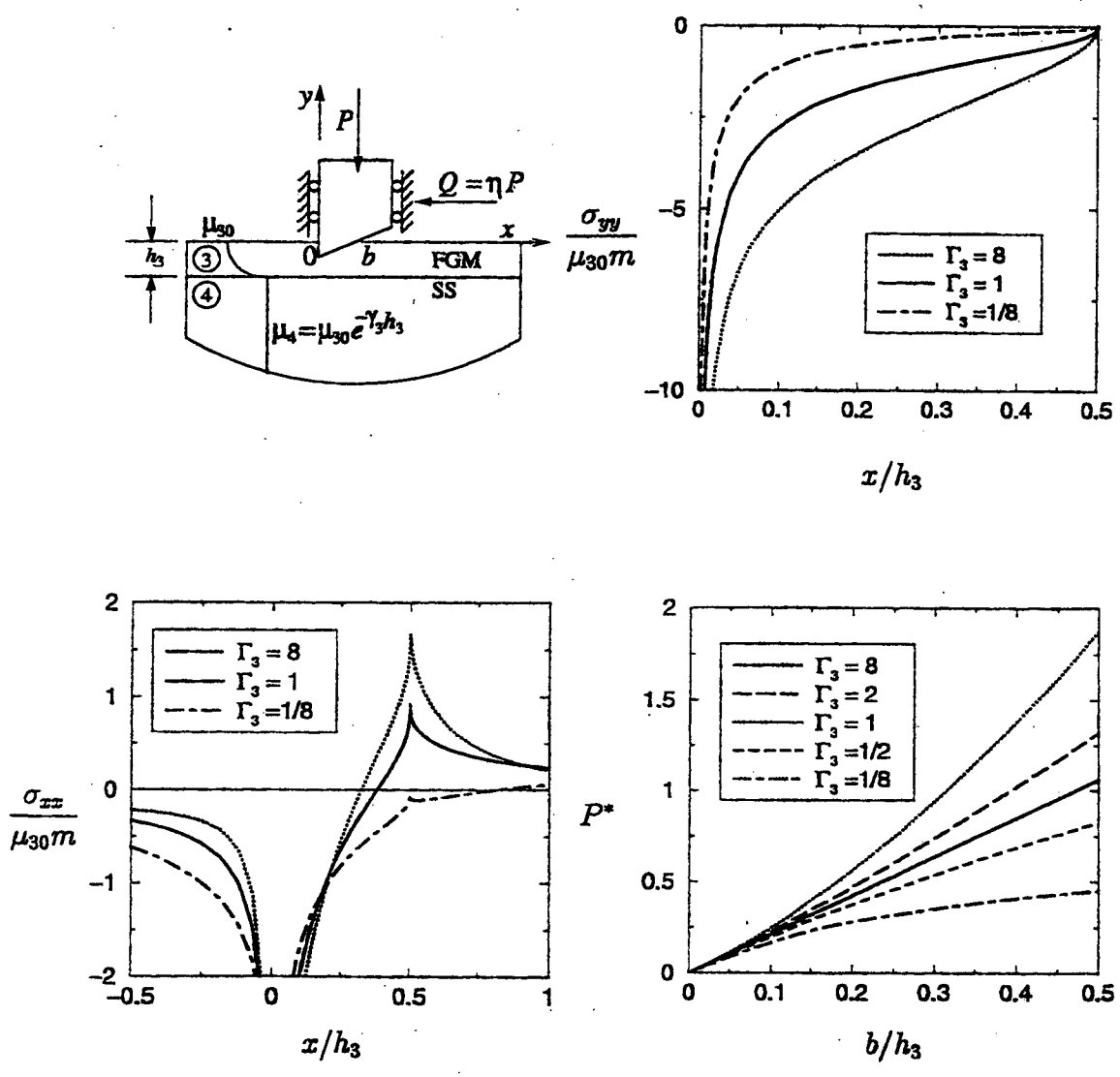

Figure 6: Stress distribution on the surface of an FGM coating loaded by a rigid triangular stamp for various values of the stiffness ratio, $\Gamma_3 = \mu_4/\mu_{30}$, $b/\mu_{30} = 0.5$, $\eta = 0.3$, $P^* = P/(\mu_{30} m h_3)$.

are also calculated. A typical example for the contacting elastic solids coated by graded layers is shown in Fig. 4 again for various values of the stiffness ratios Γ_2 and Γ_3.

The general formulation of the problem, the details of the analysis and extensive results for various typical stamp profiles, namely the flat, circular, semi-circular and triangular stamps, and contacting elastic materials with positive/positive and positive/negative curvatures are given in the AFOSR Technical Project Report [15].

5.2 Surface Cracking of Homogeneous Materials due to Sliding Contact

The problem under consideration (for an arbitrary stamp profile) is described in Figure 7. With the application to fretting fatigue in mind, the main objective of this study is to investigate the problem of contact mechanics in elastic solids. The physical problem is the initiation and propagation of surface cracks under repeated loading. Examination of crack initiation requires the determination of σ_{xx} in addition to contact stresses σ_{yy} and σ_{xy} on the surface (Fig. 7). Crack propagation requires the evaluation of stress intensity factors k_1 and k_2 at the crack tip (Fig. 7). It is assumed that the contacting solids are in relative motion and contact stresses are related through $\sigma_{xy}(x,0) = \eta\sigma_{yy}(x,0)$. First the contact problem for an elastic solid loaded by a moving rigid stamp of arbitrary profile is considered. The contact stresses σ_{yy} and σ_{xy} and the in-plane stress σ_{xx} on the surface are calculated by varying the coefficient of friction η.

The coupled crack/contact problem for a half plane with a surface crack and loaded by a moving rigid stamp of an arbitrary profile is then formulated, leading to a system of three-by-three singular integral equations of the second kind. The singular behavior of the solution and fundamental functions of the problem are obtained by using the function-theoretic method. Figs. 8 and 9 show some sample results giving the modes I and II stress intensity factors at the crack tip $y = -d$ in a homogeneous half plane with a surface crack. The details of the solution and extensive results are given in AFOSR Technical Project Report [16].

5.3 Surface Cracking of Graded Materials due to Sliding Contact

This is the same problem as that considered in Section 5.2 of this report, except that here the material properties are graded in $y-$ direction (Fig. 7). The main problem studied is the initiation and growth of surface cracks in graded materials due to sliding contact. The problem is summarized in a manuscript which is appended to this report (Appendix

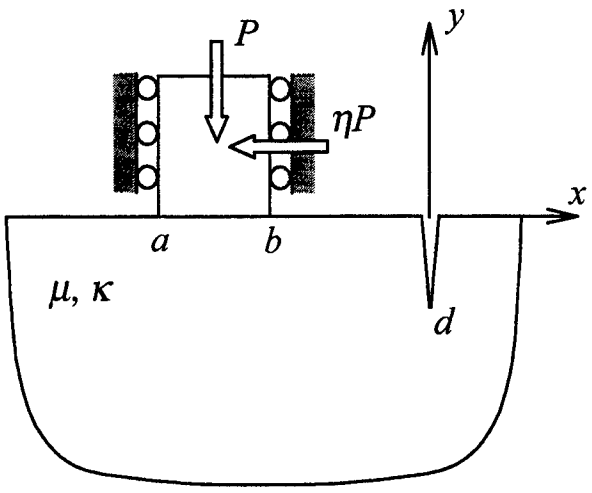

Figure 7: Geometry of the problem

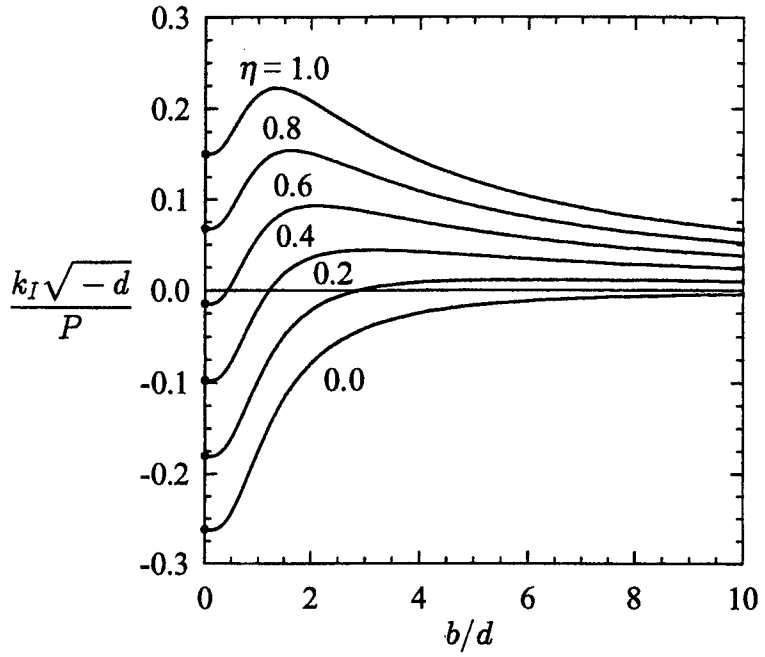

Figure 8: Mode I stress intensity factors for an edge crack in a homogeneous half-plane indented by a flat punch as shown in Figure 7. $(a-b)/d = 0.1, \nu = 0.25$.

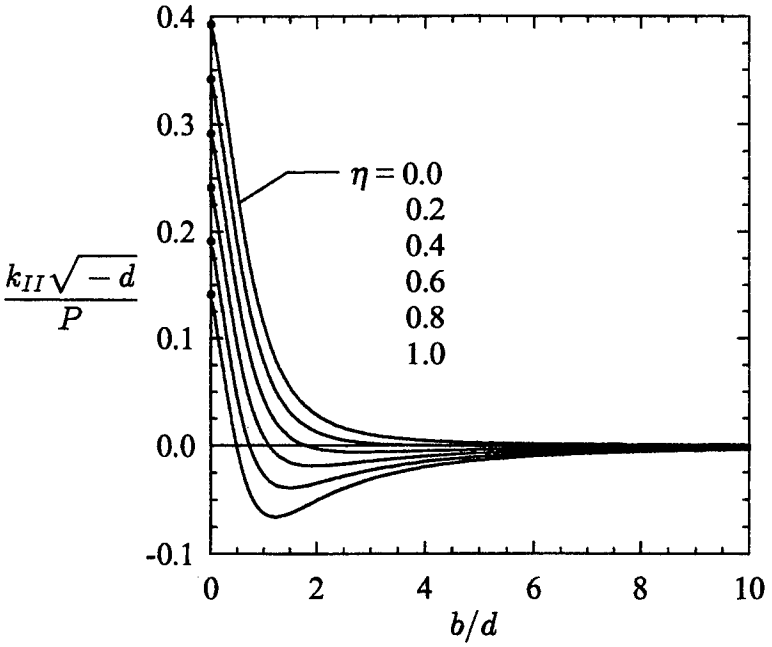

Figure 9: Mode II stress intensity factors for an edge crack in a homogeneous half-plane indented by a flat punch as shown in Figure 7. $(a-b)/d = 0.1, \nu = 0.25$.

C). The detailed analysis and extensive results are presented in the AFOSR Technical Project Report [17]. The main results of this study consist of the contact stresses, the in-plane component of the stress on the surface and modes I and II stress intensity factors at the crack tip. The elastic properties of the medium are assumed to vary exponentially in the direction perpendicular to the surface.

The solution of the problem leads to two somewhat nonintuitive conclusions. The first is that the contact problem for a graded medium with an exponentially decaying stiffness (i.e., for $\gamma < 0$ in $\mu(x) = \mu_0 \exp(\gamma x)$, Fig. 4, Appendix C where μ is the shear modulus) is not a well-posed mechanics problem. Secondly, for a flat stamp (Fig. 4, Appendix C) if $a = 0$, the point $y = 0$, $x = 0$ is a singular point with a power $|\alpha|$ which is dependent on the friction coefficient η and Poisson's ratio ν, and for sufficiently large values of η, $|\alpha|$ can be greater than the standard $1/2$ and the end point flat stamp singularities ω and β (Fig. 2, Appendix C).

Other conclusions which may be drawn from this solution is that (i) The trailing end of the sliding rigid stamp with friction is a likely location of surface crack initiation, due to greater tensile stress concentration (see the Appendix C and Report [17]), (ii) In the medium containing a surface crack and loaded by a sliding rigid stamp, the mixed mode stress state at the crack tip is such that the cracks tend to be periodic and curved backward and (iii) In the coupled crack/contact problems for a graded medium the singularities α, β and ω are independent of the material nonhomogeneity constants γ and $\mu_0 = \mu(0)$ and depend on the friction coefficient η and the surface value of the Poisson's ratio only.

6. Elastodynamics of Graded Materials

A benchmark problem concerning the elastodynamics in graded materials was considered in [21]. The problem is a one-dimensional elastodynamic problem for an FGM plate having free-free or fixed-free boundary conditions. The former may approximate the impact problem in an unconstrained layer and the latter may simulate an FGM layer bonded to a very stiff substrate. The impact loading is approximated by a rectangular compressive pulse of a very short duration (0.2 μsec). Numerical results are obtained for a 5 mm thick Nickel-Zirconoa FGM layer, two hypothetical FGMs with $E_1/E_2 = 1/2$, $\rho_1/\rho_2 = 1/3$ and $E_1/E_2 = 2$, $\rho_1/\rho_2 = 3$ and, for comparison, a homogeneous Ni plate, where E and ρ are the Young's modulus and mass density, respectively.

For the general variations in density $\rho(x)$ and stiffness $E(x)$, $(E' = E(1-\nu)/(1+\nu)(1-2\nu))$, the closed form solution is not possible. However, one can obtain an asymptotic solution which appears to be highly accurate.

The problem is first solved by assuming $E'(x) = E_0\exp(\alpha x)$, $\rho(x) = \rho_0\exp(\alpha x)$ giving a constant propagation velocity $c = \sqrt{E_0/\rho_0}$. In this case the solution can be obtained in closed form as well as asymptotically. The comparison of the two results shows that the error in a simple one term asymptotic approximation is less then 2% and a six digit accuracy is obtained by retaining the first six terms in the expansion. Next, a more general material property distribution is considered by assuming $E'(x) = E_0(ax+1)^m$ and $\rho(x) = \rho_0(ax+1)^n$ where $E_0 = E'(0)$, $\rho_0 = \rho(0)$ and a, m and n are arbitrary constants. It was shown that an estimate of maximum (spallation) stress may be obtained without solving the detailed wave propagation problem. This estimate is $\left[\sigma_{xx}(x)\right]_{\max} = \sigma_0\varphi_0(x)$ for the free/free case and $\left[\sigma_{xx}(x)\right]_{\max} = 2\sigma_0\varphi_0(x)$ for the fixed/free case, where σ_0 is the amplitude of the input pulse and $\varphi_0(x) = \left[(ax+1)/al+1\right]^{(m+n)/4}$, l being the thickness of the layer $(0 < x < l)$.

In the general problem for which no closed form solution is feasible, it is shown that one may use the total energy balance as the criterion for the accuracy of the results (or for the convergence of extended asymptotic solutions). In the nondissipative system under consideration the conservation of energy requires that at any given time the total work done by the external loads be equal to the sum of kinetic and strain energies. The calculated results show that the error in this comparison is less than three percent which is within the acceptable range.

7. Some Concluding Remarks

From the viewpoint of failure mechanics the *functionally graded materials* seem to offer certain advantages among which one may mention the following

- By eliminating the discontinuity in material property distributions, the mathematical anomalies regarding the crack tip stress oscillations for the interface cracks and the non-square-root singularities for the cracks intersecting the interfaces are also eliminated. In practice the importance of this result lies in the fact that in FGMs one can now use the crack tip finite element modeling developed for the ordinary square-root singularity and apply the methods of energy balance-based theories of the conventional fracture mechanics.

- Use of FGMs as coatings and interfacial zones would reduce the magnitude of residual and thermal stresses.
- Use of FGM coatings and interfaces would eliminate the stress singularities at the points of intersection of interfaces and stress-free ends in bonded materials.
- Replacing homogeneous coatings by FGM layers would enhance the bonding strength, reduce the crack driving force, enhance the surface properties and provide the medium with an $R-$curve behavior (thereby increasing the toughness).
- Most likely areas of applications of the concept of material property grading in the near future are high temperature components, load transfer components, components with improved impact resistance and improved bonding strength.
- Some of the engineering systems that would benefit from the application of the concept of material property grading are: Air systems (gas turbines and other hot section components), Space systems (thermoelectric cells, improved bonding and spallation resistance), Standard machinery (improved performance of bearings, gears, cams, machine tools and other load-bearing components) and Military (impact resistant components).

8. References

[1] Yamanouchi, M., Koizumi, M., Hirai, T. and Shiota, I. eds., 1990, *FGM-90, Proc. 1st International Symposium on Functionally Gradient Materials*, FGM Forum, Tokyo, Japan.

[2] Holt, J.B., Koizumi, M., Hirai, T. and Munir, Z.A. eds., 1993, *FGM-92, Proc. 2nd International Symposium on Functionally Gradient Materials*, The American Ceramic Society, Westerville, Ohio.

[3] Ilschner, B. and Cherradi, N. eds., 1995, *FGM-94, Proc. 3rd International Symposium on Structural and Functional Gradient Materials*, Presses Polytechniques et Universitaires Romandes, Lausanne, Switzerland.

[4] Shiota, I. and Miyamoto, Y., eds., 1997, *FGM-96, Proc. 4th International Symposium on Functionally Graded Materials,* Elsevier Science, Amsterdam, The Netherlands.

[5] Kaysser, W.A. ed., 1999, *FGM-98, Proc. 5th International Symposium on Functionally Graded Materials,* Trans Tech Publications, Enfield, New Hampshire.

[6] Miyamoto, M., Kaysser, W.A., Rabin, B.H., Kawasaki, A. and Ford, R.G. eds., 1999, *Functionally Graded Materials: Design, Processing and Applications*, Kluwer Academic Publishers, Norwell, Massachusetts.

[7] Sampath, S., Herman, H., Shimoda, N. and Saito, T., 1995, MRS Bulletin, p. 27.

[8] Lee, Y.-D. and Erdogan, F., 1994, "Residual/Thermal Stresses in FGM and Laminated Thermal Barrier Coatings," AFOSR Project Report. (Also published in Int. J. Frac., **69**, pp. 145-165, 1995).

[9] Kurihara, K., Sasaki, K. and Kawarada, M., 1990, *FGM-90*, FGM Forum, Tokyo, Japan, p.65.

[10] Erdogan, F. and Kasmalkar, M., 2000, "The Surface Crack Problem for a Functionally Graded Coating Bonded to a Homogeneous Layer," AFOSR Project Report.

[11] Erdogan, F. and Chiu, T. C., 2000, "Buckling of Graded Coatings - A Continuum Model," AFOSR Project Report.

[12] Erdogan, F. and Ozturk, M., 2001, "The Collinear Crack Problem in a Graded Medium," AFOSR Project Report.

[13] Ozturk, M. and Erdogan, F., 1999, "The Mixed Mode Crack Problem in an Inhomogenous Orthotropic Medium," Int. J. Frac., **98**, pp. 243-261.

[14] Lee, W.Y., Stinton, C.C., Berndt, C.C., Erdogan, F. Lee, Y.-D., and Mutasim, Z., 1996, "Concept of Functionally Graded Materials for Advanced Thermal Barrier Coating Applications," J. Amer. Ceram. Soc., **79**, pp. 3003-3012

[15] Erdogan, F. and Guler, M.A., 2000, "Contact Mechanics of FGM Coatings," AFOSR Project Report.

[16] Erdogan, F. and Dag, S., 2001, "Cracking of a Homogeneous Half Plane Due to Sliding Contact," AFOSR Project Report.

[17] Erdogan, F. and Dag, S., 2001, "Cracking of a Graded Half Plane Due to Sliding Contact," AFOSR Project Report.

[18] Friedlander, F. G., 1946, *Proc. Cambridge Philosophical Society, Mathematical and Physical Science*, **43**, pp. 360-373.

[19] Karal, F.C. and Keller, J.B., 1959, The J. Acoustical Society of America, **31**, pp. 694-705.

[20] Pekeris, C.L., 1946, The J. Acoustical Society of America, **18**, pp. 295-315.

[21] Chiu, T.C. and Erdogan, F., 1999, "One Dimensional Wave Propagation in a Functionally Graded Elastic Medium," J. Sound and Vibration, **222**, pp. 453-487.

[22] Rowe, D.M., ed., 1995, *CRC Handbook of Thermoelectrics*, *Chemical Rubber*, Roca Bacon, Florida.

[23] Hirai, T., 1996, "Functional Gradient Materials", *Materials Science and Technology,* Cahn, R.W., Haasen, P. and Kramer, E.J. eds., VCH Verlagsgesellschaft mbH, Germany.

[24] Erdogan, F., 1998, "Crack Problems in Nonhomogeneous Materials," *Fracture, A Topical Encyclopedia of Current Knowledge,* Cherepanov, G.P., ed., Krieger Publishing Company, Malabar, Florida, pp. 72-98.

[25] Konda, N. and Erdogan F., 1994, Eng. Frac. Mech., **47**, pp. 533-545.

[26] Delale, F. and Erdogan F., 1983, ASME J. Appl. Mech., **50**, pp. 609-614.

[27] Ozturk, M. and Erdogan F., 1993, ASME J. Appl. Mech., **60**, pp. 406-413.

[28] Ozturk, M. and Erdogan F., 1997, Int. J. Engng. Sci., **35**, pp. 869-883.

[29] Erdogan, F. and Wu, B.-H., 1997, ASME J. Appl. Mech., **64**, pp. 449-456.

[30] Erdogan, F. and Wu, B.-H., 1996, "Crack Problems in FGM Layers under Thermal Stresses," J. Thermal Stresses, **19**, pp. 237-265.

[31] Erdogan, F. and Gupta, G.D., 1971, Int. J. Solids Structures, **7**, pp. 39-61.

[32] Erdogan, F. and Gupta, G.D., 1971, Int. J. Solids Structures, **7**, pp. 1089-1107.

[33] Cook, T.S. and Erdogan, F., 1972, Int. J. Engng. Sci., **10**, pp. 667-696.

[34] Erdogan, F., Kaya, A.C. and Joseph, P.F., 1991, ASME J. Appl. Mech., **58**, pp. 400-418.

[35] Erdogan, F. and Biricikoglu, V., 1973, Int. J. Engng. Sci., **11**, pp. 645-766.

[36] Erdogan, F. and Yildirim, B., 2001, "Crack Problems in Graded Coatings," AFOSR Project Report.

[37] Sahin, A., 2001, "Interface Crack Problems in Graded Materials," Ph.D. Dissertation, Lehigh University, Bethlehem, Pennsylvania.

[38] Sahin, A., 1996, "The Axisymmetric Crack Problem in a Semi-Infinite Nonhomogeneous Medium," M.S. Thesis, Lehigh University, Bethlehem, Pennsylvania.

9. Personnel

Principle Investigator: Fazil Erdogan
G. Whitney Synder Professor of Mechanical Engineering and Mechanics

Post-Doctoral Associate: Murat Ozturk

Research Assistants: Tz. C. Chiu, M. A. Guler, B. Yildirim, A. Sahin, S. Dag

10. List of AFOSR Technical Project Reports and Articles

10.1 Technical Reports

[1] F. Erdogan and M. Kasmalkar, "The Surface Crack Problem for a Functionally Graded Coating Bonded to a Homogeneous Layer."
[2] F. Erdogan and M. A. Guler, "Contact Mechanics of FGM Coatings."
[3] F. Erdogan and Tz Cheng Chiu, "Buckling of Graded Coatings - A Continuum Model."
[4] B. Yildirim and F. Erdogan, "Crack Problems in Graded Coatings."
[5] M. Ozturk and F. Erdogan, "The Collinear Crack Problem in a Graded Medium."
[6] F. Erdogan and S. Dag, "Cracking of a Homogeneous Half Plane Due to Sliding Contact."
[7] F. Erdogan and S. Dag, "Cracking of a Graded Half Plane Due to Sliding Contact."

10.2 Journal Articles

[1] Ozturk, M. and Erdogan, F., 1999, "The Mixed Mode Crack Problem in an Inhomogenous Orthotropic Medium," Int. J. Frac., **98**, pp. 243-261.
[2] Chiu, T.C. and Erdogan, F., 1999, "One Dimensional Wave Propagation in a Functionally Graded Elastic Medium," J. Sound and Vibration, **222**, pp. 453-487.
[3] Erdogan, F., 1999, "Fracture Mechanics," Int. J. Solids Structures, **37**, pp. 171-183.
[4] Lee, Y.-D. and Erdogan F., "Interface Cracking of Graded Coatings," Int. J. Frac. (in print).

[5] Ozturk, M. and Erdogan, F., 1999, "Mode I Crack Problem in an Inhomogeneous Orthotropic Medium," Int. J. Engng. Sci., **35**, pp. 869-883.

[6] Lee, Y.-D. and Erdogan, F., 1988, "Interface Cracking of FGM Coatings under Steady-State Heat Flow," Engng. Frac. Mech., **59**, pp. 361-380.

[7] Schulze, G.W. and Erdogan, F., 1998, "Periodic Cracking of Elastic Coatings," Int. J. Solids Structures, **35**, pp. 3615-3634.

[8] Dag, S. and Erdogan, F., "Surface Crack in a Graded Medium under General Loading Conditions," Manuscript submitted for publication to the ASME J. Appl. Mech. (Appendix B).

[9] Dag, S. and Erdogan, F., "Fracture of Graded Materials Due to Sliding Contact," Manuscript submitted for publication to the Engng. Frac. Mech. (Appendix C).

10.3 Proceedings Articles

[1] Chiu, Tz-C. and Erdogan, F., 1999, "On the Spallation of FGM Coatings," *FGM-98, Proc. 5th International Symposium on Functionally Graded Materials,* Kaysser, W.A., ed., Trans Tech Publications, Enfield, New Hampshire, pp. 917-922.

[2] Chiu, Tz-C. and Erdogan, F., 1998, "Spallation of FGM Coatings - A Nonlinear Model," *Proc. 8th Japan - US Conference on Composite Materials,* Newaz, G. M. and Gibson, R.F., eds., Technamic Publishing Company, Lancaster - Basel, pp. 365-373.

[3] Chiu, Tz-C. and Erdogan, F., 1998, "Wave Propagation in a Functionally Graded Elastic Medium," ibid, pp. 374-382.

[4] Yildirim, B. and Erdogan, F., 1998, "Interface Cracking of FGM Coatings," ibid, pp. 388-396.

[5] Guler, M. A. and Erdogan, F., 1998, "Contact Mechanics of FGM Coatings," ibid, pp. 397-406.

[6] Sahin, A. and Erdogan, F., 1998, "The Axisymmetric Crack Problem in a Functionally Graded Semi-Infinite Medium," ibid, pp. 189-198.

[7] Erdogan, F., 1997, "Fracture Mechanics of Interfaces," *Proc. 1st Int. Conf. on Damage and Failure of Interfaces,* Rossmanith, H. P., ed., A.A. Balkema/Rotterdam/Brookfield, pp. 3-36.

APPENDIX A

Axisymmetric Crack Problem in a Functionally Graded Semi-infinite Medium

Ali Sahin and Fazil Erdogan
Department of Mechanical Engineering and Mechanics
Lehigh University, Bethlehem, PA 18015

Abstract

In this study the axisymmetric crack problem in a functionally graded semi-infinite medium is considered. It is assumed that the penny-shaped crack is located parallel to the free surface and the mechanical properties of the medium vary in depth direction only. By using a superposition technique the problem is reduced to a perturbation problem in which crack surface tractions are the only external forces. The corresponding mixed boundary value problem is then reduced to an integral equation with a generalized Cauchy kernel and solved numerically to obtain stress intensity factors and crack opening displacements. Results obtained for different nonhomogeneity and length parameters are presented and discussed. The problem has applications to the investigation of the general question of spallation fracture.

Introduction

In recent years the requirements for high temperature applications of structural materials have become increasingly more stringent. Since very often the conventional materials were not adequate for modern technologies, various forms of composites and bonded materials have been used in such technological applications as power generation, transportation, aerospace and microelectronics. In high temperature applications, metals and metal alloys appear to be very susceptible to oxidation, creep and generally to loss of structural integrity [1]. Similarly, low strength and low toughness have always been the disadvantages of ceramics. Thus, as an alternative to conventional homogeneous thermal barrier ceramic coatings, the concept of

functionally graded materials (FGM) was proposed. FGMs are essentially two-phase particulate composites synthesized in a such way that the volume fractions of the constituents vary continuously in the thickness direction to give a predetermined composition profile.

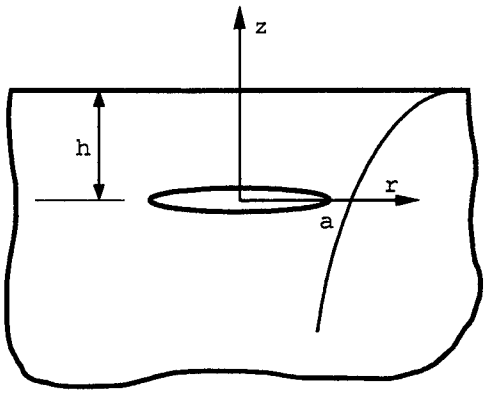

Figure 1 Crack geometry and notations

In this study it is assumed that the functionally graded medium contains an initial dominant flaw which can be approximated by a penny-shaped crack parallel to the surface (Figure 1). With the applications to fatigue and fracture in mind, the primary objective of the study has been the calculation of the stress intensity factors and the crack opening displacements. The previous studies have shown that in linear elastic crack problems for FGMs the fracture mechanics parameters are not very sensitive to the Poisson's ratio, ν, [2],[3]. Thus, in this study, too, it is assumed that ν is constant throughout the medium. It is also assumed that the Young's modulus may be represented by an exponential function of the depth coordinate z (Figure 1). Under these assumptions the problem becomes analytically tractable and may be reduced to a system of singular integral equations by using the Hankel transforms [4].

Formulation of the Problem

Consider the axisymmetric crack problem in a nonhomogeneous semi-infinite medium described in Figure 1 with the crack radius a and the distance h. Let the Lame 's constants be approximated by

$$\mu(z) = \mu_0 \exp(\alpha z), \qquad \lambda(z) = \lambda_0 \exp(\alpha z). \tag{1}$$

For the perturbation problem under consideration the only nonvanishing external loads are assumed to be

$$\sigma_{1zz}(r, 0^+) = \sigma_{2zz}(r, 0^-) = p_1(r), \qquad 0 \le r < a, \tag{2a}$$

$$\sigma_{1rz}(r,0^+) = \sigma_{2rz}(r,0^-) = p_2(r), \qquad 0 \le r < a, \tag{2b}$$

Using the kinematic relation and the Hooke's law in the absence of body forces, the equilibrium equations can be expressed as follows :

$$(\kappa+1)\left(\frac{\partial^2 u}{\partial r^2} + \frac{1}{r}\frac{\partial u}{\partial r} - \frac{u}{r^2} + \frac{\partial^2 w}{\partial r \partial z}\right) + (\kappa-1)\alpha\left(\frac{\partial u}{\partial z} + \frac{\partial w}{\partial r}\right) + (\kappa-1)\left(\frac{\partial^2 u}{\partial z^2} - \frac{\partial^2 w}{\partial r \partial z}\right) = 0, \tag{3a}$$

$$(\kappa+1)\left(\frac{\partial^2 u}{\partial r \partial z} + \frac{1}{r}\frac{\partial u}{\partial z} + \frac{\partial^2 w}{\partial z^2}\right) - (3-\kappa)\alpha\left(\frac{\partial u}{\partial r} + \frac{u}{r}\right) + (\kappa+1)\alpha\frac{\partial w}{\partial z} - (\kappa-1)\left(\frac{\partial^2 u}{\partial r \partial z} - \frac{\partial^2 w}{\partial r^2}\right) - \frac{(\kappa-1)}{r}\left(\frac{\partial u}{\partial z} - \frac{\partial w}{\partial r}\right) = 0, \tag{3b}$$

where $\kappa = 3 - 4\nu$, $\lambda/\mu = 2\nu/(1-2\nu)$, ν being the Poisson's ratio. The function $u(r,z)$ and $w(r,z)$ are the r and z components of the displacement vector. Equation (3) may be solved by using Hankel transforms with the following boundary and continuity conditions:

$$\sigma_{1zz}(r,h) = 0, \qquad \sigma_{1rz}(r,h) = 0, \qquad 0 < r < \infty, \tag{4a}$$

$$\sigma_{1zz}(r,0) = \sigma_{2zz}(r,0), \quad \sigma_{1rz}(r,0) = \sigma_{2rz}(r,0), \quad 0 < r < \infty, \tag{4b}$$

$$w_1(r,0^+) - w_2(r,0^-) = 0, \qquad a < r < \infty, \tag{4c}$$

$$u_1(r,0^+) - u_2(r,0^-) = 0, \qquad a < r < \infty, \tag{4d}$$

where subscripts 1 and 2 refer to the domains $0 < z < h$ and $z < 0$, respectively. After some lengthy analysis the mixed boundary conditions (2a,b) and (4c,d) may be reduced to the following system of integral equations

$$\frac{1}{\pi}\int_{-a}^{a}\frac{\phi_1(s)}{s-r}\,ds + \frac{1}{\pi}\int_0^a \sum_{j=1}^{2} k_{1j}(s,r)\phi_j(s)\,ds = \frac{(\kappa+1)}{2\mu_0}p_1(r), \qquad 0 \le r < a \tag{5a}$$

$$\frac{1}{\pi}\int_{-a}^{a}\frac{\phi_2(s)}{s-r}\,ds + \frac{1}{\pi}\int_0^a \sum_{j=1}^{2} k_{2j}(s,r)\phi_j(s)\,ds = -\frac{(\kappa+1)}{2\mu_0}p_2(r), \quad 0 \le r < a \tag{5b}$$

$$\int_{-a}^{a} \phi_1(s)\,ds = 0, \qquad \int_{-a}^{a} s\,\phi_2(s)\,ds = 0 \tag{5c,d}$$

where

$$\phi_1(r) = \frac{\partial}{\partial r}(w(r,0^+) - w(r,0^-)), \qquad 0 \le r < \infty, \tag{6a}$$

$$\phi_2(r) = \frac{1}{r}\frac{\partial}{\partial r}(ru(r,0^+) - ru(r,0^-)), \qquad 0 \le r < \infty \tag{6b}$$

ϕ_1 and ϕ_2 are unknown functions and the Fredholm kernels $k_{ij}(s,r)$, $(i,j=1,2)$, are square integrable in the domain $0 \le (r,s) \le a$. Although in practice these kernels are generally bounded and continuous in the interval $(0,a)$, in axisymmetric problems $k_{ij}(s,r)$ invariably contains a logarithmic singularity at $r = s$ [5]. Since there is no "closed form" solution for (5), an effective numerical solution may be developed by using a quadrature formula of the Gaussian type to evaluate the integral with Fredholm kernels for appropriately selected values of r_i, $(i = 1,..,n)$, and reducing the problem to a system of linear algebraic equations in the unknowns $\phi(s_j)$, $(j = 1,..,n)$. It can also be shown that the solution of the integral equations (5) may be expressed in terms of the following infinite series :

$$\phi_1(s) = \frac{1}{\sqrt{1-\left(\frac{s}{a}\right)^2}} \sum_{n=0}^{\infty} A_n T_n\left(\frac{s}{a}\right), \tag{7a}$$

$$\phi_2(s) = \frac{1}{\sqrt{1-\left(\frac{s}{a}\right)^2}} \sum_{n=0}^{\infty} B_n T_n\left(\frac{s}{a}\right), \tag{7b}$$

where the orthogonal functions T_n are Chebyshev polynomials of the first kind and $T_0 = 1$. A_n and B_n are the new unknowns which may be determined from the linear algebraic system obtained by substituting (7) into (5) and by using a method of reduction.

Results and Discussion

The main results of this study are the stress intensity factors calculated for various loading conditions as functions of the dimensionless nonhomogeneity constant αa defined by (1) and the basic dimensionless length parameter h/a. For a homogeneous infinite medium modes I and II crack problems are uncoupled and the stress intensity factors are given by

$$k_1 = -\frac{2}{\pi\sqrt{a}}\int_0^a \frac{rp_1(r)}{\sqrt{a^2-r^2}}dr, \qquad k_2 = -\frac{2}{\pi\sqrt{a^3}}\int_0^a \frac{r^2p_2(r)}{\sqrt{a^2-r^2}}dr. \tag{8}$$

In Figures 2-17, the stress intensity factors and the crack opening displacements are shown for two different loading conditions, namely $p_1(r) = -p_0$, $p_2(r) = 0$ and $p_2(r) = -q_0(r/a)$, $p_1(r) = 0$. For the problem under consideration the normalized stress intensity factors and the crack opening displacements are calculated for a constant Poisson's

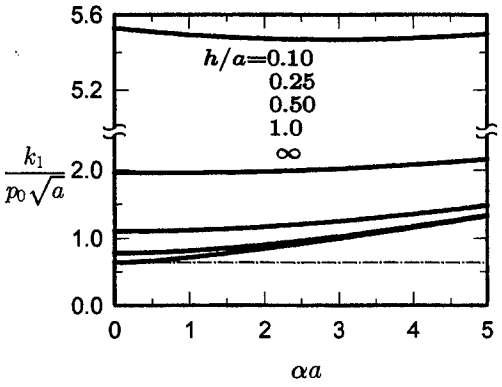

Figure 2 Normalized SIF for various h/a,
$\sigma_{zz}(r,0) = -p_0$, $\sigma_{rz}(r,0) = 0$

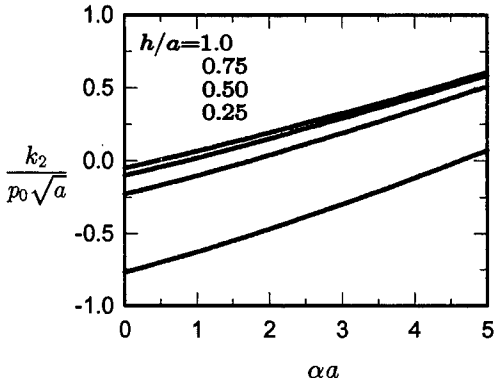

Figure 3 Normalized SIF for various h/a,
$\sigma_{zz}(r,0) = -p_0$, $\sigma_{rz}(r,0) = 0$

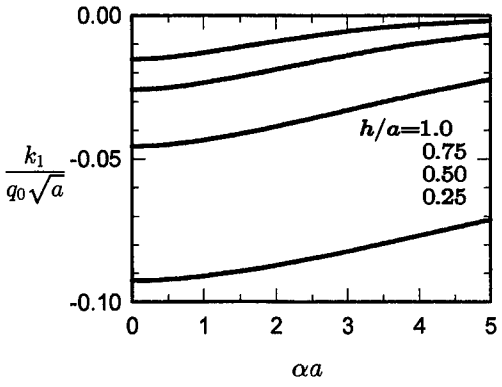

Figure 4 Normalized SIF for various h/a,
$\sigma_{zz}(r,0) = 0$, $\sigma_{rz}(r,0) = -q_0$

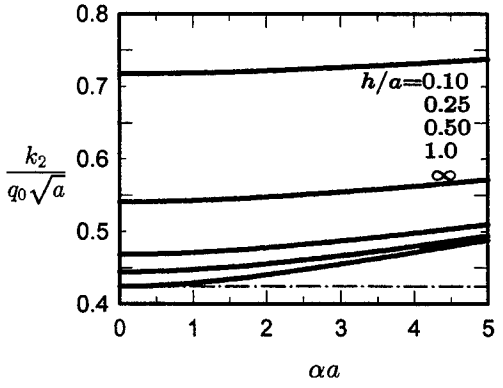

Figure 5 Normalized SIF for various h/a,
$\sigma_{zz}(r,0) = 0$, $\sigma_{rz}(r,0) = -q_0$

ratio ($\nu = 0.3$) by varying h/a and αa. Note that the problem is formulated and can be solved for arbitrary crack surface tractions. Figure 2-9 show the normalized mode I and mode II stress intensity factors k_1 and k_2 for two primary loading conditions with the dimensionless

constants αa and h/a as the variables. For large h/a values, the calculated stress intensity factors agree with the results given in [3].

When there was only normal loading ($\sigma_{zz}(r,0) = -p_0,\ \sigma_{rz}(r,0) = 0$), it was observed that for large values of h/a, normalized stress intensity factor k_1 increases slowly as the nonhomogeneity parameter αa increases. However, for small values of h/a, (such as $h/a = 0.10$), the normalized stress intensity factor k_1 first decreases and then slowly

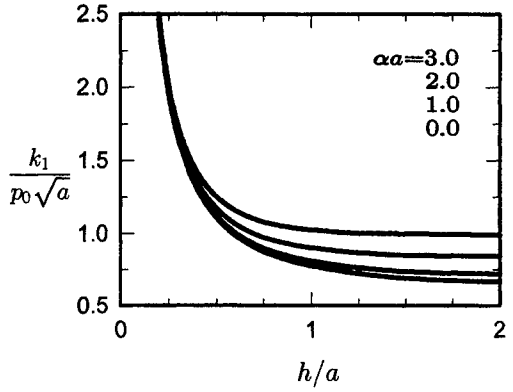

Figure 6 Normalized SIF for various αa, $\sigma_{zz}(r,0) = -p_0,\ \sigma_{rz}(r,0) = 0$

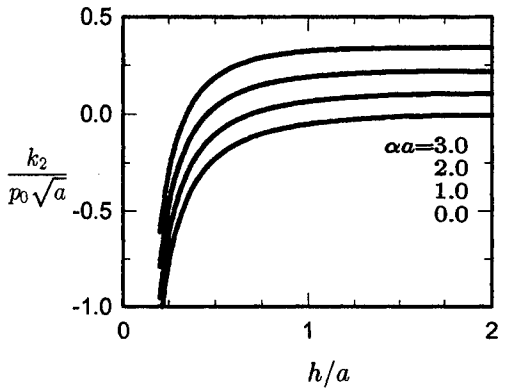

Figure 7 Normalized SIF for various αa, $\sigma_{zz}(r,0) = -p_0,\ \sigma_{rz}(r,0) = 0$

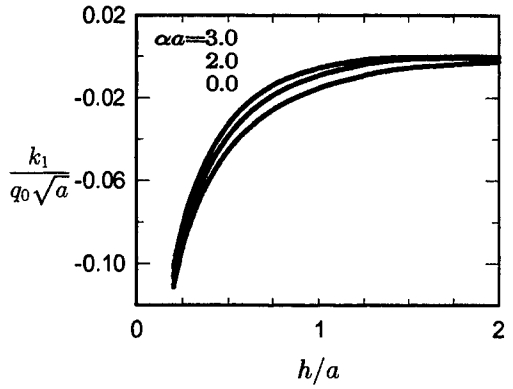

Figure 8 Normalized SIF for various αa, $\sigma_{zz}(r,0) = 0,\ \sigma_{rz}(r,0) = -q_0$

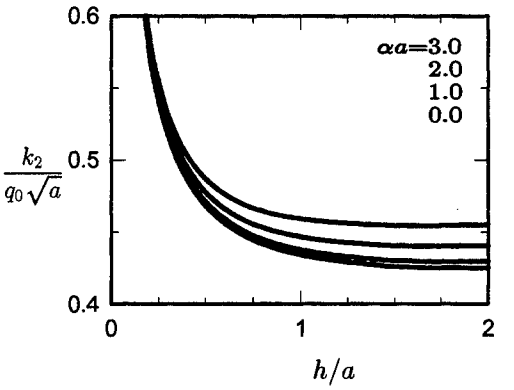

Figure 9 Normalized SIF for various αa, $\sigma_{zz}(r,0) = 0,\ \sigma_{rz}(r,0) = -q_0$

increases with increasing αa (Figure 2). Under the same loading k_2 increases with increasing αa for all values of h/a. On the other hand for shear loading ($\sigma_{zz}(r,0) = 0$, $\sigma_{rz}(r,0) = -q_0$), stress intensity factor k_1 increases for all values of h/a with increasing αa, however, the values of k_1 are small. Similarly, k_2 increases for all values of h/a with increasing αa, but the values of k_2 are small compared to k_1 under the normal loading.

rom Figures 10 and 11 it may also be observed that values of k_1 under normal loading and k_2 nder shear loading were almost symmetric with respect to αa $(-5 < \alpha a < 5)$ for large values of h/a. Since the stress intensity factors do not depend on the magnitude of the shear modulus μ_0 for a crack in an infinite medium, this result is expected.

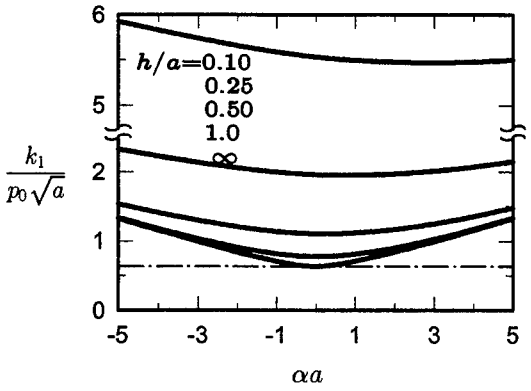

Figure 10 Normalized SIF for various h/a,
$\sigma_{zz}(r,0) = -p_0,\ \sigma_{rz}(r,0) = 0$

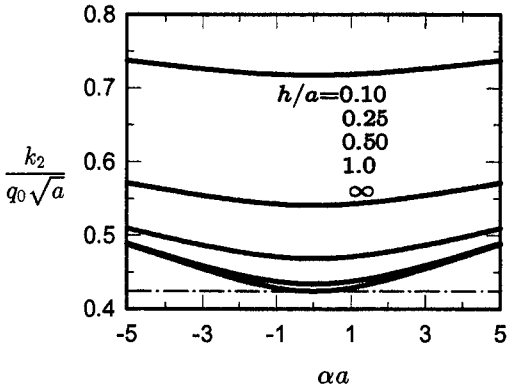

Figure 11 Normalized SIF for various h/a,
$\sigma_{zz}(r,0) = 0,\ \sigma_{rz}(r,0) = -q_0$

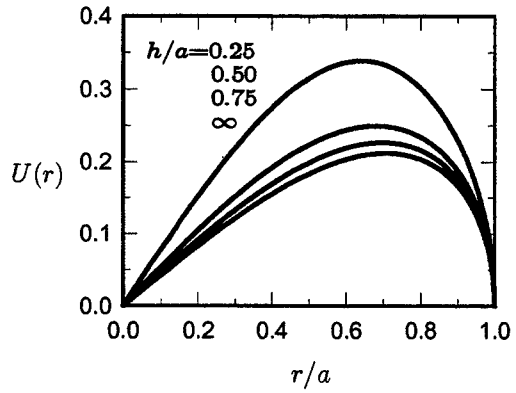

Figure 12 Normalized COD for $\alpha a = 0$,
$\sigma_{zz}(r,0) = 0,\ \sigma_{rz}(r,0) = -q_0$

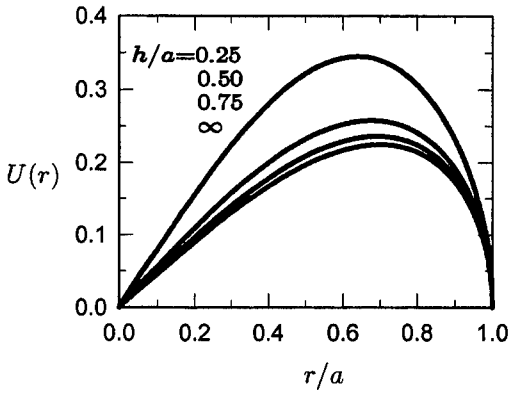

Figure 13 Normalized COD for $\alpha a = 2$,
$\sigma_{zz}(r,0) = 0,\ \sigma_{rz}(r,0) = -q_0$

It was also observed that stress intensity factors k_1 and k_2 under respectively normal and shear loading tend to certain limiting values as h/a increases. On the other hand as expected, same stress intensity factors tend to infinity when h/a goes to zero. For large values of h/a the results agree with [3].

Also, for fixed values of αa the stress intensity factors $k_1$and k_2 under shear and normal loading, respectively, tend to certain limiting values which are, however, negligibly small. Figures 12-17, show some sample results for the normalized crack opening displacements

$U(r)$ and $W(r)$, which are respectively the r and z components of the relative crack opening defined by (Figure 1)

$$U(r) = \frac{u(r,0^+) - u(r,0^-)}{\frac{aq_0(\kappa+1)}{2\mu}}, \qquad W(r) = \frac{w(r,0^+) - w(r,0^-)}{\frac{ap_0(\kappa+1)}{2\mu}} \tag{9}$$

The figures show that the influence of the nonhomogeneity constant αa on the crack opening displacements is not very significant. On the other hand $U(r)$ and $W(r)$ are seen to be rather heavily dependent on h/a (particularly for small values of h/a). Again, for large values of h/a the results agree with that given in [3].

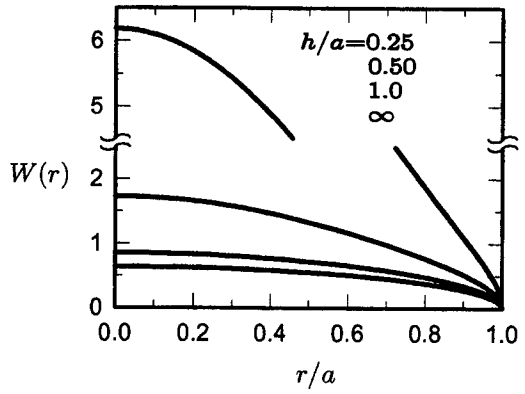

Figure 14 Normalized COD for $\alpha a = 0$,
$\sigma_{zz}(r,0) = -p_0,\ \sigma_{rz}(r,0) = 0$

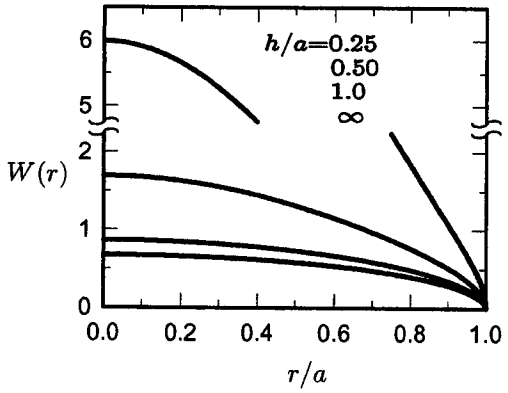

Figure 15 Normalized COD for $\alpha a = 0.5$,
$\sigma_{zz}(r,0) = -p_0,\ \sigma_{rz}(r,0) = 0$

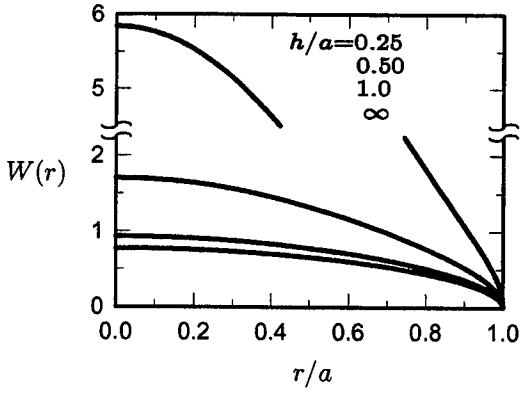

Figure 16 Normalized COD for $\alpha a = 1$,
$\sigma_{zz}(r,0) = -p_0,\ \sigma_{rz}(r,0) = 0$

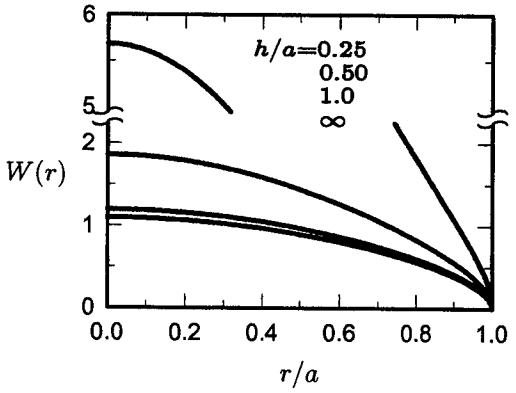

Figure 17 Normalized COD for $\alpha a = 2$,
$\sigma_{zz}(r,0) = -p_0,\ \sigma_{rz}(r,0) = 0$

TABLE 1 THE VARIATION OF SIF WITH ν FOR $h/a = 2.0$ AND $\sigma_{zz}(r,0) = -p_0,\ \sigma_{rz}(r,0) = 0$.

ν	$\alpha a = 0.1$		$\alpha a = 1.0$		$\alpha a = 2.0$		$\alpha a = 4.0$	
	$\frac{k_1}{p_0\sqrt{a}}$	$\frac{k_2}{p_0\sqrt{a}}$	$\frac{k_1}{p_0\sqrt{a}}$	$\frac{k_2}{p_0\sqrt{a}}$	$\frac{k_1}{p_0\sqrt{a}}$	$\frac{k_2}{p_0\sqrt{a}}$	$\frac{k_1}{p_0\sqrt{a}}$	$\frac{k_2}{p_0\sqrt{a}}$
0.00	.6676	.0037	.7041	.1021	.7962	.2162	1.0598	.4636
0.10	.6677	.0037	.7094	.1024	.8101	.2170	1.0870	.4657
0.20	.6678	.0037	.7157	.1028	.8266	.2179	1.1186	.4682
0.30	.6679	.0037	.7236	.1033	.8465	.2189	1.1562	.4711
0.40	.6681	.0037	.7337	.1038	.8710	.2201	1.2021	.4747
0.45	.6681	.0037	.7398	.1041	.8857	.2208	1.2292	.4768

TABLE 2 THE VARIATION OF SIF WITH ν FOR $h/a = 2.0$ AND $\sigma_{zz}(r,0) = 0,\ \sigma_{rz}(r,0) = -q_0$.

ν	$\alpha a = 0.1$		$\alpha a = 1.0$		$\alpha a = 2.0$		$\alpha a = 4.0$	
	$\frac{k_1}{q_0\sqrt{a}}$	$\frac{k_2}{q_0\sqrt{a}}$	$\frac{k_1}{q_0\sqrt{a}}$	$\frac{k_2}{q_0\sqrt{a}}$	$\frac{k_1}{q_0\sqrt{a}}$	$\frac{k_2}{q_0\sqrt{a}}$	$\frac{k_1}{q_0\sqrt{a}}$	$\frac{k_2}{q_0\sqrt{a}}$
0.00	−.0025	.4253	−.0018	.4285	−.0008	.4370	−.0001	.4638
0.10	−.0025	.4254	−.0017	.4288	−.0007	.4380	−.0001	.4659
0.20	−.0025	.4254	−.0016	.4292	−.0006	.4391	.0000	.4683
0.30	−.0025	.4254	−.0015	.4296	−.0005	.4406	.0000	.4712
0.40	−.0025	.4254	−.0013	.4303	−.0004	.4423	.0000	.4747
0.45	−.0025	.4254	−.0012	.4307	−.0003	.4434	.0000	.4768

TABLE 3 THE VARIATION OF SIF WITH ν FOR $h/a = 0.25$ AND $\sigma_{zz}(r,0) = -p_0,\ \sigma_{rz}(r,0) = 0$.

ν	$\alpha a = 0.1$		$\alpha a = 1.0$		$\alpha a = 2.0$		$\alpha a = 4.0$	
	$\frac{k_1}{p_0\sqrt{a}}$	$\frac{k_2}{p_0\sqrt{a}}$	$\frac{k_1}{p_0\sqrt{a}}$	$\frac{k_2}{p_0\sqrt{a}}$	$\frac{k_1}{p_0\sqrt{a}}$	$\frac{k_2}{p_0\sqrt{a}}$	$\frac{k_1}{p_0\sqrt{a}}$	$\frac{k_2}{p_0\sqrt{a}}$
0.00	1.9598	−.7568	1.9490	−.6297	1.9564	−.4780	2.0285	−.1435
0.10	1.9598	−.7568	1.9502	−.6289	1.9606	−.4753	2.0407	−.1362
0.20	1.9598	−.7568	1.9517	−.6280	1.9657	−.4720	2.0552	−.1276
0.30	1.9599	−.7568	1.9536	−.6267	1.9720	−.4679	2.0729	−.1173
0.40	1.9599	−.7567	1.9560	−.6251	1.9802	−.4627	2.0952	−.1045
0.45	1.9599	−.7567	1.9576	−.6241	1.9852	−.4596	2.1088	−.0969

TABLE 4 THE VARIATION OF SIF WITH ν FOR $h/a = 0.25$ AND $\sigma_{zz}(r,0) = 0,\ \sigma_{rz}(r,0) = -q_0$.

	$\alpha a = 0.1$		$\alpha a = 1.0$		$\alpha a = 2.0$		$\alpha a = 4.0$	
ν	$\frac{k_1}{q_0\sqrt{a}}$	$\frac{k_2}{q_0\sqrt{a}}$	$\frac{k_1}{q_0\sqrt{a}}$	$\frac{k_2}{q_0\sqrt{a}}$	$\frac{k_1}{q_0\sqrt{a}}$	$\frac{k_2}{q_0\sqrt{a}}$	$\frac{k_1}{q_0\sqrt{a}}$	$\frac{k_2}{q_0\sqrt{a}}$
0.00	− .0925	.5412	− .0915	.5425	− .0887	.5463	− .0799	.5591
0.10	− .0925	.5412	− .0914	.5426	− .0883	.5467	− .0790	.5601
0.20	− .0925	.5412	− .0912	.5428	− .0878	.5472	− .0780	.5612
0.30	− .0925	.5412	− .0910	.5430	− .0872	.5478	− .0768	.5626
0.40	− .0925	.5412	− .0907	.5432	− .0865	.5486	− .0754	.5642
0.45	− .0925	.5412	− .0906	.5434	− .0860	.5490	− .0745	.5652

The problem was solved under the assumption that the Poisson's ratio ν is constant. Theoretically this is not possible. The assumption can only be justified if the fracture mechanics parameters of interest, in this case the stress intensity factors, prove to be relatively insensitive to variations in the Poisson's ratio. In the problem considered, it was observed that stress intensity factors are relatively insensitive to variations in the Poisson's ratio for small values of nonhomogeneity parameter αa and for all values of h/a. But for large αa and small h/a the effect of Poisson's ratio may not be negligible. Some results are presented in Tables 1-4 to give an idea about the influence of the variation in ν on the stress intensity factors. It may be seen that, generally, the influence of ν on the stress intensity factors is not very significant.

Acknowledgement

This study was partially supported by AFOSR under the Grant F49620-98-1-0028 and by ARO under the Grant DAAH04-95-1-0232.

References

1. W.Y. Lee, Y.W. Bae, C.C. Berndt, F. Erdogan, Y.D. Lee and Z. Mutasim, 1996. "The Concept of FGMs for Advanced Thermal Barrier Coating Applications." *Journal of American Ceramic Society*, 79 [12] : 3003-3012.

2. F. Delale and F. Erdogan, 1988. "Interface Crack In Nonhomogeneous Medium." *Int. Journal of Engineering Science*, Vol. 26, pp. 559-568.

3. M. Ozturk and F. Erdogan, 1993. "Axisymmetric Crack Problem in a Nonhomogeneous Medium." *ASME Journal of Applied Mechanics*, Vol. 60, pp. 406-414.

4. F. Erdogan, G.D. Gupta and T.S. Cook, 1973. "Numerical Solution of Singular Integral Equations." in *Method of Analysis and Solution of Crack Problems,* G.C. Sih, eds. Leyden: Noordhoff Int. Publ., pp: 368-425.

5. F. Erdogan, 1965. "Simultaneous Dual Integral Equations with Trigonometric and Bessel Kernels." *Zeitschrift Fur Angewandte Mathematik und Mechanik,* Vol.48 n4 pp:217-225

APPENDIX B

Surface Crack in a Graded Medium under General Loading Conditions

Serkan Dag and Fazil Erdogan

Department of Mechanical Engineering and Mechanics

Lehigh University, Bethlehem, PA 18015

Abstract

In this study the problem of a surface crack in a semi-infinite elastic graded medium under general loading conditions is considered. It is assumed that first by solving the problem in the absence of a crack, it is reduced to a local perturbation problem with arbitrary self-equilibrating crack surface tractions. The local problem is then solved by approximating the normal and shear tractions on the crack surfaces by polynomials and the normalized modes I and II stress intensity factors are given. As an example the results for a graded half plane loaded by a sliding rigid circular stamp are presented.

1 Introduction

Graded materials, also known as *functionally graded materials* (FGMs) are generally multi-phase composites with continuously varying thermomechanical properties. Used as coatings and interfacial zones they tend to reduce stresses resulting from the material property mismatch, increase the bonding strength, improve the surface properties and provide protection against severe thermal and chemical environments. Thus, the concept of grading the thermomechanical properties of materials provides the material scientists and engineers with an important tool to design new materials having highly favorable properties in certain specific applications [1-6].

To take full advantage of this new tool research is needed not only for developing efficient material processing and characterization techniques but also for carrying out basic studies relating to the safety and durability of FGM components. Typical current and potential applications for this new class of materials include thermal barrier coatings and abradable seals in gas turbines, preparation of wear-resistant surfaces in load transfer components such as gears, bearings, cams and machine tools, various interlayers in microlectronic and

optoelectronic devices, high-speed graded index polymer optical fibers, impact resistant components, and thermoelectric cells [6].

The primary interest in this study is in initiation and propagation of surface cracks in graded materials. Initially it is assumed that the conditions of crack initiation on the surface of the uncracked graded medium have been met and a surface crack has been initiatiated. Since the material on the surface of FGM is generally 100% ceramic and consequently rather brittle, this can be verified by applying a simple maximum tensile stress criterion. The main problem is, therefore, that of a surface crack subjected to general mixed-mode loading conditions. The corresponding mode I problem was considered in [7] and [8]. The more general mode I problem of a graded layer bonded to a homogeneous substrate was studied in [9]. In recent years the crack and contact problems for FGMs has been attracting quite considerable attention. In addition to the references cited in [1-6], the review articles [10] and [11] may be of particular interest.

2 Formulation of the Problem

The geometry of the crack problem is shown in Figure 1. The graded half plane contains a surface crack of length d. The crack surfaces are assumed to be subjected to general mixed mode loading. Largely, for mathematical expediency and for the fact that main results of the crack problems in graded materials are rather insensitive to the variations in Poisson's ratio, in this study it is assumed that the elastic properties of the medium may be approximated by

$$\mu(x) = \mu_0 \exp(\gamma x), \qquad \kappa = \text{constant}, \tag{1a,b}$$

where μ is the shear modulus, γ is a nonhomogeneity parameter, $\kappa = 3 - 4\nu$ for plane strain and $\kappa = (3-\nu)/(1+\nu)$ for generalized plane stress, ν being the Poisson's ratio. By using the Hooke's law

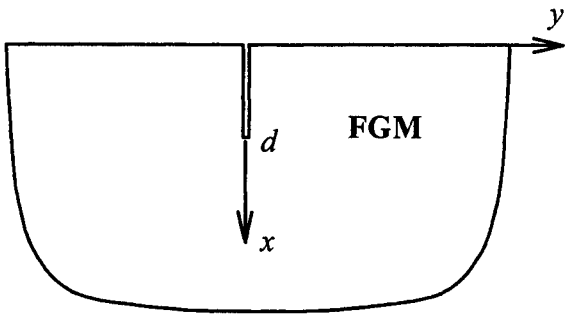

Figure 1: Surface crack in a graded medium

$$\sigma_{xx}(x,y)=\frac{\mu(x)}{\kappa-1}\Big\{(\kappa+1)\frac{\partial u}{\partial x}+(3-\kappa)\frac{\partial v}{\partial y}\Big\}, \tag{2a}$$

$$\sigma_{yy}(x,y)=\frac{\mu(x)}{\kappa-1}\Big\{(\kappa+1)\frac{\partial v}{\partial y}+(3-\kappa)\frac{\partial u}{\partial x}\Big\}, \tag{2b}$$

$$\sigma_{xy}(x,y)=\mu(x)\Big\{\frac{\partial u}{\partial y}+\frac{\partial v}{\partial x}\Big\} \tag{2c}$$

the equilibrium conditions $\sigma_{ij,j}=0$ can be expressed as

$$(\kappa+1)\frac{\partial^2 u}{\partial x^2}+(\kappa-1)\frac{\partial^2 u}{\partial y^2}+2\frac{\partial v}{\partial x\partial y}+\gamma(\kappa+1)\frac{\partial u}{\partial x}+\gamma(3-\kappa)\frac{\partial v}{\partial y}=0, \tag{3a}$$

$$(\kappa+1)\frac{\partial^2 v}{\partial y^2}+(\kappa-1)\frac{\partial^2 v}{\partial x^2}+2\frac{\partial^2 u}{\partial x\partial y}+\gamma(\kappa-1)\frac{\partial v}{\partial x}+\gamma(\kappa-1)\frac{\partial u}{\partial y}=0. \tag{3b}$$

Equations (3) must be solved under the following external loads:

$$\sigma_{xx}(0,y)=0, \qquad \sigma_{xy}(0,y)=0, \qquad -\infty<y<\infty, \tag{4a}$$

$$\sigma_{yy}(x,0)=-p(x), \qquad \sigma_{xy}(x,0)=-q(x), \qquad 0<x<d, \tag{4b}$$

$$\sigma_{ij}(x,y)\to 0 \text{ as } (x^2+y^2)\to\infty, \ (i,j=x,y), \tag{4c}$$

where $p(x)$ and $q(x)$ are the crack surface tractions which are obtained from the solution of the original problem in the absence of the crack. We observe that the unknown functions that are convenient in this problem are the derivatives of the relative crack opening displacements defined by

$$\frac{2\mu_0}{\kappa+1}\frac{\partial}{\partial x}(v(x,+0)-v(x,-0))=f_1(x), \qquad 0<x<d, \tag{5a}$$

$$\frac{2\mu_0}{\kappa+1}\frac{\partial}{\partial x}(u(x,+0)-u(x,-0))=f_2(x), \qquad 0<x<d. \tag{5b}$$

2.1 *The Opening Mode Problem*

In the graded half plane problem having a symmetry with respect to the $y=0$ plane in geometry and material property distribution, the mode I (or the opening mode) and mode II (or the sliding mode) problems turn out to be uncoupled. Therefore, the problems may be

formulated separately. Furthermore, the solution to each problem may be expressed as the sum of two solutions, namely the infinite medium with a crack and a half plane $x > 0$ without a crack.

We consider first the infinite medium with a crack. Defining the displacements by

$$u_1^{(i)}(x,y) = \frac{1}{2\pi}\int_{-\infty}^{\infty} U_1^{(i)}(\omega,y)\exp(i\omega x)d\omega \tag{6a}$$

$$v_1^{(i)}(x,y) = \frac{1}{2\pi}\int_{-\infty}^{\infty} V_1^{(i)}(\omega,y)\exp(i\omega x)d\omega, \tag{6b}$$

from Eq. (3) it follows that

$$(\kappa-1)\frac{d^2U_1^{(i)}}{dy^2} + (\kappa+1)\big(\gamma i\omega - \omega^2\big)U_1^{(i)} + (2i\omega + \gamma(3-\kappa))\frac{dV_1^{(i)}}{dy} = 0, \tag{7a}$$

$$(2i\omega + \gamma(\kappa-1))\frac{dU_1^{(i)}}{dy} + (\kappa+1)\frac{d^2V_1^{(i)}}{dy^2} + (\kappa-1)\big(\gamma i\omega - \omega^2\big)V_1^{(i)} = 0. \tag{7b}$$

where superscript i and subscript 1 refer to infinite medium and opening mode problem respectively. Assuming the solution of Eq. (7) in the form $\exp(ny)$, the characteristic equation, its roots, and the displacements are found to be

$$\big(n^2 - \delta_1 n + i\omega(\gamma + i\omega)\big)\big(n^2 + \delta_1 n + i\omega(\gamma + i\omega)\big) = 0, \quad \delta_1 = \gamma\sqrt{\frac{3-\kappa}{\kappa+1}}, \tag{8a,b}$$

$$n_1 = -\frac{1}{2}\delta_1 + \frac{1}{2}\sqrt{4\omega^2 - 4i\omega\gamma + \delta_1^2}, \qquad \Re(n_1) > 0, \tag{9a}$$

$$n_2 = \frac{1}{2}\delta_1 + \frac{1}{2}\sqrt{4\omega^2 - 4i\omega\gamma + \delta_1^2}, \qquad \Re(n_2) > 0, \tag{9b}$$

$$n_3 = -\frac{1}{2}\delta_1 - \frac{1}{2}\sqrt{4\omega^2 - 4i\omega\gamma + \delta_1^2}, \qquad \Re(n_3) < 0, \tag{9c}$$

$$n_4 = \frac{1}{2}\delta_1 - \frac{1}{2}\sqrt{4\omega^2 - 4i\omega\gamma + \delta_1^2}, \qquad \Re(n_4) < 0, \tag{9d}$$

$$u_1^{(i^-)}(x,y) = \frac{1}{2\pi}\int_{-\infty}^{\infty}\sum_{j=1}^{2} C_j(\omega)\exp(n_j y + i\omega x)d\omega, \tag{10a}$$

$$v_1^{(i^-)}(x,y) = \frac{1}{2\pi}\int_{-\infty}^{\infty}\sum_{j=1}^{2} C_j(\omega)A_j(\omega)\exp(n_j y + i\omega x)d\omega, \tag{10b}$$

for $y < 0$, and

$$u_1^{(i^+)}(x,y) = \frac{1}{2\pi}\int_{-\infty}^{\infty}\sum_{j=3}^{4} C_j(\omega)\exp(n_j y + i\omega x)d\omega, \tag{11a}$$

$$v_1^{(i^+)}(x,y) = \frac{1}{2\pi}\int_{-\infty}^{\infty}\sum_{j=3}^{4} C_j(\omega)A_j(\omega)\exp(n_j y + i\omega x)d\omega, \tag{11b}$$

for $y > 0$. In Eqs. (10) and (11) $C_j(\omega)$, $(j = 1,2,3,4)$ are unknown and A_j are given by

$$A_j(\omega) = -\frac{n_j^2(\kappa-1) + (i\omega\gamma - \omega^2)(\kappa+1)}{n_j(2i\omega + \gamma(3-\kappa))}, \qquad (j = 1,2,3,4). \tag{12}$$

Consider now the half plane problem for $x > 0$ without the crack. By observing that the problem has a symmetry with respect to $y = 0$ plane the solution may be expressed as

$$u_1^{(h)}(x,y) = \int_0^{\infty} U_1^{(h)}(x,\alpha)\cos(\alpha y)d\alpha, \tag{13a}$$

$$v_1^{(h)}(x,y) = \int_0^{\infty} V_1^{(h)}(x,\alpha)\sin(\alpha y)d\alpha, \tag{13b}$$

where superscript h and subscript 1 refer to the half plane and the opening mode, respectively. From Eqs. (3) and (13) it follows that

$$(\kappa+1)\frac{d^2U_1^{(h)}}{dx^2} + \gamma(\kappa-1)\frac{dU_1^{(h)}}{dx} - \alpha^2(\kappa-1)U_1^{(h)} + 2\alpha\frac{dV_1^{(h)}}{dx} + \gamma(3-\kappa)V_1^{(h)} = 0, \tag{14a}$$

$$2\alpha\frac{dU_1^{(h)}}{dx} + \gamma\alpha(\kappa-1)U_1^{(h)} - (\kappa-1)\frac{d^2V_1^{(h)}}{dx^2} - \gamma(\kappa-1)\frac{dV_1^{(h)}}{dx} + \alpha^2(\kappa+1)V_1^{(h)} = 0. \tag{14b}$$

Assuming the solution for Eq. (14) of the form $\exp(px)$, we find

$$\left(p^2 + \gamma p - \alpha^2 - i\alpha\delta_1\right)\left(p^2 + \gamma p - \alpha^2 + i\alpha\delta_1\right) = 0, \tag{15}$$

$$p_1 = -\frac{1}{2}\gamma + \frac{1}{2}\sqrt{\gamma^2 + 4\alpha^2 + 4i\alpha\delta_1}, \qquad \Re(p_1) > 0, \tag{16a}$$

$$p_2 = -\frac{1}{2}\gamma + \frac{1}{2}\sqrt{\gamma^2 + 4\alpha^2 - 4i\alpha\delta_1}, \qquad \Re(p_2) > 0, \tag{16b}$$

$$p_3 = -\frac{1}{2}\gamma - \frac{1}{2}\sqrt{\gamma^2 + 4\alpha^2 + 4i\alpha\delta_1}, \qquad \Re(p_3) < 0, \tag{16c}$$

$$p_4 = -\frac{1}{2}\gamma - \frac{1}{2}\sqrt{\gamma^2 + 4\alpha^2 - 4i\alpha\delta_1}, \qquad \Re(p_4) < 0, \tag{16d}$$

$$u_1^{(h)}(x,y) = \int_0^\infty (B_3 \exp(p_3 x) + B_4 \exp(p_4 x))\cos(\alpha y) d\alpha, \tag{17a}$$

$$v_1^{(h)}(x,y) = \int_0^\infty (B_3 D_3 \exp(p_3 x) + B_4 D_4 \exp(p_4 x))\sin(\alpha y) d\alpha, \tag{17b}$$

$$D_j = -\frac{p_j^2(\kappa+1) + \alpha^2(1-\kappa) + \gamma p_j(1+\kappa)}{\alpha(2p_j + \gamma(3-\kappa))}, \tag{18}$$

where δ_1 is given by Eq. (8b) and $B_3(\alpha)$ and $B_4(\alpha)$ are unknown functions. We now express the solution of the mode I problem as follows:

$$u_1(x,y) = u_1^{(i)}(x,y) + u_1^{(h)}(x,y), \tag{19a}$$

$$v_1(x,y) = v_1^{(i)}(x,y) + v_1^{(h)}(x,y), \tag{19b}$$

$$\sigma_{kj1}(x,y) = \sigma_{kj1}^{(i)}(x,y) + \sigma_{kj1}^{(h)}(x,y), \qquad (k,j = x,y). \tag{19c}$$

where displacements are given in terms of six unknown functions $C_1, \ldots, C_4, B_3, B_4$ which are determined from the following six conditions:

$$\sigma_{xx1}(0,y) = 0, \quad \sigma_{xy1}(0,y) = 0, \quad -\infty < y < \infty, \tag{20a,b}$$

$$\sigma_{yy1}(x,+0) = \sigma_{yy1}(x,-0), \quad \sigma_{xy1}(x,+0) = \sigma_{xy1}(x,-0), \quad 0 < x < \infty, \tag{21a,b}$$

$$u_1(x,+0) = u_1(x,-0), \qquad 0 < x < \infty, \tag{22}$$

$$\sigma_{yy1}(x,0) = -p(x), \qquad 0 < x < d, \tag{23a}$$

$$v_1(x,+0) = v_1(x,-0), \qquad d < x < \infty. \tag{23b}$$

The homogeneous conditions (20)-(22) may be used to eliminate five of the unknown functions. The mixed boundary conditions (23) would then determine the sixth unknown.

By using the definitions given by Eq. (5), observing that for the mode I problem under consideration $f_2(x) = 0$ and $q(x) = 0$, replacing the condition (23a) by (5a), and substituting from (10), (11), (17), (19) and (2) into (20)-(23), we obtain the following expressions giving $C_1, \ldots, C_4, B_3, B_4$ in terms of $f_1(x)$:

$$C_j(\omega) = \frac{\kappa+1}{2\mu_0} P_j(\omega) \int_0^d f_1(t) \exp(-i\omega t) dt, \tag{24a}$$

$$\sum_{j=3}^{4} (i\omega(3-\kappa) + A_j n_j (1+\kappa)) P_j(\omega) - \sum_{j=1}^{2} (i\omega(3-\kappa) + A_j n_j (1+\kappa)) P_j(\omega) = 0, \tag{24b}$$

$$\sum_{j=3}^{4} (n_j + i\omega A_j) P_j(\omega) - \sum_{j=1}^{2} (n_j + i\omega A_j) P_j(\omega) = 0, \tag{24c}$$

$$i\omega \left\{ \sum_{j=3}^{4} A_j P_j(\omega) - \sum_{j=1}^{2} A_j P_j(\omega) \right\} = 1, \tag{24d}$$

$$P_4(\omega) + P_3(\omega) - P_2(\omega) - P_1(\omega) = 0, \tag{24e}$$

$$\int_0^\infty \sum_{j=3}^{4} ((\kappa+1) p_j + D_j \alpha (3-\kappa)) B_j(\alpha) \cos(\alpha y)$$
$$+ \frac{1}{2\pi} \int_{-\infty}^{\infty} \sum_{j=3}^{4} (i\omega(\kappa+1) + A_j n_j (3-\kappa)) C_j(\omega) \exp(n_j y) d\omega = 0, \qquad 0 < y < \infty, \tag{25a}$$

$$\int_0^\infty \sum_{j=3}^{4} (D_j p_j - \alpha) B_j(\alpha) \sin(\alpha y)$$
$$+ \frac{1}{2\pi} \int_{-\infty}^{\infty} \sum_{j=3}^{4} (n_j + i\omega A_j) C_j(\omega) \exp(n_j y) d\omega = 0, \qquad 0 < y < \infty. \tag{25b}$$

$f_1(x)$ is the new unknown function and is determined from Eq. (23a). Because of symmetry in this problem it is sufficient to consider $0 < y < \infty$ only. Evaluating some of the integrals in closed form by using the theory of residues, Eqs. (25) may be reduced to

$$\sum_{j=3}^{4} ((\kappa+1) p_j + D_j \alpha (3-\kappa)) B_j^*(\alpha, t) = R_{xx1}(\alpha, t), \tag{26a}$$

$$\sum_{j=3}^{4} (D_j p_j - \alpha) B_j^*(\alpha, t) = R_{xy1}(\alpha, t), \tag{26b}$$

where

$$B_j(\alpha) = \frac{\kappa+1}{2\mu_0} \int_0^d B_j^*(\alpha, t) \exp\left(\left(\frac{\gamma}{2} - \lambda_1 \right) t \right) f_1(t) dt, \tag{27}$$

and R_{xx1}, R_{xy1} and λ_1 are given in Appendix A.

2.2 *The Sliding Mode Problem*

Referring to Fig. 1, in this section it is assumed that $y = 0$ is plane of anti symmetry. Consequently, in Eq. (4) $p(x) = 0$ and in Eq. (5) $f_1(x) = 0$. Thus, following a procedure similar to that of Section 2.1, the displacements for the graded infinite medium with a crack along the $x-$ axis may be written as

$$u_2^{(i^-)}(x,y) = \frac{1}{2\pi}\int_{-\infty}^{\infty}\sum_{j=1}^{2}E_j(\omega)\exp(n_j y + i\omega x)d\omega, \tag{28a}$$

$$v_2^{(i^-)}(x,y) = \frac{1}{2\pi}\int_{-\infty}^{\infty}\sum_{j=1}^{2}E_j(\omega)A_j(\omega)\exp(n_j y + i\omega x)d\omega, \tag{28b}$$

for $y < 0$ and

$$u_2^{(i^+)}(x,y) = \frac{1}{2\pi}\int_{-\infty}^{\infty}\sum_{j=3}^{4}E_j(\omega)\exp(n_j y + i\omega x)d\omega, \tag{29a}$$

$$v_2^{(i^+)}(x,y) = \frac{1}{2\pi}\int_{-\infty}^{\infty}\sum_{j=3}^{4}E_j(\omega)A_j(\omega)\exp(n_j y + i\omega x)d\omega, \tag{29b}$$

for $y > 0$. In Eqs. (28) and (29) $E_1(\omega), \ldots, E_4(\omega)$ are unknown and n_j and A_j are given by Eqs. (9) and (12), respectively. Similarly, the general solution for the graded half plane $x > 0$ under antisymmetric loading conditions may be expressed as

$$u_2^{(h)}(x,y) = \int_0^{\infty}(G_3(\alpha)\exp(p_3 x) + G_4(\alpha)\exp(p_4 x))\sin(\alpha y)d\alpha, \tag{30a}$$

$$v_2^{(h)}(x,y) = \int_0^{\infty}(G_3(\alpha)H_3(\alpha)\exp(p_3 x) + G_4(\alpha)H_4(\alpha)\exp(p_4 x))d\alpha, \tag{30b}$$

where $G_3(\alpha)$ and $G_4(\alpha)$ are unknown, the characteristic equation and its roots p_j, $(j = 1, \ldots, 4)$ are given by Eqs. (18) and (19) and $H_3(\alpha)$ and $H_4(\alpha)$ are

$$H_j(\alpha) = \frac{\gamma p_j(\kappa+1) + \alpha^2(1-\kappa) + p_j^2(\kappa+1)}{\alpha(2p_j + \gamma(3-\kappa))}, \qquad (j = 3, 4). \tag{31}$$

We now express the displacements and stresses in the cracked half plane under antisymmetric loading in terms of the following sums

$$u_2(x,y) = u_2^{(i)}(x,y) + u_2^{(h)}(x,y), \tag{32a}$$

$$v_2(x,y) = v_2^{(i)}(x,y) + v_2^{(h)}(x,y), \tag{32b}$$

$$\sigma_{kj2}(x,y) = \sigma_{kj2}^{(i)}(x,y) + \sigma_{kj2}^{(h)}(x,y), \qquad (k,j = x,y). \tag{33}$$

In the surface crack problem under anti symmetric loading the solution given by Eqs. (32) and (33) must satisfy the following boundary and continuity conditions:

$$\sigma_{xx2}(0,y) = 0, \quad \sigma_{xy2}(0,y) = 0, \quad -\infty < y < \infty, \tag{34}$$

$$\sigma_{yy2}(x,+0) = \sigma_{yy2}(x,-0), \quad \sigma_{xy2}(x,+0) = \sigma_{xy2}(x,-0), \quad 0 < x < \infty, \tag{35}$$

$$v_2(x,+0) = v_2(x,-0), \qquad 0 < x < \infty, \tag{36}$$

$$\sigma_{xy2}(x,0) = -q(x), \qquad 0 < x < d, \tag{37a}$$

$$u_2(x,+0) = u_2(x,-0), \qquad d < x < \infty. \tag{37b}$$

Again, by replacing Eq. (37a) by Eq. (5b) and using the solution given by Eqs. (28)-(31), the conditions (34)-(37) may be reduced to a system of equations expressing the unknown functions $E_j(\omega)$, $(j = 1,\ldots,4)$, $G_3(\alpha)$ and $G_4(\alpha)$ in terms of the new unknown function $f_2(x)$ as follows:

$$E_j(\omega) = \frac{\kappa+1}{2\mu_0} Z_j(\omega) \int_0^d f_2(t)\exp(-i\omega t)dt, \tag{38}$$

$$\sum_{j=3}^{4}(i\omega(3-\kappa) + A_j n_j(1+\kappa))Z_j(\omega) - \sum_{j=1}^{2}(i\omega(3-\kappa) + A_j n_j(1+\kappa))Z_j(\omega) = 0, \tag{39a}$$

$$\sum_{j=3}^{4}(n_j + i\omega A_j)Z_j(\omega) - \sum_{j=1}^{2}(n_j + i\omega A_j)Z_j(\omega) = 0, \tag{39b}$$

$$\sum_{j=3}^{4} A_j Z_j(\omega) - \sum_{j=1}^{2} A_j Z_j(\omega) = 0, \tag{39c}$$

$$i\omega\Big\{Z_4(\omega) + Z_3(\omega) - Z_2(\omega) - Z_1(\omega)\Big\} = 1. \tag{39d}$$

$$\int_0^\infty \sum_{j=3}^{4}((\kappa+1)p_j - H_j\alpha(3-\kappa))G_j(\alpha)\sin(\alpha y)$$

$$+\frac{1}{2\pi}\int_{-\infty}^{\infty}\sum_{j=3}^{4}(i\omega(\kappa+1)+A_jn_j(3-\kappa))E_j(\omega)\exp(n_jy)d\omega = 0,\ \ 0<y<\infty, \tag{40a}$$

$$\int_0^\infty \sum_{j=3}^{4}(H_jp_j+\alpha)G_j(\alpha)\cos(\alpha y)$$

$$+\frac{1}{2\pi}\int_{-\infty}^{\infty}\sum_{j=3}^{4}(n_j+i\omega A_j)E_j(\omega)\exp(n_jy)d\omega = 0, \qquad 0<y<\infty. \tag{40b}$$

In this problem, too, because of symmetry it is sufficient to consider $y > 0$ half of the medium only. Also, by evaluating some of the integrals in closed from Eqs. (40a,b) may be reduced to

$$\sum_{j=3}^{4}((\kappa+1)p_j - H_j\alpha(3-\kappa))G_j^*(\alpha,t) = R_{xx2}(\alpha,t), \tag{41a}$$

$$\sum_{j=3}^{4}(H_jp_j+\alpha)G_j^*(\alpha,t) = R_{xy2}(\alpha,t), \tag{41b}$$

where

$$G_j(\alpha) = \frac{\kappa+1}{2\mu_0}\int_0^d G_j^*(\alpha,t)\exp\Big(\Big(\frac{\gamma}{2}-\lambda_1\Big)t\Big)f_2(t)dt, \tag{42}$$

and R_{xx2}, R_{xy2} and λ_1 are given in Appendix A.

3 The Integral Equations

By using the solution developed in Section 2 all stress and displacement components can be expressed in terms of $f_1(x)$ and $f_2(x)$ with appropriate kernels. Specifically, observing that the problem is uncoupled, using Eqs. (22) and (36), the conditions (23a) and (37a) which are yet to be satisfied may be written as

$$\sigma_{yy}(x,0) = \lim_{y\to 0}\int_0^d k_{11}(x,y,t)f_1(t)dt = -p(x), \quad 0<x<d, \tag{43}$$

$$\sigma_{xy}(x,0) = \lim_{y\to 0}\int_0^d k_{22}(x,y,t)f_2(t)dt = -q(x), \quad 0<x<d, \tag{44}$$

where the kernels k_{11} and k_{22} are given in Appendix B. Note that unlike the homogeneous half plane, in the graded medium with a surface crack $k_{11}(x,0,t)$ and $k_{22}(x,0,t)$ are not equal. The singular nature of the integral equations (43) and (44) and that of the solutions f_1 and f_2 may be determined by examining the asymptotic behavior of the integrands $K_{ss}^{(r)}$, $(r = i,h;\ s = 1,2)$ given in Appendix B. After performing the necessary analysis the integral equations (43) and (44) may be reduced to

$$\int_0^d \left[\frac{1}{\pi}\frac{1}{t-x} + h_{11s}(x,t) + h_{11f}(x,t)\right] f_1(t)dt = -\exp(-\gamma x)p(x),\ 0 < x < d, \quad (45a)$$

$$\int_0^d \left[\frac{1}{\pi}\frac{1}{t-x} + h_{22s}(x,t) + h_{22f}(x,t)\right] f_2(t)dt = -\exp(-\gamma x)q(x),\ 0 < x < d, \quad (45b)$$

where h_{11s} and h_{22s} are generalized Cauchy kernels (of the order $1/t$) that become unbounded as the arguments x and t tend to the end point zero simultaneously. The limits of these singular kernels are found to be:

$$\lim_{(x,t)\to 0} h_{11s}(x,t) = \lim_{\gamma\to 0} h_{11s}(x,t) = \lim_{(x,t)\to 0} h_{22s}(x,t) = \lim_{\gamma\to 0} h_{22s}(x,t) =$$

$$= \frac{1}{\pi}\left(\frac{1}{t+x} + \frac{2t}{(t+x)^2} - \frac{4t^2}{(t+x)^3}\right), \qquad 0 < (t,x) < d. \quad (46)$$

The expressions for h_{kks} and h_{kkf}, $(k = 1,2)$ are given in [12]. It may be observed that (46) is the standard expression found for edge cracks in homogeneous materials [13]. Thus, the solution of the integral equations may be expressed as

$$f_1(x) = (d-x)^{-1/2} f_1^*(x), \qquad 0 < x < d, \quad (47a)$$

$$f_2(x) = (d-x)^{-1/2} f_2^*(x), \qquad 0 < x < d, \quad (47b)$$

where $f_1^*(x)$ and $f_2^*(x)$ are unknown bounded functions. Note that, there is no singularity at the crack mouth $x = 0$, $y = 0$ while the standard square-root singularity is retained at the crack tip.

4 On the Solution of the Integral Equations

The integral equations are solved by using a collocation technique. First the intervals $(0,d)$ in (45) are normalized by defining,

$$f_i(t) = \phi_i(r), \qquad i = 1,2, \qquad -1 < r < 1, \tag{48a}$$

$$t = \frac{d}{2}r + \frac{d}{2}, \qquad 0 < t < d, \qquad -1 < r < 1, \tag{48b}$$

$$x = \frac{d}{2}s + \frac{d}{2}, \qquad 0 < x < d, \qquad -1 < s < 1. \tag{48c}$$

The solution may then be expressed as

$$\phi_1(r) = (1-r)^{-1/2}\sum_{n=0}^{\infty} A_{1n} P_n^{(-1/2,0)}(r), \tag{49a}$$

$$\phi_2(r) = (1-r)^{-1/2}\sum_{n=0}^{\infty} A_{2n} P_n^{(-1/2,0)}(r), \tag{49b}$$

where $P_n^{(-1/2,0)}(r)$, $-1 < r < 1$, are Jacobi polynomials. Substituting (49) in (45), truncating the infinite series at N and regularizing the singular terms, the integral equations become

$$\sum_{n=0}^{N}\left\{ -\frac{\Gamma(-1/2)\Gamma(n+1)}{\sqrt{2}\pi\Gamma(n+1/2)}\mathrm{F}(n+1, -n+1/2; 3/2; (1-s)/2) + m_{11n}(s)\right\} A_{1n} =$$

$$= -\exp(-\gamma d(1+s)/2) p(d(1+s)/2), \quad -1 < s < 1, \tag{50a}$$

$$\sum_{n=0}^{N}\left\{ -\frac{\Gamma(-1/2)\Gamma(n+1)}{\sqrt{2}\pi\Gamma(n+1/2)}\mathrm{F}(n+1, -n+1/2; 3/2; (1-s)/2) + m_{22n}(s)\right\} A_{2n} =$$

$$= -\exp(-\gamma d(1+s)/2) q(d(1+s)/2), \quad -1 < s < 1, \tag{50b}$$

where $\Gamma()$ is the Gamma function and $\mathrm{F}()$ is the hypergeometric function. Expressions for $m_{kkn}(s)$, $(k = 1,2)$ are given in Appendix B. Equations (50) are solved numerically using a collocation technique. The following roots of the Chebyshev polynomials are used as the collocation points:

$$s_j = \cos\left(\frac{\pi(2j-1)}{2(N+1)}\right), \qquad j = 1, \ldots, N+1. \tag{51}$$

After solving the integral equations for f_1 and f_2 stress intensity factors at the crack tip $(d, 0)$ may be evaluated by using the results. The stress intensity factors are defined by and calculated from

$$k_1 = \lim_{x\to d+0}\sqrt{2(x-d)}\sigma_{yy}(x,0) =$$

$$= -\lim_{x\to d-0}\frac{2\mu(x)}{\kappa+1}\sqrt{2(d-x)}\frac{\partial}{\partial x}(v(x,0^+)-v(x,0^-)), \tag{52a}$$

$$k_2 = \lim_{x\to d+0}\sqrt{2(x-d)}\sigma_{xy}(x,0) =$$

$$= -\lim_{x\to d-0}\frac{2\mu(x)}{\kappa+1}\sqrt{2(d-x)}\frac{\partial}{\partial x}(u(x,0^+)-u(x,0^-)). \tag{52b}$$

From (49) and (52) it then follows that

$$k_1 = -\exp(\gamma d)\sqrt{d}\sum_{n=0}^{N}A_{1n}P_n^{(-1/2,0)}(1), \tag{53a}$$

$$k_2 = -\exp(\gamma d)\sqrt{d}\sum_{n=0}^{N}A_{2n}P_n^{(-1/2,0)}(1). \tag{53b}$$

5 Results

The main results of this study are the variation of the stress intensity factors as functions of the material nonhomogeneity parameter γ. Some sample results are also obtained giving the crack opening displacements. Assuming that in practical applications the crack surface tractions for the perturbation problem would be sufficiently well-behaved continuous functions and may be approximated by fourth degree polynomials with sufficient accuracy, the input functions may be expressed as

$$p(x) = \sum_{n=0}^{4}\sigma_n(x/d)^n, \qquad q(x) = \sum_{n=0}^{4}\tau_n(x/d)^n, \tag{54a,b}$$

where the coefficients σ_n and τ_n are known constants. To facilitate the application of the results, the normalized stress intensity factors are given in Tables 1 and 2 in tabular form. It should be remarked that even though there are no restrictions on the coefficients τ_n, $\sigma_0, \ldots \sigma_4$ must be such that the resultant k_1 is positive. Otherwise the mode I problem has to be reconsidered as a crack closure problem and the contact region on the crack surface must be determined (by using $k_1(c_i) = 0$ as the closure criterion, c_i being the end points of the contact regions)

The calculated stress intensity factors for crack surface tractions (54) are also shown in Figures 2 and 3. The figures are self-explanatory: as the material nonhomogeneity parameter γ decreases, both k_1 and k_2 tend to increase, k_1 and k_2 are much more sensitive to the variations in γ for $\gamma < 0$ (for the "softening" material) than for $\gamma > 0$ and generally for a given γ the amplitude of k_1 is greater than that of k_2, particularly for $\gamma < 0$. The standard normalized stress intensity factors $k_1/\left(\sigma_0\sqrt{d}\right) = k_2/\left(\sigma_0\sqrt{d}\right) = 1.1215$ in an homogeneous half plane with a surface crack subjected to uniform pressure σ_0 and shear τ_0 are shown in Table 1 and Figures 2 - 4 as reference.

Figure 4 shows the results for fixed grip tensile $(\epsilon_{yy}(x, \mp\infty) = \epsilon_0)$ and shear $(\gamma_{xy}(x, \mp\infty) = \gamma_0)$ loading. Note that as the nonhomogeneity parameter γ increases, the normalized k_2 (dashed lines) monotonically increases, whereas k_1 goes through a minimum near $\gamma = 0$. The figure also shows the mode I results for a graded half plane under fixed grip loading ϵ_0 obtained in [9] (full circles). Not only is the agreement quite good, also somewhat paradoxial result concerning the slight increase in k_1 for $\gamma < 0$ is independently verified.

Figure 5 shows the influence of the Poisson's ratio ν on the modes I and II stress intensity factors in a graded half plane with a surface crack loaded by uniform crack surface tractions $p(x) = \sigma_0$ and $q(x) = \tau_0$. As shown in the previous studies, the effect of ν on k_1 does not seem to be significant. However, particularly for large values of γ, the influence of ν on k_2 could be significant.

Figures 7-10 show some sample results for the normalized crack opening displacements (COD). It may be observed that in all cases as γ increases (or as the stiffness of the medium increases), the crack opening displacements decrease, the influence of γ on COD is more significant for $\gamma < 0$ than for $\gamma > 0$, and generally for $\gamma < 0$ COD under mode I loading (σ_0 and σ) is greater than that under mode II loading (τ_0 and τ). These are all intuitively expected results.

Figure 11 describes a sample problem concerning a graded half plane with a surface crack loaded by a sliding rigid circular stamp. It is assumed that along the contact area $a < y < b$ the condition of Coulomb friction is valid with η as the coefficient of friction. For the geometry and the direction of loading shown, the results are given in Figures 12-14. Figures 12 and 13 show the modes I and II stress intensity factors, respectively. Figure 14 shows the normalized force P for a given contact area $((b-a)/R = 0.1)$ as a function of the stamp location. As expected, P increases with increasing material stiffness (or γ) and distance a. However, for (approximately) $(a/R) > 1$ P is very nearly constant. For details and extensive results see [12] and [13].

Acknowledgment

This study was supported by AFOSR under the grant F49620-98-1-0028.

Appendix A

Various Functions Used in the Solution of the Mixed Mode Crack Problem

$$R_{xx1}(\alpha,t)=\frac{1}{\pi}\frac{\kappa-1}{\kappa+1}\frac{\alpha^2}{\lambda_1\lambda_2(\lambda_1^2+\lambda_2^2)}\Big\{\gamma\lambda_2\cos(\lambda_2 t)+\big(\gamma\lambda_1-2\big(\lambda_1^2+\lambda_2^2\big)\sin(\lambda_2 t)\big)\Big\} \tag{A1}$$

$$R_{xy1}(\alpha,t)=-\frac{2}{\pi}\frac{1}{\kappa+1}\frac{\alpha}{\lambda_1\lambda_2(\lambda_1^2+\lambda_2^2)}\times$$

$$\times\Big\{\lambda_2\big(\lambda_1^2+\lambda_2^2+\gamma^2/4\big)\cos(\lambda_2 t)-\lambda_1\big(\lambda_1^2+\lambda_2^2-\gamma^2/4\big)\sin(\lambda_2 t)\Big\} \tag{A2}$$

$$R_{xx2}(\alpha,t)=-\frac{2}{\pi}\frac{\kappa-1}{\kappa+1}\frac{\alpha^3}{\lambda_1\lambda_2(\lambda_1^2+\lambda_2^2)}\Big\{\lambda_2\cos(\lambda_2 t)+\lambda_1\sin(\lambda_2 t)\Big\}, \tag{A3}$$

$$R_{xy2}(\alpha,t)=-\frac{1}{\pi}\frac{1}{\kappa+1}\frac{\alpha^2}{\lambda_1\lambda_2(\lambda_1^2+\lambda_2^2)}\times$$

$$\times\Big\{\gamma\lambda_2\cos(\lambda_2 t)+\Big(2\big(\lambda_1^2+\lambda_2^2\big)+\gamma\lambda_1\Big)\sin(\lambda_2 t)\Big\}, \tag{A4}$$

$$\lambda_1=\sqrt{\frac{R_1+R_2}{2}},\qquad \lambda_2=\sqrt{\frac{R_1-R_2}{2}}, \tag{A5a,b}$$

$$R_1=\sqrt{\left(\gamma^2/4+\alpha^2\right)^2+\alpha^2\gamma^2(3-\kappa)/(\kappa+1)}, \tag{A6}$$

$$R_2=\gamma^2/4+\alpha^2, \tag{A7}$$

Appendix B

Expressions for the Kernels $k_{11}(x,y,t)$ and $k_{22}(x,y,t)$

$$k_{11}(x,y,t)=k_{11}^{(i)}(x,y,t)+k_{11}^{(h)}(x,y,t), \tag{B1}$$

$$k_{22}(x,y,t)=k_{22}^{(i)}(x,y,t)+k_{22}^{(h)}(x,y,t), \tag{B2}$$

$$k_{11}^{(i)}(x,y,t)=\frac{\kappa+1}{\kappa-1}\frac{\exp(\gamma x)}{4\pi}\int_{-\infty}^{\infty}K_{11}^{(i)}(\omega,y)\exp(i\omega(x-t))d\omega, \tag{B3}$$

$$k_{11}^{(h)}(x,y,t) = \frac{\kappa+1}{\kappa-1}\frac{\exp(\gamma x)}{2}\int_0^\infty K_{11}^{(h)}(\alpha,t,x)\cos(\alpha y)d\alpha, \tag{B4}$$

$$k_{22}^{(i)}(x,y,t) = (\kappa+1)\frac{\exp(\gamma x)}{4\pi}\int_{-\infty}^\infty K_{22}^{(i)}(\omega,y)\exp(i\omega(x-t))d\omega, \tag{B5}$$

$$k_{22}^{(h)}(x,y,t) = (\kappa+1)\frac{\exp(\gamma x)}{2}\int_0^\infty K_{22}^{(h)}(\alpha,t,x)\cos(\alpha y)d\alpha, \tag{B6}$$

where the integrands are given as

$$K_{11}^{(i)}(\omega,y) = \sum_{j=3}^{4}(i\omega(3-\kappa)+A_j n_j(1+\kappa))P_j(\omega)\exp(n_j y), \tag{B7}$$

$$K_{22}^{(i)}(\omega,y) = \sum_{j=3}^{4}(n_j+i\omega A_j)Z_j(\omega)\exp(n_j y), \tag{B8}$$

$$K_{11}^{(h)}(\alpha,t,x) = \sum_{j=3}^{4}(p_j(3-\kappa)+D_j\alpha(1+\kappa))B_j^*(\alpha,t)\exp(p_j x+(\gamma/2-\lambda_1)t), \tag{B9}$$

$$K_{22}^{(h)}(\alpha,t,x) = \sum_{j=3}^{4}(\alpha+H_j p_j)G_j^*(\alpha,t)\exp(p_j x+(\gamma/2-\lambda_1)t). \tag{B10}$$

The terms used in Eq. (50) are in the following form:

$$m_{11n}(s) = \int_{-1}^{1}(1-r)^{-1/2}H_{11}(s,r)P_n^{(-1/2,0)}(r)dr, \tag{B11}$$

$$m_{22n}(s) = \int_{-1}^{1}(1-r)^{-1/2}H_{22}(s,r)P_n^{(-1/2,0)}(r)dr, \tag{B12}$$

$$H_{11}(s,r) = \frac{d}{2}\left\{h_{11s}\left(\frac{d}{2}s+\frac{d}{2},\frac{d}{2}r+\frac{d}{2}\right)+h_{11f}\left(\frac{d}{2}s+\frac{d}{2},\frac{d}{2}r+\frac{d}{2}\right)\right\}, \tag{B13}$$

$$H_{22}(s,r) = \frac{d}{2}\left\{h_{22s}\left(\frac{d}{2}s+\frac{d}{2},\frac{d}{2}r+\frac{d}{2}\right)+h_{22f}\left(\frac{d}{2}s+\frac{d}{2},\frac{d}{2}r+\frac{d}{2}\right)\right\}. \tag{B14}$$

References

[1] Yamanouchi, M., Koizumi, M., Hirai, T. and Shiota, I. eds., 1990, *FGM-90, Proc. 1st International Symposium on Functionally Gradient Materials*, FGM Forum, Tokyo, Japan.

[2] Holt, J.B., Koizumi, M., Hirai, T. and Munir, Z.A. eds., 1993, *FGM-92, Proc. 2nd International Symposium on Functionally Gradient Materials*, The American Ceramic Society, Westerville, Ohio.

[3] Ilschner, B. and Cherradi, N. eds., 1995, *FGM-94, Proc. 3rd International Symposium on Structural and Functional Gradient Materials*, Presses Polytechniques et Universitaires Romandes, Lausanne, Switzerland.

[4] Shiota, I. and Miyamoto, Y., eds., 1997, *FGM-96, Proc. 4th International Symposium on Functionally Graded Materials,* Elsevier Science, Amsterdam, The Netherlands.

[5] Kaysser, W.A. ed., 1999, *FGM-98, Proc. 5th International Symposium on Functionally Graded Materials,* Trans Tech Publications, Enfield, New Hampshire.

[6] Miyamoto, M., Kaysser, W.A., Rabin, B.H., Kawasaki, A. and Ford, R.G. eds., 1999, *Functionally Graded Materials: Design, Processing and Applications*, Kluwer Academic Publishers, Norwell, Massachusetts.

[7] Erdogan, F. and Wu, B.H., 1997, "The Surface Crack Problem for a Plate with Functionally Graded Properties," ASME J. Appl. Mech., **64**, pp. 449-456.

[8] Erdogan, F. and Wu, B.H., 1996, "Crack Problems in FGM Layers under Thermal Stresses," J. Thermal Stresses, **19**, pp. 237-265.

[9] Kasmalkar M., 1997, "The Surface Crack Problem for a Functionally Graded Coating Bonded to a Homogeneous Layer," Ph.D. Thesis, Lehigh University, Bethlehem, Pennsylvania.

[10] Erdogan, F., 1995, "Fracture Mechanics of Functionally Graded Materials," Composites Engineering, **5**, pp. 753-770.

[11] Erdogan, F., 1998, "Crack Problems in Nonhomogeneous Materials," *Fracture, A Topical Encyclopedia of Current Knowledge,* Cherepanov, G.P., ed., Krieger Publishing Company, Malabar, Florida, pp. 72-98.

[12] Dag, S. and Erdogan, F., 2001, "Cracking of a Graded Half Plane Due to Sliding Contact," Technical Report, AFOSR Grant F49620-98-1-0028.

[13] Dag, S. and Erdogan, F., 2001, "Cracking of a Homogeneous Half Plane Due to Sliding Contact," Technical Report, AFOSR Grant F49620-98-1-0028.

Table 1 Normalized mode I Stress Intensity factors

	$k_1/(\sigma_n d^{1/2})$				
γd	σ_0	$\sigma_1(x/d)$	$\sigma_2(x/d)^2$	$\sigma_3(x/d)^3$	$\sigma_4(x/d)^4$
-3.0	4.4345	1.9324	1.2148	0.8897	0.7076
-2.0	3.1238	1.4495	0.9525	0.7209	0.5879
-1.0	1.9846	1.0196	0.7152	0.5663	0.4774
-0.5	1.4988	0.8317	0.6099	0.4970	0.4274
0.0001	1.1215	0.6828	0.5255	0.4410	0.3868
0.5	1.0225	0.6439	0.5035	0.4264	0.3763
1.0	0.9930	0.6328	0.4974	0.4225	0.3735
2.0	0.9807	0.6289	0.4956	0.4215	0.3729
3.0	0.9884	0.6329	0.4981	0.4233	0.3743

Table 2 Normalized mode II Stress Intensity Factors

	$k_2/(\tau_n d^{1/2})$				
γd	τ_0	$\tau_1(x/d)$	$\tau_2(x/d)^2$	$\tau_3(x/d)^3$	$\tau_4(x/d)^4$
-3.0	1.6704	0.9273	0.6738	0.5437	0.4635
-2.0	1.4765	0.8398	0.6202	0.5063	0.4355
-1.0	1.2825	0.7534	0.5678	0.4700	0.4083
-0.5	1.1940	0.7144	0.5443	0.4539	0.3964
0.0001	1.1215	0.6829	0.5255	0.4410	0.3868
0.5	1.0727	0.6620	0.5132	0.4327	0.3807
1.0	1.0429	0.6497	0.5062	0.4280	0.3773
2.0	1.0164	0.6397	0.5008	0.4245	0.3749
3.0	1.0128	0.6394	0.5011	0.4249	0.3753

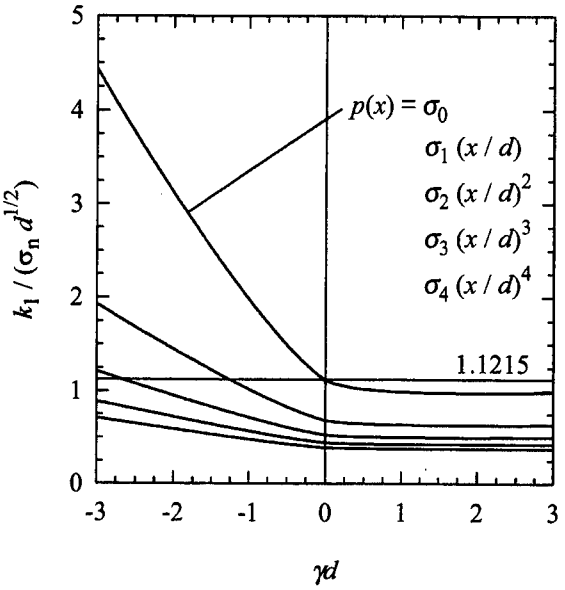

Fig. 2 Normalized mode I stress intensity factors, $\kappa = 2$, $\mu(x) = \mu_0 \exp(\gamma x)$.

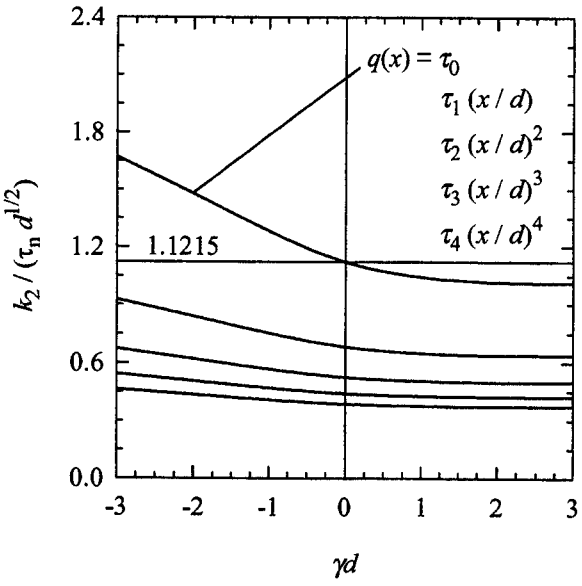

Fig. 3 Normalized mode II stress intensity factors, $\kappa = 2$, $\mu(x) = \mu_0 \exp(\gamma x)$.

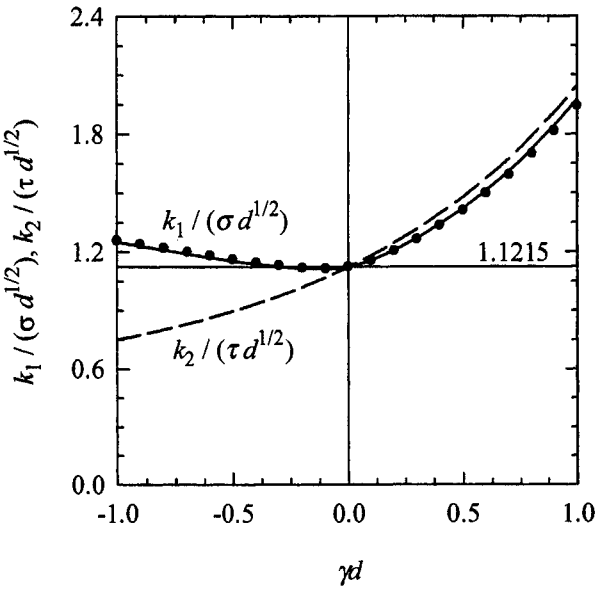

Fig. 4 Normalized modes I and II stress intensity factors for fixed grip tensile and shear loading, $\kappa = 1.8, \mu(x) = \mu_0 \exp(\gamma x)$, $\sigma = 8\mu_0\epsilon_0/(\kappa+1)$, $\tau = 8\mu_0\gamma_0/(\kappa+1)$.

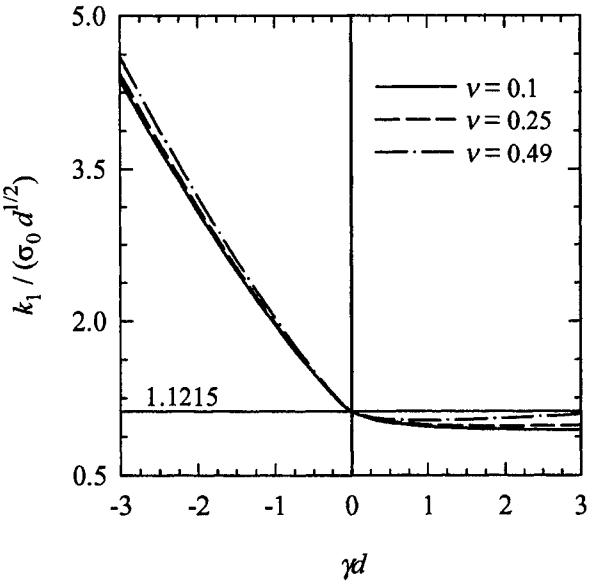

Fig. 5 Normalized mode I stress intensity factors for plane strain and for different values of Poisson's ratio, $\mu(x) = \mu_0 \exp(\gamma x)$.

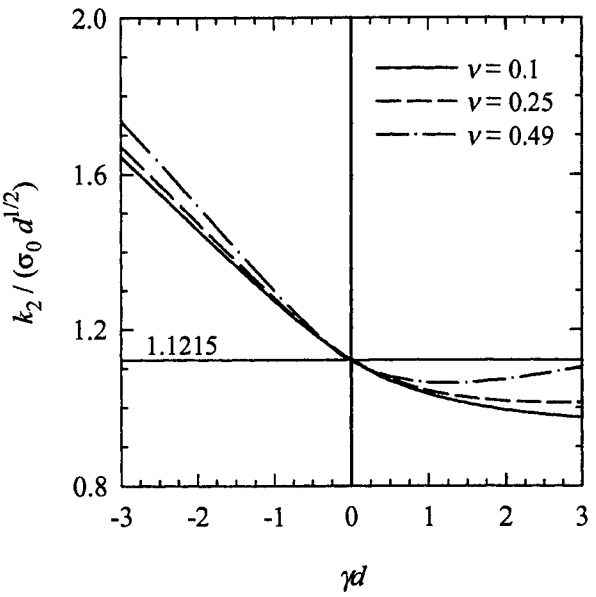

Fig. 6 Normalized mode II stress intensity factors for plane strain and for different values of Poisson's ratio, $\mu(x) = \mu_0 \exp(\gamma x)$.

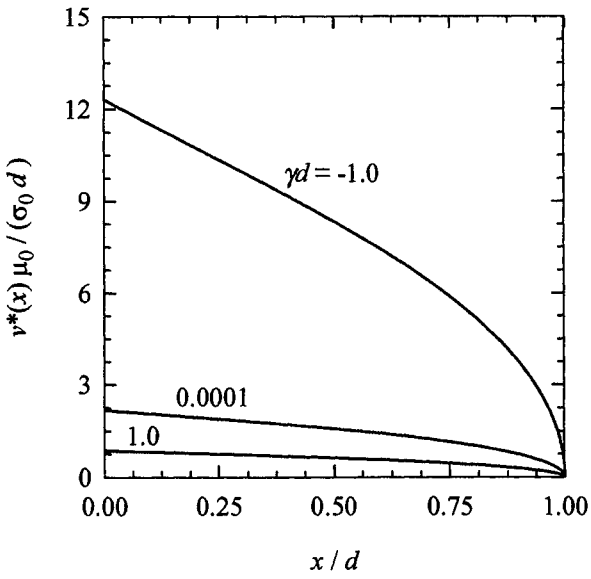

Fig. 7 Normal crack opening displacement, $v^*(x) = v(x, +0) - v(x, -0)$, $\sigma_{yy}(x, 0) = -\sigma_0$, $\kappa = 2$, $\mu = \mu_0 \exp(\gamma x)$.

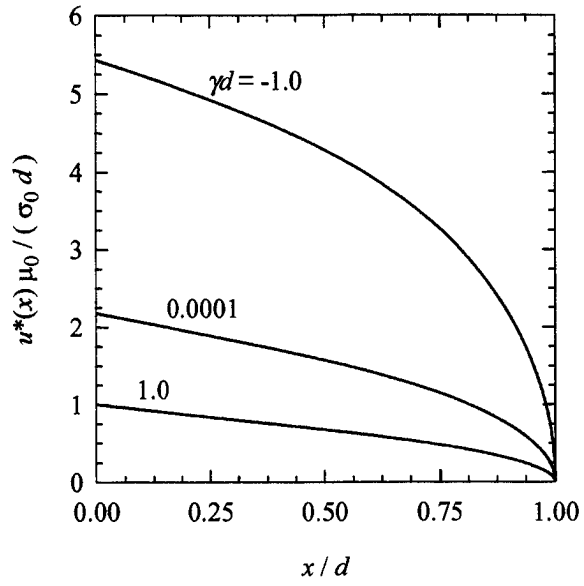

Fig. 8 Tangential crack opening displacement, $u^*(x) = u(x, +0) - u(x, -0)$, $\sigma_{xy}(x, 0) = -\tau_0$, $\kappa = 2$, $\mu = \mu_0 \exp(\gamma x)$.

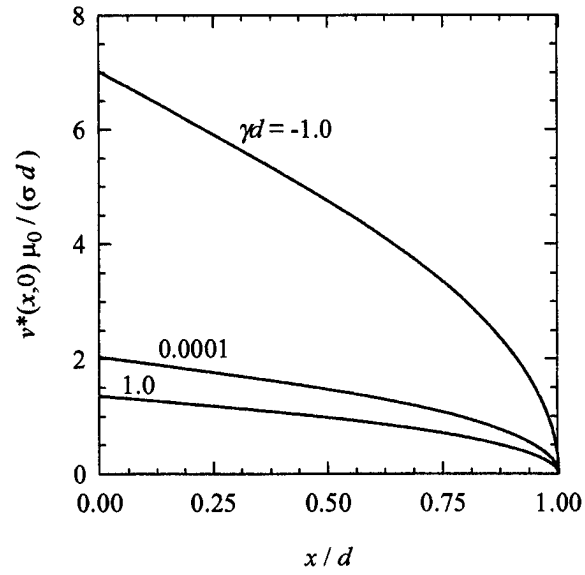

Fig. 9 Normal crack opening displacement for fixed grip loading, $v^*(x) = v(x, +0) - v(x, -0)$, $\sigma = 8\mu_0\epsilon_0/(\kappa + 1)$, $\kappa = 1.8$, $\mu = \mu_0 \exp(\gamma x)$.

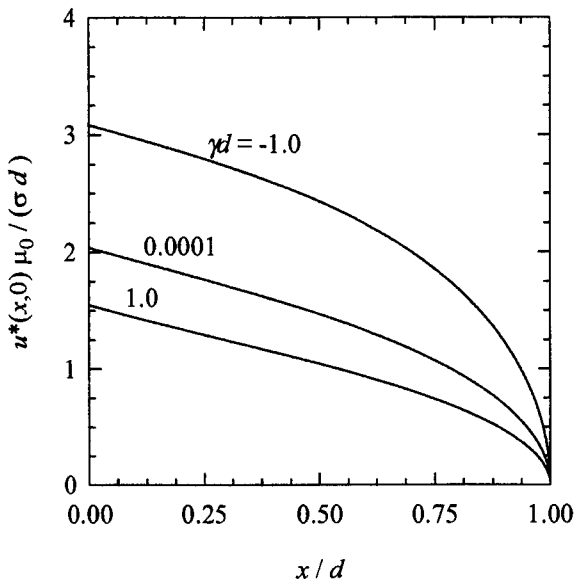

Fig.10 Tangential crack opening displacement for fixed grip loading, $u^*(x) = u(x, +0) - u(x, -0), \tau = 8\mu_0\gamma_0/(\kappa+1)$, $\kappa = 1.8$, $\mu(x) = \mu_0 \exp(\gamma x)$.

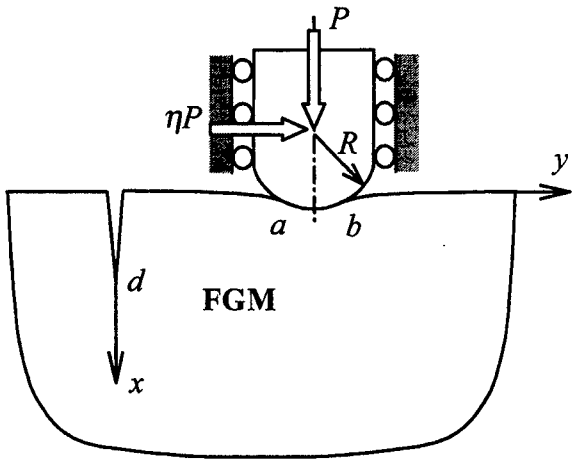

Fig. 11 A graded half plane with a surface crack loaded by a sliding rigid circular stamp.

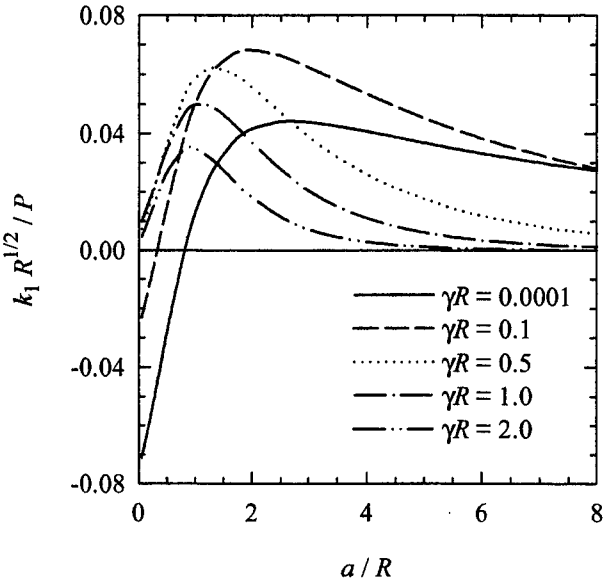

Fig. 12 Mode I stress intensity factors for a graded half plane loaded by a sliding circular stamp as shown in Figure 12, $(b-a)/R = 0.1$, $d/R = 0.1$, $\eta = 0.4$, $\kappa = 2$, $\mu(x) = \mu_0 \exp(\gamma x)$.

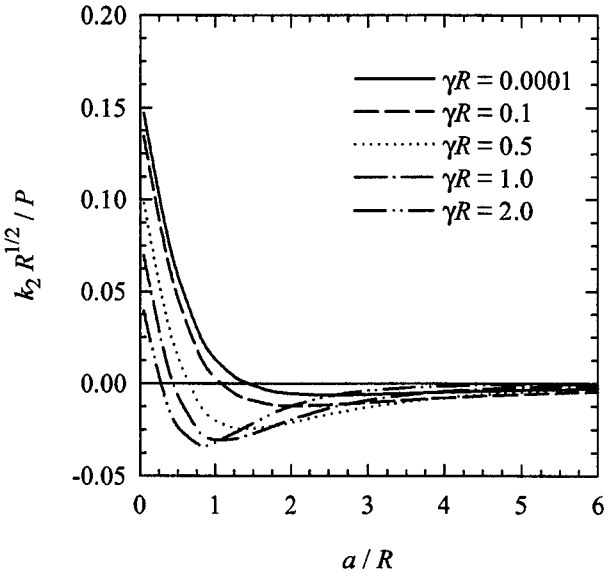

Fig. 13 Mode II stress intensity factors for a graded half plane loaded by a sliding circular stamp as shown in Figure 12, $(b-a)/R = 0.1$, $d/R = 0.1$, $\eta = 0.4$, $\kappa = 2$, $\mu(x) = \mu_0 \exp(\gamma x)$.

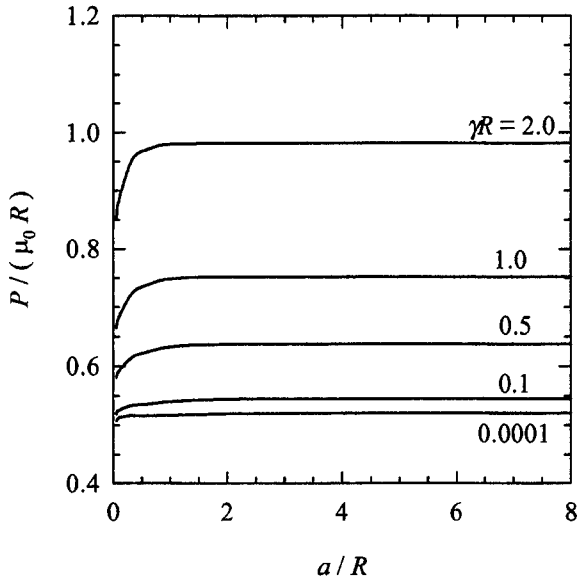

Fig. 14 Normalized force required for a given contact area $(b-a)/R = 0.1$, $d/R = 0.1$, $\eta = 0.4$, $\kappa = 2.0$, $\mu(x) = \mu_0 \exp(\gamma x)$.

APPENDIX C

Fracture of graded materials due to sliding contact

Serkan Dag, Fazil Erdogan*

Department of Mechanical Engineering and Mechanics, Lehigh University,

19 Memorial Drive West, Bethlehem, PA 18015, USA

Abstract

In this article the initiation and subcritical growth of surface cracks in graded materials due to sliding contact are considered. After a brief introduction the general coupled crack/contact problem for a semi-infinite graded medium subjected to a sliding rigid stamp of arbitrary profile is formulated. Solving the problem in the absence of any cracks, the complete stress state on the surface of the medium is evaluated and the critical stress that would cause the surface crack initiation is identified. The coupled problem is then solved, stress intensity factors are calculated and some results are presented.

Keywords: Functionally graded materials; Sliding contact/crack problems; Stress intensity factors.

1. Introduction

Graded materials, also known as *functionally graded materials* (FGMs) are multiphase composites with continuously varying volume fractions and, as a result, thermomechanical properties. Used as coatings and interfacial zones they reduce the residual and thermal stresses resulting from the material property mismatch, increase the bonding strength, improve surface properties and provide protection against severe thermal and chemical environments. Many of the present and potential applications of FGMs involve contact problems. These are mostly load transfer problems in deformable solids, generally in the presence of friction as in, for example, bearings, gears, cams, machine tools and abradable seals in gas turbines. In such applications the concept of

* Corresponding author. Tel.: + 1-610-758-4099; Fax: + 1-610-758-6224.

E-mail address: fe00@lehigh.edu (F. Erdogan).

material property grading appears to be ideally suited to improve the surface properties and wear-resistance of the components that are in contact.

From the standpoint of failure mechanics an important aspect of contact problems is the surface cracking which is caused by friction forces and which invariably leads to fretting fatigue. In most applications material property grading near the surface is used as a substitute for homogeneous ceramic coatings. In both cases that is, in both homogeneous and graded coatings the surface of the composite medium consists of 100% ceramic which generally is a brittle solid. Hence, the "maximum tensile stress" criterion may be used for crack initiation on the surface. Once the crack is initiated, its subcritical growth under repeated loading by a sliding stamp is controlled by stress intensity factors at the crack tip. The main objective of this study is, therefore, the evaluation of peak tensile stresses on the surface for the purpose of studying crack initiation and the stress intensity factors for modeling the subcritical crack growth. Specifically, the objective is the examination of the influence of friction coefficient and material nonhomogeneity parameters on the peak surface stresses and stress intensity factors. The problem is considered under the assumptions of plane strain, Coulomb friction and linear nonhomogeneous elasticity.

Studies in contact mechanics in elastic solids were originated by Hertz [1]. The technical literature on the subject is very extensive. A thorough description of the underlying solid mechanics problems in homogenous materials may be found, for example, in [2]. Some sample solutions for frictionless contact problems in a semi-infinite graded medium are given in [3]-[5]. Details of the analysis of homogeneous substrates with FGM coatings having positive or negative curvatures and extensive results regarding the stress distribution under plane strain conditions and sliding contact are discussed in [6]. The crack/contact problem described in Figure 1 has also been considered in [7] for a homogeneous half-plane by using the conformal mapping technique. Even though the square root singularity at the crack tip is embedded in the technique, the procedure used in [7] does not account for the singularities at the end points of the contact region a and b, particularly when $a = 0$ (see, Figure 2). Also, for some reason in [7] the mode II stress intensity factor k_2 is calculated to be negative, implying that under the loading by a sliding stamp the surface crack would tend to curve forward in the direction of the moving stamp, whereas the experimental results (e.g., [8]) and the results found in this study show the opposite.

2. Formulation of the general crack/contact problem

The coupled crack/contact problem for a nonhomogeneous half plane considered in this study is described in Figure 1. Largely for mathematical expediency it will be assumed that the elastic parameters of the medium may be approximated by

$$\mu(x) = \mu_0 \exp(\gamma x), \qquad \kappa = \text{constant} \tag{1a,b}$$

where μ is the shear modulus, γ is the nonhomogeneity parameter, $\kappa = 3 - 4\nu$ for plane strain and $\kappa = (3-\nu)/(1+\nu)$ for the generalized plane stress, ν being the Poisson's ratio. By using the Hooke's law

$$\sigma_{xx}(x,y) = \frac{\mu(x)}{\kappa - 1}\left\{(\kappa+1)\frac{\partial u}{\partial x} + (3-\kappa)\frac{\partial v}{\partial y}\right\}, \tag{2a}$$

$$\sigma_{yy}(x,y) = \frac{\mu(x)}{\kappa - 1}\left\{(\kappa+1)\frac{\partial v}{\partial y} + (3-\kappa)\frac{\partial u}{\partial x}\right\}, \tag{2b}$$

$$\sigma_{xy}(x,y) = \mu(x)\left\{\frac{\partial u}{\partial y} + \frac{\partial v}{\partial x}\right\}, \tag{2c}$$

the equilibrium equations $\sigma_{ij,j} = 0$ become

$$(\kappa+1)\frac{\partial^2 u}{\partial x^2} + (\kappa-1)\frac{\partial^2 u}{\partial y^2} + 2\frac{\partial^2 v}{\partial x \partial y} + \gamma(\kappa+1)\frac{\partial u}{\partial x} + \gamma(3-\kappa)\frac{\partial v}{\partial y} = 0, \tag{3a}$$

$$(\kappa+1)\frac{\partial^2 v}{\partial y^2} + (\kappa-1)\frac{\partial^2 v}{\partial x^2} + 2\frac{\partial^2 u}{\partial x \partial y} + \gamma(\kappa-1)\frac{\partial v}{\partial x} + \gamma(\kappa-1)\frac{\partial u}{\partial y} = 0. \tag{3b}$$

In previous studies (e.g., [9]) it was shown that the stress intensity factors in graded materials are not significantly influenced by the variation in ν. Thus, in this study, too, the Poisson's ratio will be assumed to be constant. Equations (3) must be solved under the following conditions:

$$\sigma_{xx}(0,y) = 0, \qquad \sigma_{xy}(0,y) = 0, \qquad -\infty < y < a, \; b < y < \infty, \tag{4a,b}$$

$$\sigma_{xy}(0,y) = \eta\sigma_{xx}(0,y), \qquad \frac{4\mu_0}{\kappa+1}\frac{\partial}{\partial y}u(0,y) = f(y), \qquad a < y < b, \tag{5a,b}$$

$$\sigma_{yy}(x,0) = 0, \qquad \sigma_{xy}(x,0) = 0, \qquad 0 < x < d, \tag{6a,b}$$

$$\int_a^b \sigma_{xx}(0,y)dy = -P, \tag{7}$$

$$\epsilon_{yy}(x,\pm\infty) = \epsilon_0, \tag{8}$$

where η is the coefficient of friction and the known function $f(y)$ defines the stamp profile. Note that, in addition to $f(y)$, the external loads are described by the resultant force P, the remote strain ϵ_0 and the crack surface tractions given by (6). We also observe that the unknown functions of the problem may be identified as follows (Figure 1):

$$\frac{2\mu_0}{\kappa+1}\frac{\partial}{\partial x}(v(x,0^+)-v(x,0^-)) = f_1(x), \qquad 0<x<d, \tag{9a}$$

$$\frac{2\mu_0}{\kappa+1}\frac{\partial}{\partial x}(u(x,0^+)-u(x,0^-)) = f_2(x), \qquad 0<x<d, \tag{9b}$$

$$\sigma_{xx}(0,y) = f_3(y), \qquad a<y<b. \tag{10}$$

By using the Fourier transforms, the mixed boundary value problem under consideration may be reduced to a system of integral equations of the following form:

$$\sigma_{yy}(x,0) = \int_0^d \Big[k_{11}(x,t)f_1(t)+k_{12}(x,t)f_2(t)\Big]dt + \int_a^b k_{13}(x,t)f_3(t)dt + E(x)\epsilon_0 = 0$$
$$0<x<d, \tag{11a}$$

$$\sigma_{xy}(x,0) = \int_0^d \Big[k_{21}(x,t)f_1(t)+k_{22}(x,t)f_2(t)\Big]dt + \int_a^b k_{23}(x,t)f_3(t)dt = 0,$$
$$0<x<d, \tag{11b}$$

$$\frac{4\mu_0}{\kappa+1}\frac{\partial}{\partial y}u(0,y) = \int_0^d \Big[k_{31}(y,t)f_1(t)+k_{32}(y,t)f_2(t)\Big]dt + \int_a^b k_{33}(y,t)f_3(t)dt =$$
$$= f(y), \qquad a<y<b, \tag{11c}$$

where the kernels k_{ij} may be expressed in terms of infinite integrals with known integrands by using MAPLE and the residue theorem. For example, consider the kernels k_{j3}, $j=1,2,3$, that arise from the contact problem, that is, in Figure 1 and (11) by letting $d=0$. Using Fourier transforms, from (3) it can be shown that

$$u_3(x,y) = \frac{1}{2\pi}\int_{-\infty}^{\infty}\sum_{j=1}^{2} M_j \exp(s_j x + i\rho y)d\rho, \tag{12a}$$

$$v_3(x,y) = \frac{1}{2\pi}\int_{-\infty}^{\infty}\sum_{j=1}^{2} M_j N_j \exp(s_j x + i\rho y)d\rho, \tag{12b}$$

where

$$N_j(\rho) = \frac{i\Big((\kappa+1)s_j^2 + \gamma(\kappa+1)s_j + \rho^2(1-\kappa)\Big)}{\rho(2s_j + \gamma(3-\kappa))}, \qquad (j=1,2) \tag{13}$$

and s_1, s_2 are the roots of characteristic equation with negative real parts. The characteristic equation and its roots are given by

$$\big(s^2 + \gamma s - \rho^2 - i|\rho|\delta\big)\big(s^2 + \gamma s - \rho^2 - i|\rho|\delta\big) = 0, \quad \delta = |\gamma|\sqrt{\frac{3-\kappa}{\kappa+1}}, \tag{14a,b}$$

$$s_1 = -\frac{1}{2}\gamma - \frac{1}{2}\sqrt{\gamma^2 + 4\rho^2 + 4i|\rho|\delta}, \qquad \Re(s_1) < 0, \tag{15a}$$

$$s_2 = -\frac{1}{2}\gamma - \frac{1}{2}\sqrt{\gamma^2 + 4\rho^2 - 4i|\rho|\delta}, \qquad \Re(s_2) < 0, \tag{15b}$$

$$s_3 = -\frac{1}{2}\gamma + \frac{1}{2}\sqrt{\gamma^2 + 4\rho^2 + 4i|\rho|\delta}, \qquad \Re(s_3) > 0, \tag{15c}$$

$$s_4 = -\frac{1}{2}\gamma + \frac{1}{2}\sqrt{\gamma^2 + 4\rho^2 - 4i|\rho|\delta}, \qquad \Re(s_4) > 0. \tag{15d}$$

The functions $M_j(\rho)$ are given as

$$M_j(\rho) = \psi_j(\rho)\int_a^b f_3(t)\exp(-i\rho t)dt \qquad (j=1,2), \tag{16}$$

where ψ_1 and ψ_2 are given by

$$\sum_{j=1}^{2}(s_j(\kappa+1) + i\rho N_j(3-\kappa))\psi_j(\rho) = \frac{\kappa-1}{\mu_0}, \tag{17a}$$

$$\sum_{j=1}^{2}(i\rho + N_j s_j)\psi_j(\rho) = \frac{\eta}{\mu_0}. \tag{17b}$$

In (12), the subscript 3 stands for the displacements due to stamp loading only. After determining u_3 and v_3, referring to (11) and using the stress-strain relations the kernels may be obtained as follows:

$$k_{13}(x,t) = \frac{1}{2\pi}\frac{\mu(x)}{\kappa-1}\int_{-\infty}^{\infty}\sum_{j=1}^{2}(s_j(3-\kappa)+i\rho N_j(\kappa+1))\psi_j(\rho)\exp(s_jx-i\rho t)d\rho, \quad (18a)$$

$$k_{23}(x,t) = \frac{\mu(x)}{2\pi}\int_{-\infty}^{\infty}\sum_{j=1}^{2}(i\rho+N_js_j)\psi_j(\rho)\exp(s_jx-i\rho t)d\rho, \quad (18b)$$

$$k_{33}(y,t) = \frac{1}{2\pi}\frac{4\mu_0}{\kappa+1}\int_{-\infty}^{\infty}i\rho(\psi_1(\rho)+\psi_2(\rho))\exp(i\rho(y-t))d\rho. \quad (18c)$$

For future reference, one may also express the in-plane component of the stress on the surface due to the stamp loading as

$$\sigma_{yy3}(0,y) = \int_a^b k_{y3}(y,t)f_3(t)dt, \quad (19)$$

$$k_{y3}(y,t) = \frac{1}{2\pi}\frac{\mu_0}{\kappa-1}\int_{-\infty}^{\infty}\sum_{j=1}^{2}(s_j(3-\kappa)+i\rho N_j(\kappa+1))\psi_j(\rho)\exp(i\rho(y-t))d\rho. \quad (20)$$

The remaining kernels k_{ij} $(i=1,2,3;\ j=1,2)$ are obtained by following a procedure which is somewhat more complicated than but essentially quite similar to that followed for the kernels, k_{j3}, $(j=1,2,3)$. The symmetry conditions require that $\sigma_{yy2}(x,0)=0$ for $f_1(t)=0$, $f_2(t)\neq 0$, $f_3(t)=0$, and $\sigma_{xy1}(x,0)=0$ for $f_1(t)\neq 0$, $f_2(t)=0$, $f_3(t)=0$, from which it follows that

$$k_{12}(x,t)=0, \qquad k_{21}(x,t)=0. \quad (21a,b)$$

The details of the analysis and derivation of the remaining kernels, k_{11}, k_{22}, k_{31} and k_{32} may be found in [10]. After obtaining the unknown functions f_1, f_2 and f_3 the stresses and displacements in the graded medium may be determined from equations (2) and (12), (16) and their equivalents for nonvanishing f_1 and f_2.

3. Singular behavior of the solution

Singular nature of the integral equations (11) and, consequently, the singular behavior of the unknown functions f_1, f_2 and f_3 are obtained by examining the singularities of the kernels k_{ij}. In the problem under consideration the kernels have the form, (see, for example, (18))

$$k_{ij}(x^*,t) = \int_{-\infty}^{\infty} K_{ij}(x^*,t,\rho)d\rho, \ (i,j=1,2,3), \tag{22}$$

where $x^* = x$ for $i = 1,2$ and $x^* = y$ for $i = 3$. It can be shown that [10] with the exception of one case that will be discussed below, the integrands K_{ij} in (22) are bounded and continuous for $\rho < \infty$ and integrable at $\rho = 0$. The singular nature of the kernels k_{ij} is, therefore, determined by examining the asymptotic behavior of $K_{ij}(x^*,t,\rho)$ as ρ tends to infinity. Designating the asymptotic values of K_{ij} by K_{ij}^{∞} and by evaluating the integrals

$$\int_{-\infty}^{\infty} K_{ij}^{\infty}(x^*,t,\rho)d\rho, \tag{23}$$

in closed form, the system of integral equations (11) may be expressed as follows:

$$\sigma_{yy}(x,0)\exp(-\gamma x) = \int_0^d \left[\frac{1}{\pi}\frac{1}{t-x} + h_{11s}(x,t) + h_{11f}(x,t)\right] f_1(t)dt$$

$$+ \int_a^b \left[h_{13s}(x,t) + h_{13f}(x,t)\right] f_3(t)dt + E_0\epsilon_0 = 0, \qquad 0 < x < d, \tag{24a}$$

$$\sigma_{xy}(x,0)\exp(-\gamma x) = \int_0^d \left[\frac{1}{\pi}\frac{1}{t-x} + h_{22s}(x,t) + h_{22f}(x,t)\right] f_2(t)dt$$

$$+ \int_a^b \left[h_{23s}(x,t) + h_{23f}(x,t)\right] f_3(t)dt = 0, \qquad 0 < x < d, \tag{24b}$$

$$\frac{4\mu_0}{1+\kappa}\frac{\partial}{\partial y}u(0,y) = \int_0^d \Big[h_{31s}(y,t) + h_{31f}(y,t)\Big] f_1(t)dt$$

$$+ \int_0^d \Big[h_{32s}(x,t) + h_{32f}(x,t)\Big] f_2(t)dt$$

$$-\frac{1}{\pi}\int_a^b \frac{f_3(t)}{t-y}dt - \eta\frac{\kappa-1}{\kappa+1}f_3(y) + \int_a^b h_{33f}(y,t)f_3(t)dt = f(y), \qquad a<y<b, \quad (24c)$$

where $h_{ijs}(x^*,t)$ are additional singular kernels (of the order $1/t$) that become unbounded as the arguments x^* and t tend to the end point zero simultaneously and are evaluated from (23) whereas $h_{ijf}(x^*,t)$ are bounded in their respective closed intervals and are evaluated (numerically) from the integrals

$$\int_{-\infty}^{\infty}\Big[K_{ij}(x^*,t,\rho) - K_{ij}^{\infty}(x^*,t,\rho)\Big]d\rho. \qquad (25)$$

Evaluating the integrals (23), the singular kernels are found to be

$$\lim_{(x,t)\to 0} h_{11s}(x,t) = \lim_{(x,t)\to 0} h_{22s}(x,t) =$$

$$= \frac{1}{\pi}\left(\frac{1}{t+x} + \frac{2t}{(t+x)^2} - \frac{4t^2}{(t+x)^3}\right), \qquad 0<(t,x)<d, \qquad (26a)$$

$$\lim_{(x,t)\to 0} h_{13s}(x,t) = \frac{1}{\pi}\left(\frac{2xt^2}{(t^2+x^2)^2} - \eta\frac{2t^3}{(t^2+x^2)^2}\right), \quad a<t<b, \quad 0<x<d, \qquad (26b)$$

$$\lim_{(x,t)\to 0} h_{23s}(x,t) = \frac{1}{\pi}\left(\eta\frac{2xt^2}{(t^2+x^2)^2} - \frac{2tx^2}{(t^2+x^2)^2}\right), \quad a<t<b, \quad 0<x<d, \qquad (26c)$$

$$\lim_{(y,t)\to 0} h_{31s}(y,t) = -\frac{1}{\pi}\frac{4t^2y}{(t^2+y^2)^2}, \quad 0<t<d, \qquad a<y<b, \qquad (26d)$$

$$\lim_{(y,t)\to 0} h_{32s}(y,t) = -\frac{1}{\pi}\frac{4t^3}{(t^2+y^2)^2}, \quad 0<t<d, \qquad a<y<b. \qquad (26e)$$

Note that the singular kernels h_{11s} and h_{22s} given by (26a) are the standard expressions found for edge cracks in homogeneous materials [10], [11].

The singular behavior of the unknown functions f_1, f_2 and f_3 at the end points of their respective intervals may be determined by carrying out a function theoretic analysis [12], [13]. The two cases, $a > 0$ and $a = 0$ are considered separately.

$a > 0$

In this case we observe that the kernels (26b-e) are bounded in their corresponding closed intervals and would not contribute to the singularities of the functions f_1, f_2 and f_3. Expressing f_i by

$$f_1(x) = x^{\theta_1}(d-x)^{\lambda_1}F_1(x), \qquad 0 < x < d, \tag{27a}$$

$$f_2(x) = x^{\theta_2}(d-x)^{\lambda_2}F_2(x), \qquad 0 < x < d, \tag{27b}$$

$$f_3(x) = (y-a)^{\omega}(b-y)^{\beta}F_3(y), \qquad a < y < b, \tag{27c}$$

and substituting in (24), the conditions of boundedness of $\sigma_{yy}(x,0)$ and $\sigma_{xy}(x,0)$ in $0 < x < d$ and $f(y)$ in $a < y < b$ would give the following equations to determine θ_1, λ_1, θ_2, λ_2, ω and β :

$$\theta_1 = 0, \quad \theta_2 = 0, \tag{28a,b}$$

$$\cot(\pi\lambda_1) = 0, \quad \cot(\pi\lambda_2) = 0, \quad (\lambda_1 = \lambda_2 = -0.5), \tag{29a,b}$$

$$\cot(\pi\omega) = \eta\frac{\kappa-1}{\kappa+1}, \quad \cot(\pi\beta) = -\eta\frac{\kappa-1}{\kappa+1}, \tag{30a,b}$$

where the acceptable roots are $\lambda_1 = -0.5$, $\lambda_2 = -0.5$, $\Re(\omega) < 0$, if a is known and is a sharp corner, $\Re(\omega) > 0$ if a is unknown and is a point of smooth contact. Similarly, $\Re(\beta) < 0$ if b is a known sharp corner and $\Re(\beta) > 0$ if b is unknown and the contact is smooth.

$a = 0$

In this case all kernels $h_{ijs}(x^*,t)$ become unbounded as $x^* \to 0$ and $t \to 0$ simultaneously and contribute to the singularity of the unknown functions. Again, we express the unknown functions in the following form:

$$f_1(x) = x^{\alpha}(d-x)^{\lambda_1}G_1(x), \qquad 0 < x < d, \tag{31a}$$

$$f_2(x) = x^{\alpha}(d-x)^{\lambda_2}G_2(x), \qquad 0 < x < d, \tag{31b}$$

$$f_3(y) = y^{\alpha}(b-y)^{\beta}G_3(y), \qquad 0 < y < b. \tag{31c}$$

Now, by substituting (31) into (24), evaluating the singular integrals by using the complex function theory [12], multiplying both sides of the equations first by $(d-x)^{-\lambda_1}$ then by $(d-x)^{-\lambda_2}$ and letting $x \to d$, and then by $(b-y)^{-\beta}$ and letting $y \to b$ we find

$$\cot(\pi\lambda_1) = 0, \qquad \cot(\pi\lambda_2) = 0, \qquad \lambda_1 = \lambda_2 = -0.5. \tag{32a, b}$$

$$\cot(\pi\beta) + \eta\frac{\kappa-1}{\kappa+1} = 0. \tag{33}$$

Similarly, after integrating all singular kernels if we multiply both sides of (24a-c) by $x^{-\alpha}$, $x^{-\alpha}$ and $y^{-\alpha}$, respectively, and let $x \to 0$, $y \to 0$, we obtain the following system of equations to determine α:

$$\begin{bmatrix} a_{11}(\alpha) & 0 & a_{13}(\alpha) \\ 0 & a_{21}(\alpha) & a_{23}(\alpha) \\ a_{31}(\alpha) & a_{32}(\alpha) & a_{33}(\alpha) \end{bmatrix} \begin{bmatrix} \sqrt{d}G_1(0) \\ \sqrt{d}G_2(0) \\ b^\beta G_3(0) \end{bmatrix} = \begin{bmatrix} 0 \\ 0 \\ 0 \end{bmatrix}, \tag{34}$$

where the coefficient matrix $a_{ij}(\alpha)$ is known in closed form. Since $G_i(0) \neq 0$, for a nontrivial solution the characteristic equation to determine α is obtained by expressing $|a_{ij}(\alpha)| = 0$, giving

$$\frac{2\alpha^2+4\alpha+1-\cos(\pi\alpha)}{(\kappa+1)\sin(\pi\alpha)} \times$$

$$\times\,(\eta(4\alpha^2+10\alpha+5+(\kappa-1)\cos(\pi\alpha)+\kappa(2\alpha+3))+(\kappa+1)\sin(\pi\alpha)) = 0. \tag{35}$$

The eigenvalue problem (34) yields the following additional compatibility equations which relate $G_1(0)$, $G_2(0)$ and $G_3(0)$ and which must be taken into consideration in the numerical solution of the integral equations (24):

$$G_1(0)\sqrt{d} = \frac{\eta\cos(\pi\alpha/2)(2+\alpha)+\sin(\pi\alpha)(1+\alpha)}{2\alpha^2+4\alpha+1-\cos(\pi\alpha)} G_3(0)b^\beta, \tag{36a}$$

$$G_2(0)\sqrt{d} = \frac{\eta\sin(\pi\alpha/2)(1+\alpha)-\cos(\pi\alpha/2)\alpha}{2\alpha^2+4\alpha+1-\cos(\pi\alpha)} G_3(0)b^\beta. \tag{36b}$$

Note that the main results of the asymptotic analysis expressed by (28)-(30) and (32)-(34) are independent of μ_0 and the material nonhomogeneity parameter γ and are dependent on the Poisson's ratio (through κ) and the coefficient of friction η only,

meaning that in the coupled problem considered the stress singularities for graded and homogeneous materials are identical.

The characteristic equation (35) has been verified independently by considering the 90-degree elastic wedge under appropriate boundary conditions and by using Mellin transforms (see Appendix A).

For a constant Poisson's ratio $\nu = 0.25$ Figure 2 shows the singularities associated with a rigid flat stamp. For $a > 0$ the contact stresses are given by $\sigma_{xx}(0,y) = f_3(y)$, $\sigma_{xy}(0,y) = \eta f_3(y)$ and referring to (27c), the singularities ω and β are obtained from (30). Note that in the case of sliding contact the physically relevant problem is related to $a \geq 0$ and $\eta > 0$, otherwise the contact stresses would tend to close the crack. Thus, for $\eta > 0$ from Figure 2 it is seen that the trailing end of the stamp has a stronger and the leading end a weaker singularity than the frictionless stamp problem, that is $-\omega > 0.5$ and $-\beta < 0.5$. Similarly, in the smooth contact case $\omega > 0$, $\beta > 0$, $\beta > 1/2 > \omega$ and again the contact stresses are concentrated near the trailing end of the stamp. Figure 2 also shows the singularity α at $a = 0$ for the flat stamp obtained from (35). α is real and negative for $\eta > 0$ and $\alpha = 0$ for $\eta = 0$. Also for $\eta < 0$, $\Re(\alpha) > 0$ and for $\eta \lesssim -0.16$ α is complex.

4. The contact problem for decreasing stiffness ($\gamma < 0$)

Consider the sliding contact problem for a graded medium without a surface crack and remote loading ϵ_0. The half-plane is thus subjected to a pair of unbalanced resultant forces P and ηP. In formulating the general problem in the previous sections it was stated that the integrands $K_{ij}(x^*,t,\rho)$ in (22) are integrable around $\rho = 0$, with one exception that being K_{33} for $\gamma < 0$. All other integrands appear to be well-behaved at $\rho = 0$ for all values of γ. From (18) and (22) the infinite integral giving k_{33} may be expressed as

$$k_{33}(y,t) = \frac{1}{2\pi}\int_0^\infty \Big[H_1(\rho)\sin(\rho(y-t)) + \eta H_2(\rho)\cos(\rho(y-t))\Big]d\rho. \tag{37}$$

For the homogeneous medium $\gamma = 0$, $K_{33} = K_{33}^{\infty}$ and the kernel k_{33} is evaluated in closed form as shown in (24c). For $\gamma \neq 0$ the asymptotic expansion of $H_1(\rho)$ and $H_2(\rho)$ near $\rho = 0$ gives

$$H_1(\rho) = a_1\rho + a_3\rho^3 + \mathrm{O}(\rho^5), \tag{38a}$$

$$a_1 = \frac{8(\kappa-1)}{\gamma(\kappa+1)^2}, \qquad a_3 = \frac{32(\kappa-3)(\kappa(1+\text{sign}(\gamma))-4)}{\gamma^3(\kappa+1)^3(1+\text{sign}(\gamma))}, \tag{38b,c}$$

$$H_2(\rho) = b_2\rho^2 + b_4\rho^4 + b_6\rho^6 + \mathrm{O}(\rho^8), \tag{39a}$$

$$b_2 = \frac{16(2-\kappa)}{\gamma^2(1+\kappa)^2}, \tag{39b}$$

$$b_4 = \frac{-64\Big(\kappa^2(1+\text{sign}(\gamma)) - \kappa(7+9\text{sign}(\gamma)) + 10 + 16\text{sign}(\gamma)\Big)}{\gamma^4(\kappa+1)^3(1+\text{sign}(\gamma))}, \tag{39c}$$

Observing that $\text{sign}(\gamma) = 1$ for $\gamma > 0$, $\text{sign}(\gamma) = -1$ for $\gamma < 0$, from (38) and (39) it is seen that H_1 and H_2 are well-behaved near $\rho = 0$ for $\gamma > 0$. However, for $\gamma < 0$ coefficients a_3 and b_4 (and possibly that of higher powers of ρ) become unbounded and as a result k_{33} as expressed by (37) also becomes unbounded. Consequently, it is seen that for a graded medium with an exponentially decaying stiffness the contact problem is not a well-posed problem. Physically the problem that is analogous to $\gamma < 0$ case is a homogeneous infinite strip of finite thickness under an unbalanced transverse load P (in thickness direction) which has no solution (see [14] for the explanation). Thus for graded half-planes with or without a crack, if $\gamma < 0$ the contact problem has no solution.

5. On the solution of integral equations

Once the exponents λ_1, λ_2, ω, β and α are determined, from (27) and (31) the weight functions w_i and the general form of the solution of the integral equations may be obtained by normalizing the intervals $(0,d)$ and (a,b) or $(0,b)$ to be $(-1,1)$, e.g. by defining

$$f_i(t) = \phi_i(r), \qquad i = 1,2,3, \qquad -1 < r < 1, \tag{40}$$

$$t = \frac{d}{2}(1+r), \qquad 0 < t < d, \qquad -1 < r < 1, \tag{41a}$$

$$t = \frac{b-a}{2}r + \frac{b+a}{2}, \qquad a < t < b, \qquad -1 < r < 1, \qquad (a > 0), \tag{41b}$$

$$t = \frac{b}{2}(1+r), \qquad 0 < t < b, \qquad -1 < r < 1, \qquad (a = 0). \tag{41c}$$

The integral equations (24) with generalized Cauchy kernels would then have the form

$$\sum_{j=1}^{3}\int_{-1}^{1} m_{ij}(s^*,r)\phi_j(r)dr = g_i(s^*), \qquad -1 < s^* < 1, \quad i = 1,2,3, \tag{42}$$

where $x = d(1+s^*)/2$ for $i = 1,2$, $y = (b-a)s^*/2 + (b+a)/2$, $(a > 0)$, $y = b(1+s^*)/2$, $(a = 0)$, for $i = 3$.

From (27)-(30) it is seen that for $a > 0$ the solution of (42) may be expressed as

$$\phi_1(r) = w_1(r)\sum_{n=0}^{\infty} A_{1n}P_n^{(-1/2,0)}(r), \qquad w_1(r) = (1-r)^{-1/2}, \tag{43a}$$

$$\phi_2(r) = w_2(r)\sum_{n=0}^{\infty} A_{2n}P_n^{(-1/2,0)}(r), \qquad w_2(r) = (1-r)^{-1/2}, \tag{43b}$$

$$\phi_3(r) = w_3(r)\sum_{n=0}^{\infty} A_{3n}P_n^{(\beta,\omega)}(r), \qquad w_3(r) = (1-r)^{\beta}(1+r)^{\omega}. \tag{43c}$$

Similarly for $a = 0$, from (31)-(33) and (35) we obtain

$$\phi_1(r) = w_1(r)\sum_{n=0}^{\infty} B_{1n}P_n^{(-1/2,\alpha)}(r), \qquad w_1(r) = (1-r)^{-1/2}(1+r)^{\alpha}, \tag{44a}$$

$$\phi_2(r) = w_2(r)\sum_{n=0}^{\infty} B_{2n}P_n^{(-1/2,\alpha)}(r), \qquad w_2(r) = (1-r)^{-1/2}(1+r)^{\alpha}, \tag{44b}$$

$$\phi_3(r) = w_3(r)\sum_{n=0}^{\infty} B_{3n}P_n^{(-1/2,\alpha)}(r), \qquad w_3(r) = (1-r)^{\beta}(1+r)^{\alpha}, \tag{44c}$$

where $P_n^{(\alpha_1,\alpha_2)}(r)$, $-1 < r < 1$, are Jacobi polynomials. The integral equations (42) are solved numerically by using (43) or (44) and an appropriate collocation technique. In this solution the eqauilibrium condition (7) and the compatibility relations (36) are used as additional conditions. Also, the following property of Jacobi polynomials is used to regularize the singular parts of the integral equations (24), that is the terms involving the Cauchy kernels and the free term

$$\frac{1}{\pi}\int_{-1}^{1}(1-r)^{\beta}(1+r)^{\alpha}P_n^{(\beta,\alpha)}\frac{dr}{r-s} = \cot(\pi\beta)(1-s)^{\beta}(1+s)^{\alpha}P_n^{(\beta,\alpha)}(s) -$$

$$-\frac{2^{(\alpha+\beta)}\Gamma(\beta)\Gamma(n+\alpha+1)}{\pi\Gamma(n+\alpha+\beta+1)}\mathrm{F}\Big(n+1, -n-\beta-\alpha; 1-\beta; \frac{1-s}{2}\Big), \tag{45}$$

where $\Gamma()$ is the gamma function and $\mathrm{F}\left(n+1, -n-\beta-\alpha; 1-\beta; \frac{1-s}{2}\right)$ is the hypergeometric function.

After solving the integral equations for f_1, f_2 and f_3 the contact stresses $\sigma_{xx}(0,y) = f_3(y) = \phi_3(s^*)$, $\sigma_{xy}(0,y) = \eta f_3(y) = \eta\phi_3(s^*)$, the in-plane component of the surface stress $\sigma_{yy}(0,y)$ (see for example (19) and (20) for the procedure to be followed) and the stress intensity factors at the crack tip $(d,0)$ may be evaluated by using the results. The stress intensity factors are defined by and calculated from

$$k_1 = \lim_{x\to d+0}\sqrt{2(x-d)}\sigma_{yy}(x,0) =$$

$$= -\lim_{x\to d-0}\frac{2\mu(x)}{\kappa+1}\sqrt{2(d-x)}\frac{\partial}{\partial x}(v(x,0^+)-v(x,0^-)), \tag{46a}$$

$$k_2 = \lim_{x\to d+0}\sqrt{2(x-d)}\sigma_{xy}(x,0) =$$

$$= -\lim_{x\to d-0}\frac{2\mu(x)}{\kappa+1}\sqrt{2(d-x)}\frac{\partial}{\partial x}(u(x,0^+)-u(x,0^-)). \tag{46b}$$

From (43), (44) and (46) it then follows that

$$k_1 = -\exp(\gamma d)\sqrt{d}\sum_{n=0}^{\infty}A_{1n}P_n^{(-1/2,0)}(1), \tag{47a}$$

$$k_2 = -\exp(\gamma d)\sqrt{d}\sum_{n=0}^{\infty}A_{2n}P_n^{(-1/2,0)}(1), \tag{47b}$$

for $a > 0$ and

$$k_1 = -2^{\alpha}\exp(\gamma d)\sqrt{d}\sum_{n=0}^{\infty}A_{1n}P_n^{(-1/2,\alpha)}(1), \tag{48a}$$

$$k_2 = -2^{\alpha}\exp(\gamma d)\sqrt{d}\sum_{n=0}^{\infty}A_{2n}P_n^{(-1/2,\alpha)}(1), \tag{48b}$$

for $a = 0$.

The other quantity of physical interest is the in-plane stress $\sigma_{yy}(0,y)$ on the surface which has a bearing on crack initiation and which may be expressed as

$$\sigma_{yy}(0,y)=\sum_{j=1}^{3}\sigma_{yyj}(0,y)=\sum_{j=1}^{2}\int_0^d k_{yj}(y,t)f_j(t)dt+\int_a^b k_{y3}(y,t)f_3(t)dt,$$
$$-\infty<y<\infty, \tag{49}$$

where $k_{yj}(y,t)$, $(j=1,2,3)$ are known kernels corresponding to the in-plane stress components $\sigma_{yyj}(0,y)$, $(j=1,2,3)$, (see, for example (19) and (20) for the in-plane stress due to sliding contact). Knowing the stress components σ_{xx}, σ_{yy} and σ_{xy} on the surface, at the critical location (that is, the trailing end $y=a$ of the contact region) the cleavage stress $\sigma_{\theta\theta}(r,\theta)$ may be expressed as

$$\sigma_{\theta\theta}(r,\theta)=\sigma_{xx}\sin^2(\theta)+\sigma_{yy}\cos^2(\theta)-\sigma_{xy}\sin(\theta)\cos(\theta), \tag{50}$$

where for $\theta=\theta_{cr}$, $\sigma_{\theta\theta}$ is maximum and positive, and it can be shown that $\theta_{cr}=0$ and $(\sigma_{\theta\theta})_{cr}=\sigma_{yy}(0,a)$, namely, the crack initiation is perpendicular to the surface.

It should be observed that the problem of remote loading by a constant strain $\epsilon_{yy}(x,\pm\infty)=\epsilon_0$ of a graded half-plane is a mode I surface crack problem and is fully uncoupled from the sliding contact/crack problem. As a result, the special cases of the previously known solutions for a graded strip [11] or bonded dissimilar graded strips [15] may be directly superimposed on the results given in this study to obtain the influence of the remote loading by constant strain. Also note that such a superposition would tend to remove negative mode I stress intensity factors resulting from certain values of the parameters γ, κ, η and normalized dimensions a/d and b/d.

6. Results and discussion

The calculated results in this study mainly consist of the contact stresses $(\sigma_{xx}(0,y)$, $\sigma_{xy}(0,y)$, $a<y<b)$, stress intensity factors $(k_1(d)$, $k_2(d))$, and the in-plane component of the stress on the surface $(\sigma_{yy}(0,y)$, $-\infty<y<\infty)$. The contact stresses are obtained directly by solving the integral equation (24) or (42) as follows:

$$\sigma_{xx}(0,y)=f_3(y)=\phi_3(s),\quad \sigma_{xy}(0,y)=\eta\phi_3(s),\quad a<y<b,\qquad -1<s<1. \tag{51}$$

For $a>0$ some sample results showing the normal component of the contact stress, $\sigma_{xx}(0,y)$, are given in Figure 3 for loading by a flat stamp as described in Figure 4. In this case the stresses are singular at the end points a and b (see equation 27c) and the

singularities ω and β are given by (30) and Figure 2. Note again, that for $\eta > 0$ $|\omega| > |\beta|$, that is the stress concentration near the trailing end a is greater than that near the leading end b. Figure 3 also shows in certain respects the competing effects of the coefficient of friction η, the material nonhomogeneity parameter γ and the relative stamp dimension $(b-a)/d$ on the contact stresses.

The contact stress distribution for $a = 0$ is shown in Figure 5. In this case the stress singularities α and β at the end points $a = 0$ and b are given by (35) and (33), respectively. Figure 2 shows that for relatively small values of (positive) η the stress singularity at b is greater than that at $a = 0$ (i.e., $-\beta > -\alpha$), hence the skewed distribution in Figures 5a and 5b where $\eta = 0.4$. On the other hand for relatively large values of η, $|\alpha| > |\beta|$ (see Figure 2) the trend seems to be reversed and there is a greater stress concentration near the end $a = 0$ (see Figures 5c and 5d).

Some results showing the modes I and II stress intensity factors k_1 and k_2 at the crack tip $x = d$ in a graded medium loaded by a flat stamp (Figure 4) are given in Figures 6-8. Figure 6 shows the results as functions of a/d for $a > 0$, $(b-a)/d = 1$ and various values of γ and η. For a frictionless stamp acting on a homogeneous medium η, γ and the tangential force that would tend to open the crack are zero, the region is mostly under compression and, consequently, k_1 is negative and k_2 is positive. As η increases the resultant friction force ηP also increases and gradually k_1 becomes positive and k_2 negative. Figure 6 shows that the influence of not only η, which is expected, but also of the material nonhomogeneity parameter γ on the stress intensity factors could be quite significant. Incidentally, the solution presented in Figures 6-8 corresponding to the values of η, γ and $(b-a)/d$ (or b/d for $a = 0$) for which $k_1 < 0$ is, of course, not valid due to crack closure. But the results can still be applicable and useful in superposition with an uncoupled solution resulting, for example, from remote strain loading $\epsilon_{yy}(x, \mp\infty)$, [11], [15], provided the resultant k_1 is positive. Otherwise, the problem needs to be formulated by taking into account the crack closure and determining the closure distance from the condition of $k_1 = 0$.

Stress intensity factors similar to that shown in Figure 6 are also given in Figure 7, the only difference being in the relative stamp size, namely $(b-a)/d = 1$ in Figure 6 and $(b-a)/d = 0.1$ in Figure 7.

In the special case of $a = 0$, Figure 8 shows the stress intensity factors k_1 and k_2 as functions of the relative stamp size b/d (see Figure 4) for $\kappa = 2$ and for various values of γ and η. For a homogeneous medium the solution is obtained in two different ways: first by assuming $\gamma d = 0.0001$ and using the nonhomogeneous material program and then by

solving the integral equations for a homogeneous medium (for which all kernels are known in closed form). In Figure 8, the results of the former solution are given as solid lines and that of the latter as closed circles. Note that for all intents and purposes the two sets of results are identical.

Some examples showing the surface stresses in a graded medium in the absence of a crack and loaded by a sliding flat stamp are given in Figure 9 (see Figure 4, $d = 0$). The figure shows the normal component of the contact stress $\sigma_{xx}(0, y)$, $a < y < b$, and the in-plane stress $\sigma_{yy}(0, y)$, $-\infty < y < \infty$, that is parallel to the surface. The shear component of the contact stress is obtained from $\sigma_{xy}(0, y) = \eta\sigma_{xx}(0, y)$. The results are given for various values of friction coefficient η, and material nonhomogeneity parameter γ. For $\eta = 0$ the results are symmetric and stresses on the surface (including σ_{yy}) have square-root singularities at $y = a$ and $y = b$. On the other hand for $\eta > 0$ there is a greater stress concentration near the trailing end of the stamp, $y = a$ and $|\omega| > |\beta|$, ω and β being the singularities at $y = a$ and $y = b$, respectively (see Figure 2). The important conclusion one may draw from Figure 9 is that at the trailing end of the stamp the in-plane component of the stress $\sigma_{yy}(0, y)$ is unbounded and and discontinuous and has a singularity of the order $(a - y)^{\omega}$, where $-\omega > 1/2$ (see Figure 2). This implies that $y = a$ is a likely location of surface crack initiation.

7. Some conclusions

1. Analytically the contact problem for a graded half-plane with exponentially decaying stiffness is not a well-posed problem.
2. The trailing end of the sliding rigid stamp with friction is a likely location of surface crack initiation due to greater stress concentration.
3. In the medium containing a surface crack and loaded by a sliding rigid stamp, the mixed mode stress state at the crack tip is such that the cracks tend to be periodic and curve backward.
4. In the coupled crack/contact problems for a graded medium the stress singularities α, β and ω are independent of the material nonhomogeneity constants γ and μ_0 and depend on the friction coefficient η and the surface value of the Poisson's ratio (through the elastic constant κ) only.

Acknowledgments

This work was partially supported by AFOSR under the grant F49620-98-1-0028. The senior author also gratefully acknowledges the support provided by Alexander von Humboldt Foundation during his stay at the FZK in Karlsruhe, Germany.

Appendix A. Mellin transform method for the derivation of the characteristic equation

The characteristic equation given by (35) can also be obtained by considering a 90-degree homogeneous elastic wedge as shown in Figure 10 and using Mellin transformation. The boundary conditions of the problem are

$$\sigma_{r\theta}(r,0) - \eta\sigma_{\theta\theta}(r,0) = 0, \qquad 0 < r < \infty, \tag{A1a}$$

$$\frac{\partial}{\partial r}u_{\theta}(r,0) = f(r), \qquad 0 < r < \infty, \tag{A1b}$$

$$\sigma_{\theta\theta}(r,\pi/2) = 0, \qquad 0 < r < \infty, \tag{A1c}$$

$$\sigma_{r\theta}(r,\pi/2) = 0, \qquad 0 < r < \infty. \tag{A1d}$$

In polar coordinates, following definition of the stresses in terms of a stress function χ, identically satisfies the equilibrium equations,

$$\sigma_{rr}(r,\theta) = \frac{1}{r}\frac{\partial\chi(r,\theta)}{\partial r} + \frac{1}{r^2}\frac{\partial^2\chi(r,\theta)}{\partial\theta^2}, \tag{A2a}$$

$$\sigma_{\theta\theta}(r,\theta) = \frac{\partial^2\chi(r,\theta)}{\partial r^2}, \tag{A2b}$$

$$\sigma_{r\theta}(r,\theta) = -\frac{\partial}{\partial r}\left(\frac{1}{r}\frac{\partial\chi(r,\theta)}{\partial\theta}\right). \tag{A2c}$$

Thus, the compatibility condition becomes,

$$\nabla^2\nabla^2\chi(r,\theta) = 0, \tag{A3}$$

where,

$$\nabla^2 = \frac{\partial^2}{\partial r^2} + \frac{1}{r}\frac{\partial}{\partial r} + \frac{1}{r^2}\frac{\partial^2}{\partial \theta^2}\,. \tag{A4}$$

It is also known that (see, for example, [16]), displacements can be expressed in terms of this biharmonic stress function χ and another harmonic function ϕ in the following form,

$$2\mu u_r(r,\theta) = -\frac{\partial \chi(r,\theta)}{\partial r} + \Big(\frac{\kappa+1}{4}\Big) r \frac{\partial \phi(r,\theta)}{\partial \theta}, \tag{A5a}$$

$$2\mu u_\theta(r,\theta) = -\frac{1}{r}\frac{\partial \chi(r,\theta)}{\partial \theta} + \Big(\frac{\kappa+1}{4}\Big) r^2 \frac{\partial \phi(r,\theta)}{\partial r}, \tag{A5b}$$

where $\chi(r,\theta)$ and $\phi(r,\theta)$ are related by,

$$\nabla^2 \chi(r,\theta) = \frac{\partial}{\partial r}\Big(r\frac{\partial \phi(r,\theta)}{\partial \theta}\Big), \tag{A6}$$

and $\phi(r,\theta)$ is a harmonic function,

$$\nabla^2 \phi(r,\theta) = 0. \tag{A7}$$

Mellin transform of a function $f(r)$ and its inverse are defined by ,

$$\widehat{f}(p) = \int_0^\infty f(r) r^{p-1} dr, \quad f(r) = \frac{1}{2\pi i}\int_{c-i\infty}^{c+i\infty} \widehat{f}(p) r^{-p} dp. \tag{A8a,b}$$

Mellin transform of the derivative can be written as,

$$\int_0^\infty \frac{d^n f(r)}{dr^n} r^{p-1+n} dr = (-1)^n \frac{\Gamma(p+n)}{\Gamma(p)} \widehat{f}(p), \tag{A9}$$

provided,

$$r^{p+m-1}\frac{d^{m-1}}{dr^{m-1}} f(r) = 0. \tag{A10}$$

as, $r \to 0$ and $r \to \infty$ for $m = 1, 2, 3, ..., n$.

Taking the Mellin transform of equations (A3), (A6) and (A7) we obtain,

$$\frac{d^4 \widehat{\chi}(\theta,p)}{d\theta^4} + \big(p^2 + (p+2)^2\big)\frac{d^2 \widehat{\chi}(\theta,p)}{d\theta^2} + p^2(p+2)^2 \widehat{\chi}(\theta,p) = 0, \tag{A11a}$$

$$\frac{d^2\widehat{\phi}(\theta,p)}{d\theta^2}+p^2\widehat{\phi}(\theta,p)=0, \tag{A11b}$$

$$\frac{d}{d\theta}\widehat{\phi}(\theta,p+2)=-\frac{1}{p+2}\Big(p^2\widehat{\chi}(\theta,p)+\frac{d^2\widehat{\chi}(\theta,p)}{d\theta^2}\Big). \tag{A11c}$$

Solving equations (A11a) and (A11b) and using (A11c) displacements and stresses can be expressed as follows,

$$\mu r^2\Big(\frac{\partial u_r}{\partial r}+i\frac{\partial u_\theta}{\partial r}\Big)=$$

$$-\frac{1}{2\pi i}\int_{c-i\infty}^{c+i\infty}(p+1)\Big(Ape^{ip\theta}+B(p+1)e^{i(p+2)\theta}+\kappa\overline{B}e^{-i(p+2)\theta}\Big)r^{-p}dp, \tag{A12a}$$

$$\frac{r^2}{2i}(\sigma_{r\theta}+i\sigma_{\theta\theta})=$$

$$\frac{1}{2\pi i}\int_{c-i\infty}^{c+i\infty}(p+1)\Big(Ape^{ip\theta}+B(p+1)e^{i(p+2)\theta}-\overline{B}e^{-i(p+2)\theta}\Big)r^{-p}dp. \tag{A12b}$$

In equations (A12), A and B are complex constants and $\overline{B}$ is the complex conjugate of B. Using equations (A12) and boundary conditions (A1) following expressions are obtained

$$\frac{\sigma_{\theta\theta}(r,0)}{4\mu}=\int_0^\infty f(t)dt\frac{1}{2\pi i}\int_{c-i\infty}^{c+i\infty}\frac{2\alpha^2+4\alpha+1-\cos(\pi\alpha)}{D(\alpha)}\frac{r^\alpha}{t^{\alpha+1}}d\alpha, \tag{A13a}$$

$$\frac{1}{2(\kappa+1)}\frac{\partial}{\partial r}u_\theta(r,\pi/2)=$$

$$\int_0^\infty f(t)dt\frac{1}{2\pi i}\int_{c-i\infty}^{c+i\infty}\frac{\eta\cos(\pi\alpha)(\alpha+2)+\sin(\pi\alpha/2)(\alpha+1)}{D(\alpha)}\frac{r^\alpha}{t^{\alpha+1}}d\alpha, \tag{A13b}$$

where,

$$D(\alpha)=\eta(4\alpha^2+10\alpha+5+(\kappa-1)\cos(\pi\alpha)+\kappa(2\alpha+3))+(\kappa+1)\sin(\pi\alpha). \tag{A14}$$

Note that $D(\alpha)$ is same as the characteristic equation (35). If one performs the inversions in (A13) by using the theory of residues, then negative roots of $D(\alpha)$ give stresses that are singular as r approaches zero. Thus, $D(\alpha)=0$ is the characteristic equation of the problem.

References

1. Hertz H. Uber die Beruhrung elastischer Korper. J. Reine und Augewandte Mathematik. 1882;92:156-171.
2. Johnson KL. Contact Mechanics. Cambridge University Press, 1985.
3. Bakirtas I. The problem of a rigid punch on a nonhomogeneous elastic half space. Int. J. Engng. Sci. 1980;18:597-610.
4. Giannakopoulos AE, Suresh S. Indentation of solids with gradients in elastic properties: Part II Axisymmetric indenters. Int. J. Solids Structures. 1997;34:2393-2428.
5. Suresh S, Giannakopoulos AE, Alcala J. Spherical indentation of compositionally graded materials: Theory and experiments. Acta Mater. 1997;45:1307-1321.
6. Guler MA. Contact mechanics of FGM coatings. Ph.D. dissertation, Lehigh University, Bethlehem, PA, USA, 2000.
7. Hasebe N, Okumura M, Nakamura T. Frictional punch and crack in plane elasticity. ASCE, J. Engng. Mech. 1989;115:1137-1149.
8. Lawn B. Fracture of brittle solids. Cambridge University Press, 1993.
9. Delale F, Erdogan F. Crack problem for a nonhomogeneous plane. ASME, J. Appl. Mech. 1983;50:609-614.
10. Dag S. Crack/contact problems for graded materials. Ph.D. dissertation, Lehigh University, Bethlehem, PA, USA, 2001.
11. Erdogan F, Wu BH. Surface crack problem for a plate with functionally graded properties. ASME, J. Appl. Mech. 1997;64:449-456.
12. Erdogan F. Mixed boundary value problems in mechanics. In: Mechanics Today, Nemat-Nasser S. ed. vol. 4. Pergamon Press, 1978. p. 1-86.
13. Muskhelishvili NI. Singular integral equations. Groningen: P. Noordhoff Ltd., 1953.
14. Ratwani M, Erdogan F. On the plane contact problem for a frictionless elastic layer. Int. J. Solids Structures. 1973;9:921-936.
15. Kasmalkar M. The surface crack problem for a functionally graded coating bonded to a homogeneous layer. Ph.D. dissertation, Lehigh University, Bethlehem, PA, USA, 1997.
16. Hein VL, Erdogan F. Stress singularities in a two-material wedge. Int. J. Frac. Mech. 1973;7:317-330.

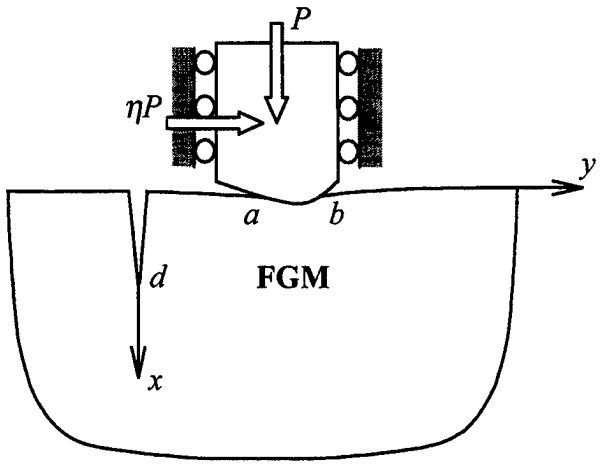

Figure 1: The general description of the crack/contact problem in a graded medium.

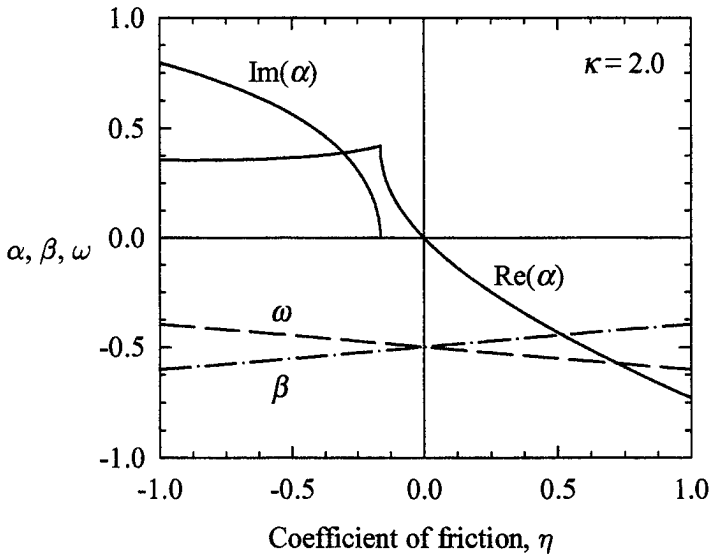

Figure 2: Variation of exponents α, β and ω with friction coefficient η.

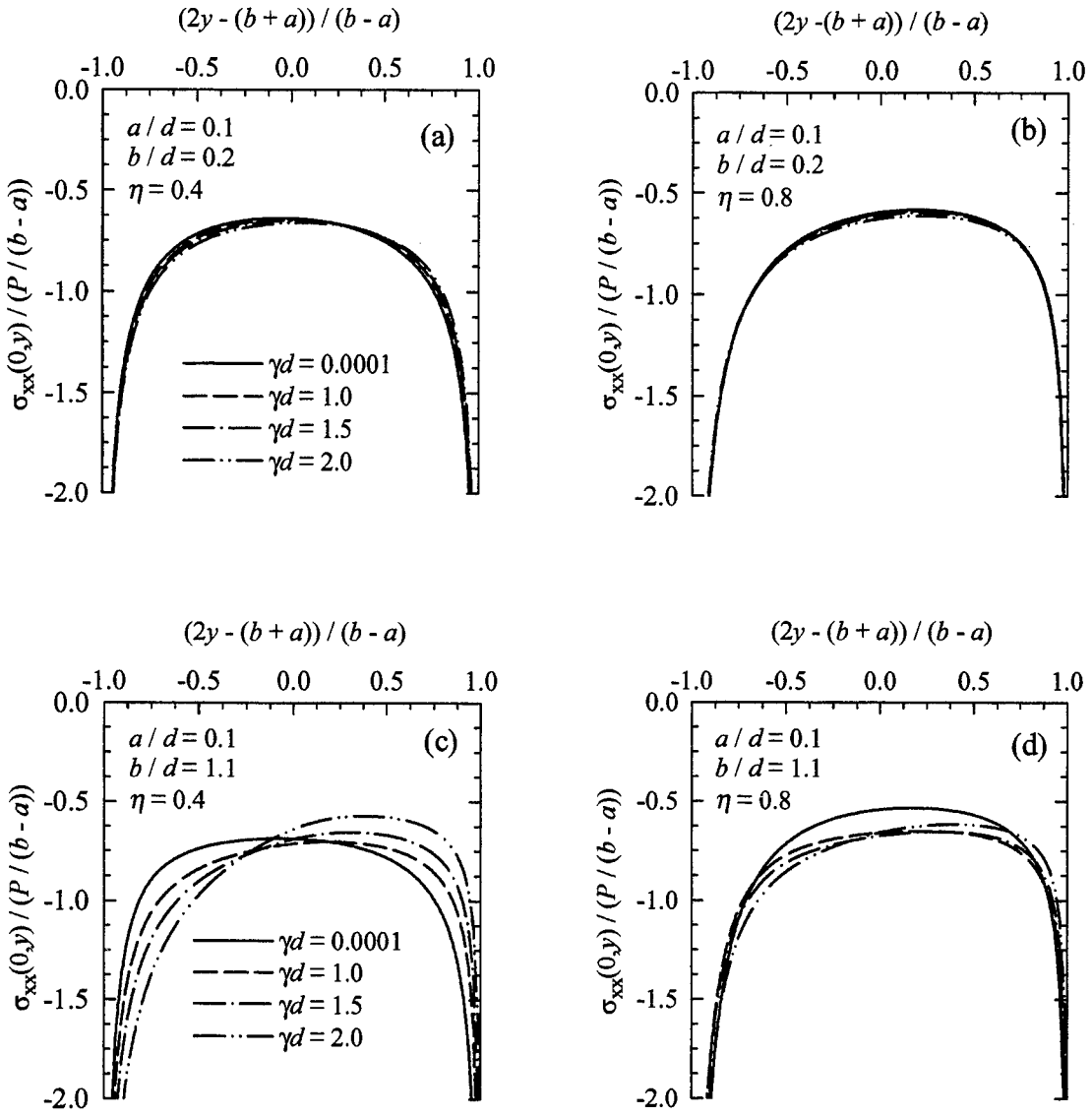

Figure (3a-d): The distribution of the normal component of contact stress for $a > 0$, $\kappa = 2$ and for various values of η, γ and the relative stamp dimension $(b - a)/d$ (see Figure 4).

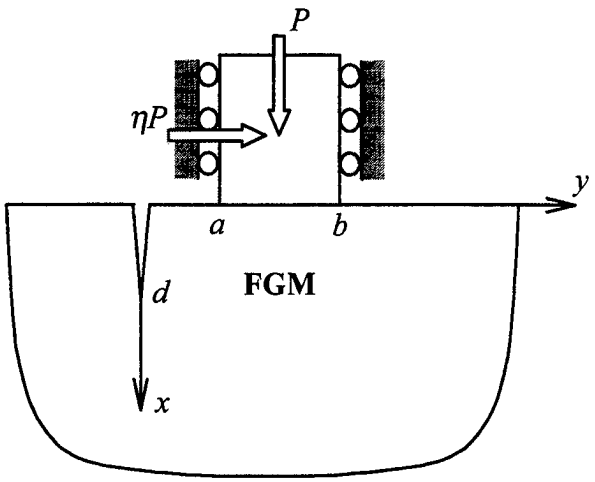

Figure 4: The geometry of crack/contact problem for a flat stamp.

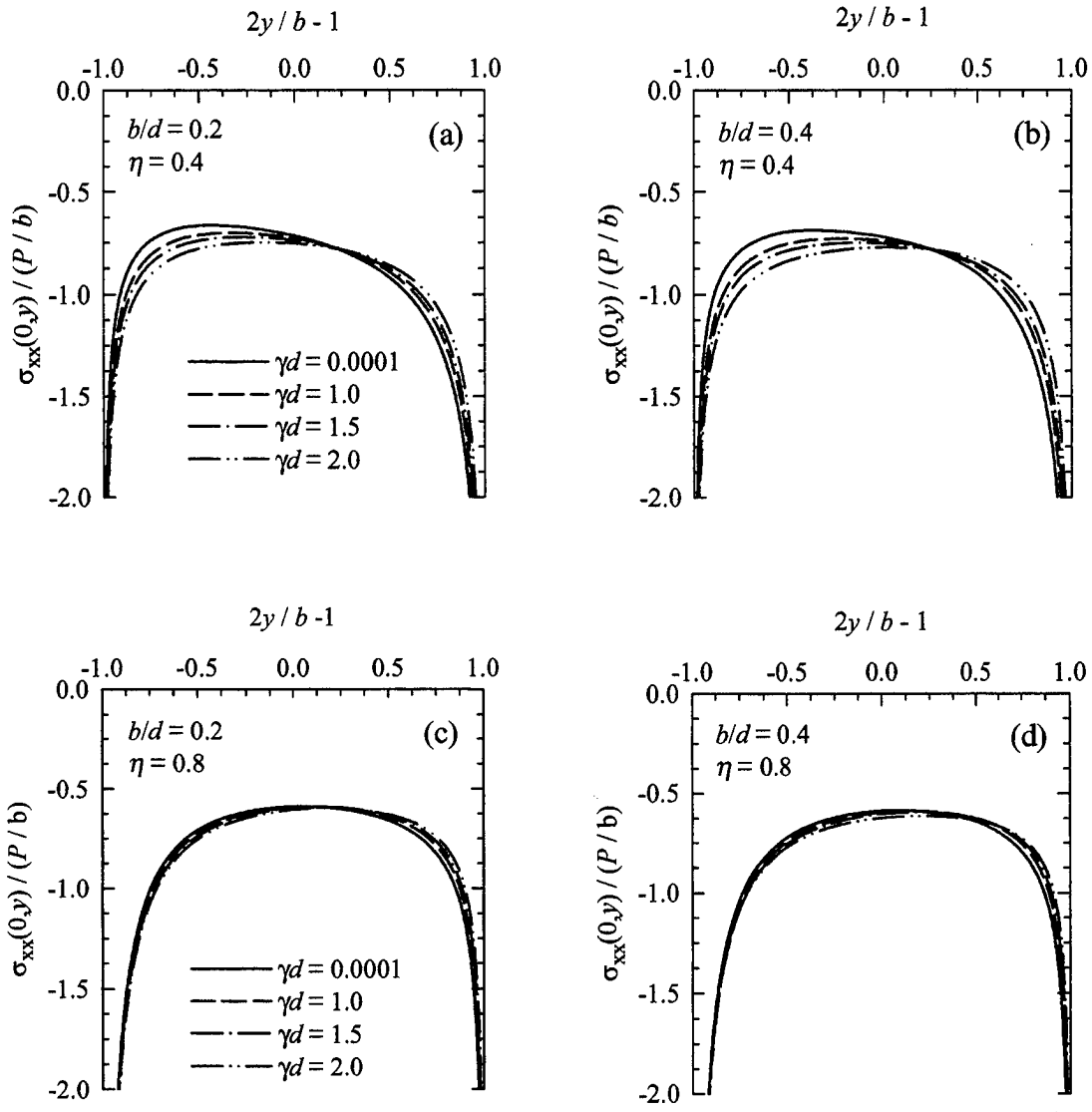

Figure (5a-d): The contact stress distribution for $a = 0$, $\kappa = 2$ and for various values of η, γ and relative stamp dimension b/d. (see Figure 4).

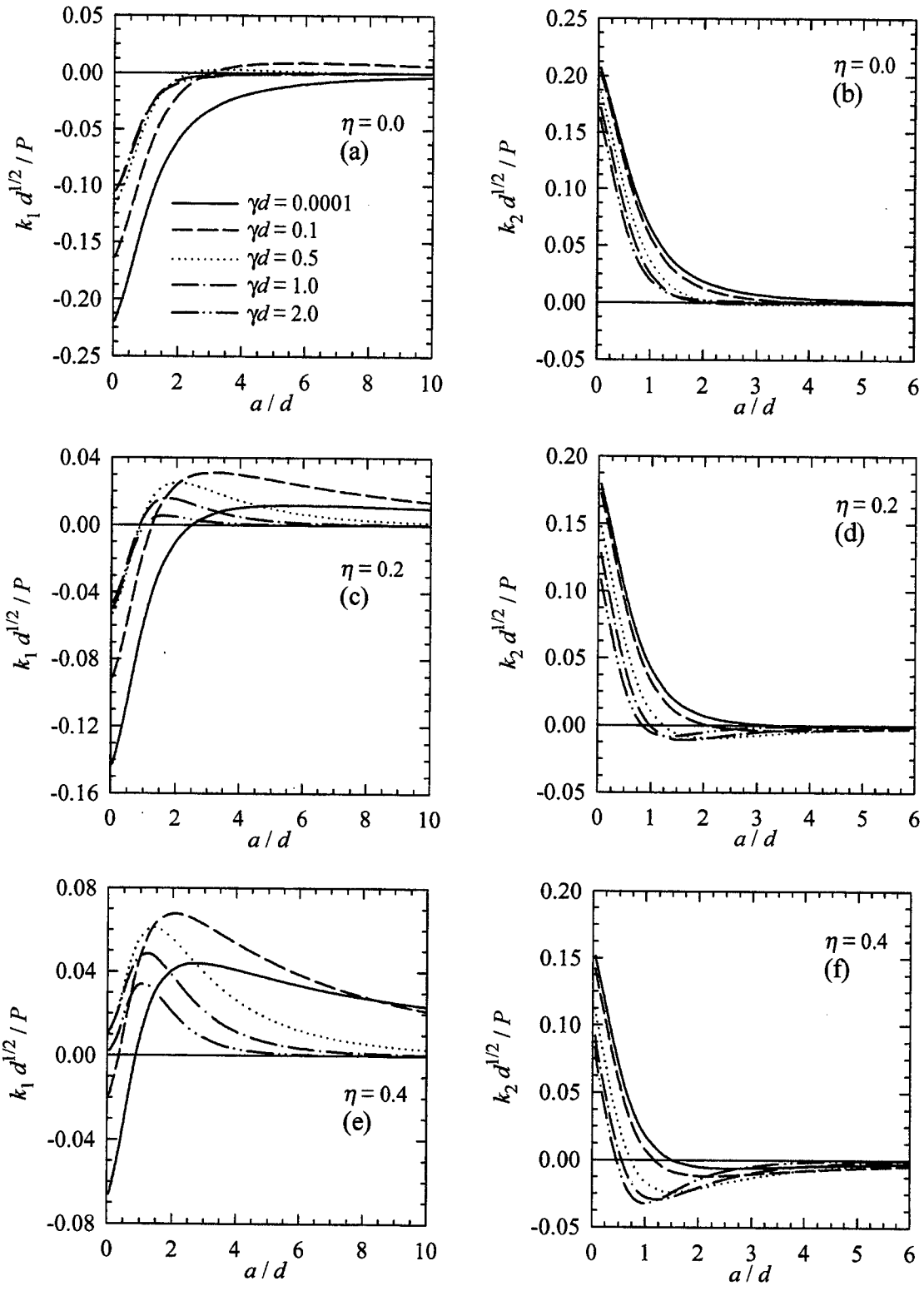

Figure (6a-l): Variation of stress intensity factors with γ, η and stamp location a/d (see Figure 4) for $\kappa = 2$, $(b-a)/d = 1.0$ and $a > 0$.

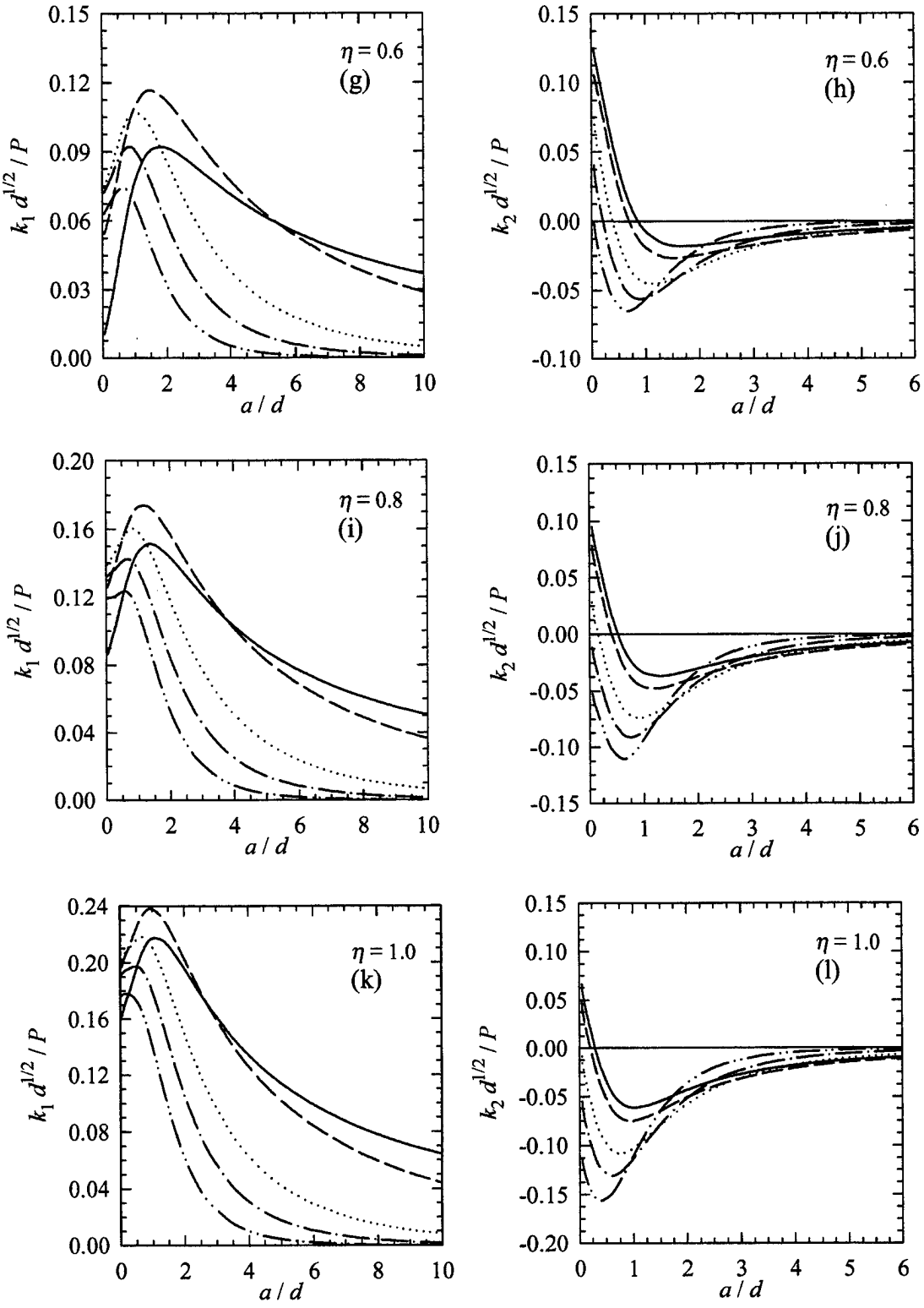

Figure (6a-l): continued.

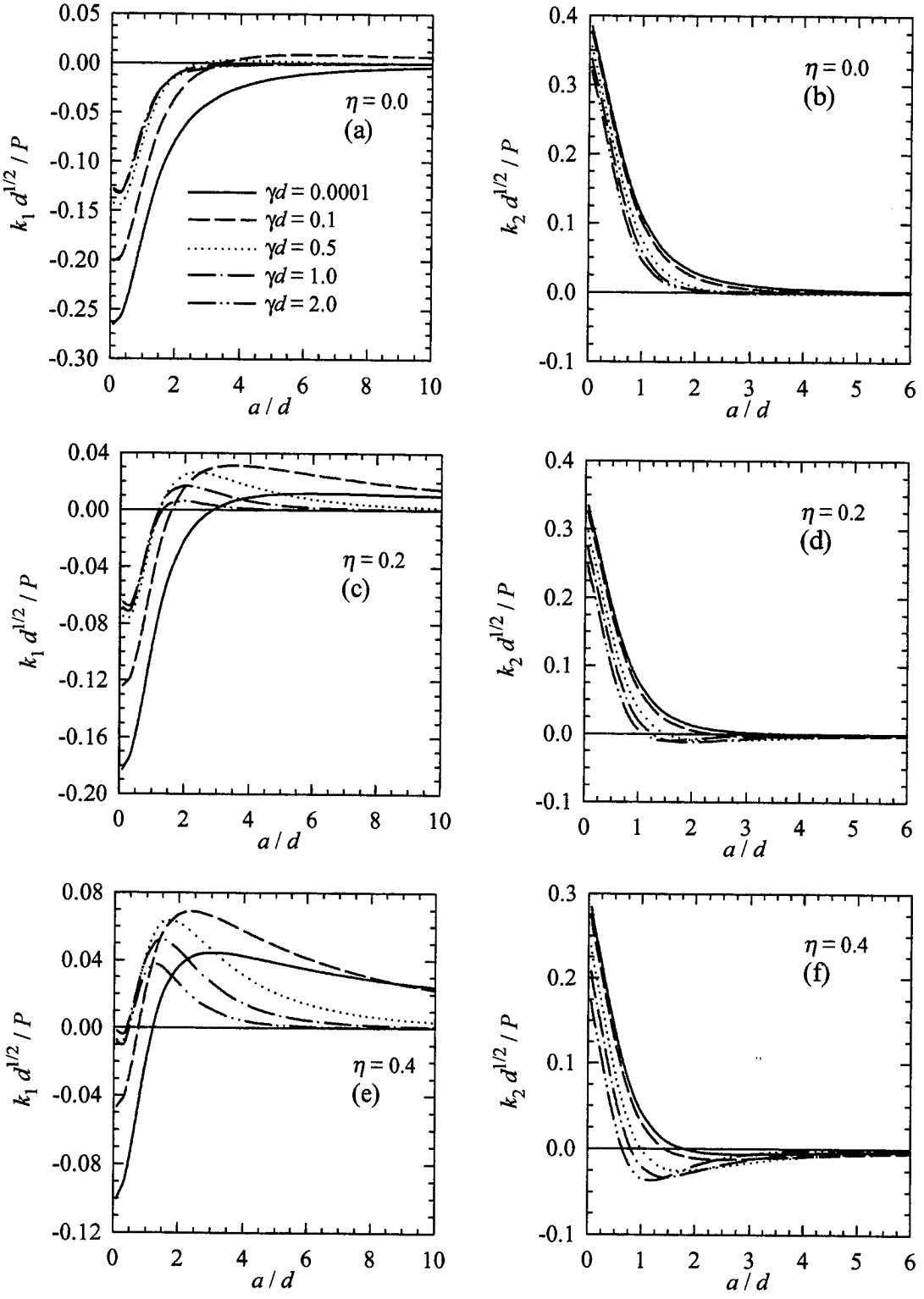

Figure (7a-l): Same as Figure 6, $(b - a)/d = 0.1$.

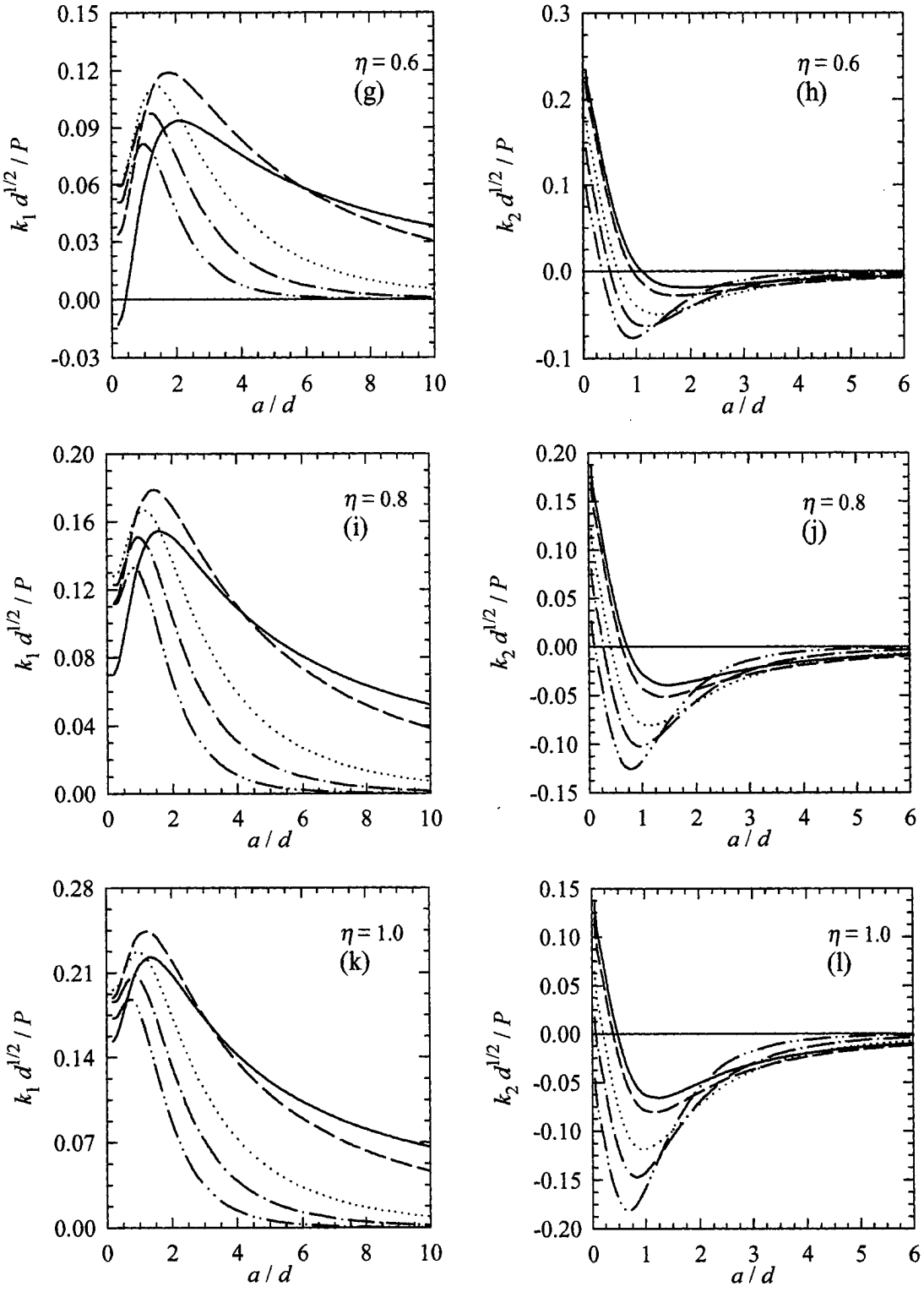

Figure (7a-l): continued.

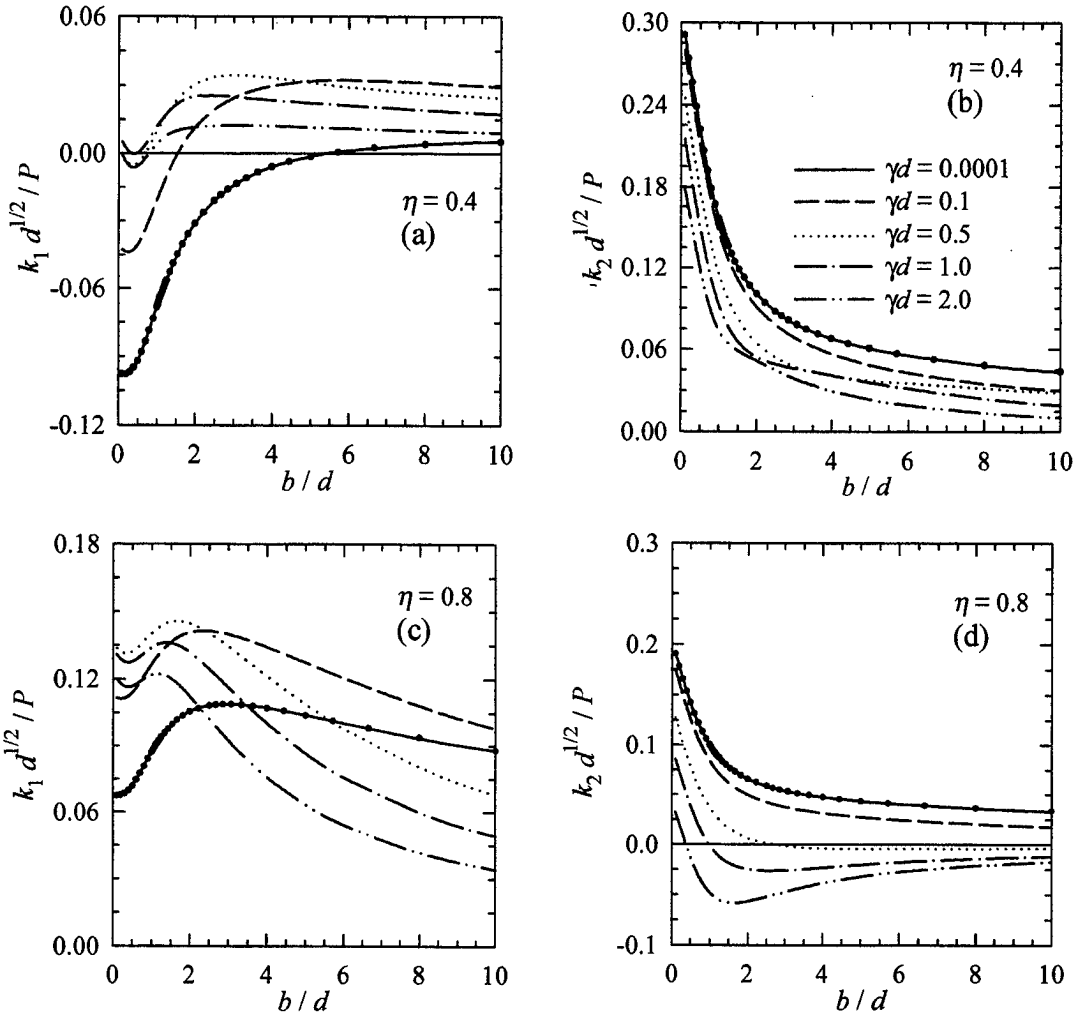

Figure (8a-d): Variation of stress intensity factors with the relative stamp size for $a = 0$, $\kappa = 2$ and for various values of γ and η (see Figure 4).

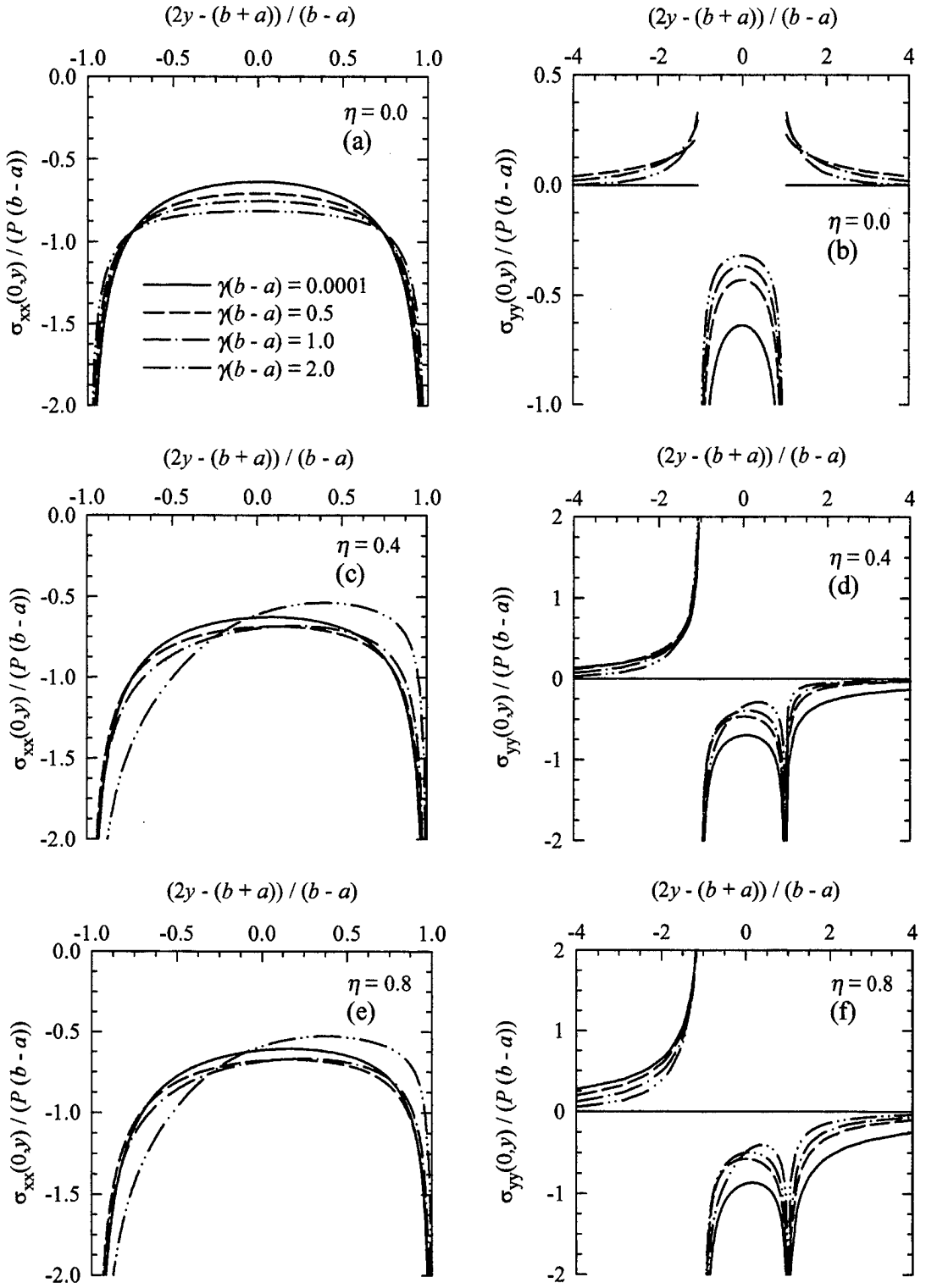

Figure (9a-f): The distribution of the contact stress $\sigma_{xx}(0, y)$ and the in-plane stress $\sigma_{yy}(0, y)$ on the surface in a graded medium loaded by a flat stamp for $\kappa = 2$ and for various values of γ and η.

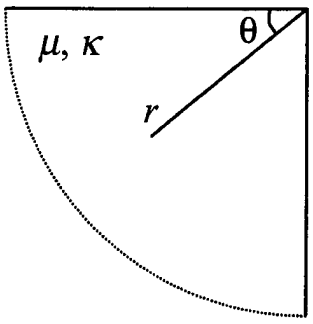

Figure 10: The geometry of the 90-degree elastic wedge.